

Montana Tech Library

Digital Commons @ Montana Tech

---

Graduate Theses & Non-Theses

Student Scholarship

---

Summer 2021

**QUATERNARY GEOLOGY OF PORTIONS OF THE MCGREGOR  
PEAK, MURR PEAK, MARION, AND HUBBART RESERVOIR, 7.5'  
QUADRANGLES, FLATHEAD COUNTY, MONTANA**

Carlos Montejo

Follow this and additional works at: [https://digitalcommons.mtech.edu/grad\\_rsched](https://digitalcommons.mtech.edu/grad_rsched)



Part of the [Geology Commons](#)

---

QUATERNARY GEOLOGY OF PORTIONS OF THE MCGREGOR PEAK,  
MURR PEAK, MARION, AND HUBBART RESERVOIR, 7.5'  
QUADRANGLES, FLATHEAD COUNTY, MONTANA

by  
Carlos Montejo

A thesis submitted in partial fulfillment of the  
requirements for the degree of

Master of Science:  
Geoscience-Geology

Montana Tech  
2021



## Abstract

Quaternary deposits in the northern Little Bitterroot River watershed record the advance and retreat of the Cordilleran Ice Sheet, transgression of Glacial Lake Missoula, and at least one partial or complete drainage of Glacial Lake Missoula during the last Pleistocene glaciation. New geologic mapping at a scale of 1:24,000 in portions of the McGregor Peak, Marion, Murr Peak, and Hubbard Reservoir quadrangles with a focus on Quaternary deposits has refined boundaries for where the Cordilleran Ice Sheet and Glacial Lake Missoula coincided. Stratigraphic analysis of three measured sections within Glacial Lake Missoula sediments along with three optically stimulated luminescence ages on quartz grains in sands below and within the glaciolacustrine sediments constrains the age of initial lake transgression to between  $21.8 \pm 1.4$  and  $20.3 \pm 1.2$  ka. These ages are consistent with regional chronological data within and outside of the lake basin. Unlike other studies on the stratigraphy of Glacial Lake Missoula sediments, stratigraphic sections in this study area do not show conclusive evidence of regression and subaerial exposure such as desiccation cracks and periglacial modification. A fan-shaped deposit containing boulders with long dimensions  $> 5$  m at the mouth of a steep canyon along the Little Bitterroot River is evidence of high-velocity flows which produced bedrock scours that were subsequently filled to form lakes. These features are interpreted to record at least one glacial outburst flood after Glacial Lake Missoula had reached its maximum elevation.

Keywords: Glacial Lake Missoula, Cordilleran Ice Sheet, Little Bitterroot River, McGregor Peak, Marion, Hubbard Reservoir, Murr Peak, rhythmites, optically stimulated luminescence

## **Dedication**

I would like to thank my parents for always supporting me and helping me pursue my educational journey. They have always been there for me no matter what. I would also like to thank my former undergraduate professor and longtime friend Dr. Dave Miller for all his help.

## **Acknowledgements**

I would like to acknowledge my advisor Dr. Larry Smith and Dr. Kaleb Scarberry for all their help and guidance in completing this project. I wish to thank Yiwen Li, Katie McDonald, and Susan Smith for taking the time to help me digitize my map. I would also like to thank Dr. Paul Conrad for graciously accepting to be on my committee. I am very grateful for the funding from the USGS EdMap program (grant award No. G20AC00153), Montana Geological Society, and Tobacco Root Geological Society.

## Table of Contents

<b>ABSTRACT .....</b>	<b>II</b>
<b>DEDICATION .....</b>	<b>III</b>
<b>ACKNOWLEDGEMENTS .....</b>	<b>IV</b>
<b>LIST OF TABLES .....</b>	<b>VIII</b>
<b>LIST OF FIGURES.....</b>	<b>IX</b>
<b>LIST OF PLATES.....</b>	<b>XIII</b>
 1. INTRODUCTION .....	 1
1.1. Purpose .....	3
1.2. Physiography and Regional Setting.....	4
1.3. Structural Setting .....	7
1.4. Previous Work .....	7
2. METHODS .....	12
2.1. Mapping of Bedrock.....	13
2.2. Mapping and Analysis of Quaternary Geology .....	13
2.3. Analysis of Glaciolacustrine Deposits.....	14
2.4. Geochronology of Glaciolacustrine Deposits.....	15
3. RESULTS.....	17
3.1. Mesoproterozoic Belt Supergroup – Ravalli Undifferentiated (Yra).....	17
3.2. Geologic Structures .....	22
3.3. Tertiary Deposits .....	22
3.3.1. Ash Flow Tuff (Ta).....	22
3.3.2. Tuffaceous Rock (Ttu).....	24
3.3.3. Weathered Volcanic Rock (Tts) .....	24

3.3.4.	Diabase Intrusions (Ti) .....	24
3.3.5.	Tertiary Sediments (Ts).....	24
3.4.	<i>Tertiary or Quaternary Gravels (QTgr)</i> .....	25
3.5.	<i>Quaternary Deposits and Geology</i> .....	28
3.5.1.	Glacial Till (Qgt) .....	28
3.5.2.	Outwash and Glaciofluvial Deposits (Qgo) .....	29
3.5.3.	Kame Terrace Deposits (Qkt).....	32
3.5.4.	Glaciolacustrine Deposits (Qgl) .....	33
3.5.4.1.	Pine Prairie Section .....	33
3.5.4.2.	Reservoir Section .....	37
3.5.4.3.	Tripp Section .....	40
3.5.5.	Colluvium Deposits (Qc) .....	44
3.5.6.	Boulder Fan Deposit .....	45
3.5.7.	Quaternary Landslide deposits (Qls) .....	48
3.5.8.	Talus Deposits (Qta) .....	48
3.5.9.	Holocene Alluvium (Qal).....	48
3.6.	<i>Glacial Landforms and Features</i> .....	48
3.6.1.	Depositional Landforms .....	49
3.6.2.	Erosional Landforms and Features .....	49
3.7.	<i>Erratics and Overflow Channels</i> .....	51
3.8.	<i>Optical Ages</i> .....	52
4.	DISCUSSION .....	54
4.1.	<i>Defining the Cordilleran Ice Sheet Margin</i> .....	54
4.2.	<i>Glacial Lake Extent and Elevation</i> .....	56
4.3.	<i>Sedimentology and Optical Ages of Glaciolacustrine Sediments</i> .....	58
4.4.	<i>Evidence for a Lake Drainage</i> .....	64
4.5.	<i>Relation to Regional Chronology of Glacial Lake Missoula</i> .....	65
5.	CONCLUSIONS.....	67

6. REFERENCES CITED.....	68
7. APPENDIX A: FINAL LUMINESCENCE REPORT .....	77



## List of Tables

Table I: Small-Aliquot OSL age information. ....	53
Table II: Presumed water content and contribution to radiation from U, Ra, Pb, Th, K, and cosmic rays.....	53

## List of Figures

- Figure 1: Map showing the southern extent of the Cordilleran Ice Sheet (CIS), Glacial Lake Missoula, Glacial Lake Columbia, and the Channeled Scabland. When not blocked by a lobe of the CIS, the .....2
- Figure 2: Study area is outlined in black and contains portions of the McGregor Lake, Marion, Murr Peak, and Hubbard Reservoir 7.5' quadrangles. McGregor Lake is located in the northwest corner of the .....6
- Figure 3: Map showing location of relevant studies near the study area. 1) Langer et al. (2011); 2) Welk (2019); 3) Lange and Zehner (1992); 4) Scarberry (in prep); 5) Scarberry et al. (in prep); 6) Capps (2004).....10
- Figure 4: Map showing the location of recent optical dates for Glacial Lake Missoula sediments in Montana. ....11
- Figure 5: Map showing locations of measured stratigraphic sections in glaciolacustrine deposits. ....15
- Figure 6: Figure showing the Ravalli Group argillite, siltite and quartzite rocks. A) Magnetite and biotite rich argillite. Magnetite shown with black arrows and black speckles in rock are biotite. Quarter for scale.....19
- Figure 7: A) Ravalli Group derived regolith that forms from weathering of the Ravalli Group below the land surface. Notebook for scale is 19 cm tall. Photo was taken in NE ¼, sec. 29, T. 26 N., R. 24 W. B) Quarry .....21
- Figure 8: A) Exposure of ash-flow tuff that occurs in NE ¼, sec. 20, T. 25 N., R. 24 W. Notebook is 19 cm long. B) Up close photo of the ash-flow tuff showing Belt and other volcanic rock clasts. Exposure .....23

Figure 9: A) Tertiary sediment exposure found in a pit. Tape measure is 2.4 m. Exposure occurs in NE  $\frac{1}{4}$ , sec. 21, T. 25 N., R. 24 W. B) Ball and pillow structures in a silt bed. Pencil length is 14 cm. Photo location is .....25

Figure 10: A) Exposure of QTgr in NW  $\frac{1}{4}$ , sec. 20, T. 25 N., R. 24 W. Yellow field book for scale is 19 cm long. B) Purple laminated quartzite clast that is common in QTgr. Glove for scale is approximately 19 cm .....27

Figure 11: Ternary diagram showing clast compositions for QTgr in an exposure south of the Hubbart Reservoir. Green circle shows that the clasts in QTgr are nearly all locally derived Ravalli Group clasts. ....28

Figure 12: A) Exposure of till along the moraine that borders the eastern edge of McGregor Lake (SW  $\frac{1}{4}$  sec. 8, T. 26 N., R. 25 W.). Notebook for scale is 19 cm tall. B) Large boulder found adjacent to moraine.....29

Figure 13: A) View of quarry in a Pine Prairie outwash terrace (SE  $\frac{1}{4}$  sec. 8, T. 26 N., R. 25 W.). Tree for scale is approximately 4 m tall. B) Exposure of gravels near the Tripp section (SW  $\frac{1}{4}$ , sec. 27, T. 25 N., R. 24 W.). ....31

Figure 14: Ternary diagram showing clast compositions for the Tripp section (Qgo1) and Pine Prairie terrace (Qgo2). Blue and red circles show that the clasts in Qgo are nearly all locally derived Ravalli Group and .....32

Figure 15: Measured stratigraphic column of the Pine Prairie section with key for all measured sections.....35

Figure 16: A) Excavated exposure of the Pine Prairie section (SW  $\frac{1}{4}$  sec. 9, T. 26 N., R. 25 W.). Shovel is approximately 1 m long. B) Rhythmic silt and clay couplets with sharp contacts between couplets. Contacts between the.....36

Figure 17: Stratigraphic column of the Reservoir section. See figure 15 for key. OSL sample R was taken from the climbing ripple cross-laminated fine sand in the lowermost couplet.

.....38

Figure 18: A) Exposure of the Reservoir section (SE  $\frac{1}{4}$  sec. 31, T. 26 N., R. 24 W.). Dashed black line shows the contact between the gravel-sand and silty sand-clay facies. B)

Transition from in-phase to .....40

Figure 19: Stratigraphic column of the Tripp section. See figure 15 for key. OSL sample LT1 was taken from the medium sand overlying the gravels. OSL sample LT3 was taken from the uppermost medium sand bed.....42

Figure 20: A) Exposure of the Tripp section (SW  $\frac{1}{4}$  sec. 27, T. 25 N., R. 24 W.). Length of tape measure is 2 m. White arrows show the edges of the intrusive feature and the black box contains the two holes that.....43

Figure 21: A) Crudely bedded colluvium exposure on a steep slope near the Hubbard Reservoir dam (SE  $\frac{1}{4}$  sec. 18, T. 25 N., R. 24 W.). Outcrop is approximately 5 m thick. B)

Undisturbed stratified colluvium overlying .....45

Figure 22: A) Boulder with long dimension of 7 m found near the upper portion of the boulder fan deposit (NE  $\frac{1}{4}$  sec. 31, T. 26 N., R. 24 W.). Field book for scale is 19 cm long. B)

Distal portion of the boulder fan deposit .....47

Figure 23: Figure showing the scoured bedrock just north of the study area. Boggy depressions and channels that are deeply incised into bedrock shown by white arrows. Study area boundary is shown in black and borders Highway 2. ....50

Figure 24: Figure showing location of three important erratics. Two of the erratics are labeled as E1 and are located at an elevation of 1256 m. The other erratic E2, is located in Granger Creek at an elevation of 1243 m. Overflow channel .....	52
Figure 25: Interpreted CIS limit within and to the north of the study area. Ice margin modified from Locke and Smith (2004).....	55
Figure 26: Interpreted northern extent of Glacial Lake Missoula in the study area at an elevation of 1256 m (light blue polygon) and at 1280 m (dark blue line). The relationship between the interpreted CIS limit and Glacial Lake .....	58

## List of Plates

Plate 1: Geologic Map with Cross Section

## 1. Introduction

The Quaternary geology of northwestern Montana is characterized by late Pleistocene glacial deposits from the advance and retreat of the Cordilleran Ice Sheet (CIS), multiple glacial lakes, and local alpine glaciers. The CIS, the smaller of the two great North American ice sheets, was centered over British Columbia and extended south into the northwestern United States and north into southern Alaska and the Yukon Territory at its greatest extent (Clark et al., 1993). In the western US, the CIS advanced along south-trending valleys to form lobes that dammed multiple proglacial lakes (Wait and Thorson, 1983). The Purcell Trench Lobe of the CIS dammed the Clark Fork River at Lake Pend Oreille near the current Montana-Idaho border and formed Glacial Lake Missoula (Figure 1) (Pardee, 1910, 1942; Alden, 1953). Glacial Lake Missoula inundated large portions of the intermontane valleys of western Montana that contained tributaries to the Clark Fork River and emptied many times as catastrophic floods, or megafloods (Waitt, 1980, 1985; Smith et al., 2018). These megafloods drained through Idaho, Washington, Oregon, and into the Pacific Ocean creating the Channeled Scabland of eastern Washington and northern Idaho (Figure 1) (Bretz, 1923, 1969; Baker, 1973; Normark and Reid, 2003; Benito and O'Connor, 2003; Balbas et al., 2017). Shorelines etched into Mount Jumbo east of Missoula show a maximum lake level elevation of 1295 m for Glacial Lake Missoula (O'Connor et al., 2020).

The chronology of Glacial Lake Missoula and its flood history were primarily inferred from downstream flood deposits outside of the Glacial Lake Missoula basin (Waitt, 1980, 1985; Atwater, 1986; Benito and O'Connor, 2003; Clague et al., 2003; Normark and Reid, 2003; Balbas et al., 2017). Recently, the use of optically stimulated luminescence (OSL) dating of quartz grains in transgressive sands below and subaerially exposed sands within glaciolacustrine

deposits has provided limited dates on lake transgression and drainage (Hanson et al., 2012; Smith et al., 2018; Welk, 2019).

Little work on mapping the boundary between the CIS and Glacial Lake Missoula has been done west of the Flathead Valley in northwestern Montana. Drainages west of the Flathead Valley contain deposits that record the chronology and relationship between glacial advance and retreat, glacial lake level history, and glacial lake drainages. These deposits cover significant portions of the northern Little Bitterroot River watershed and have been mapped as Quaternary glacial deposits undifferentiated or Qg (Johns, 1970; Harrison et al., 1986, 1992). This study focuses on problems related to Quaternary geology in the northern Little Bitterroot River area (Figure 1).

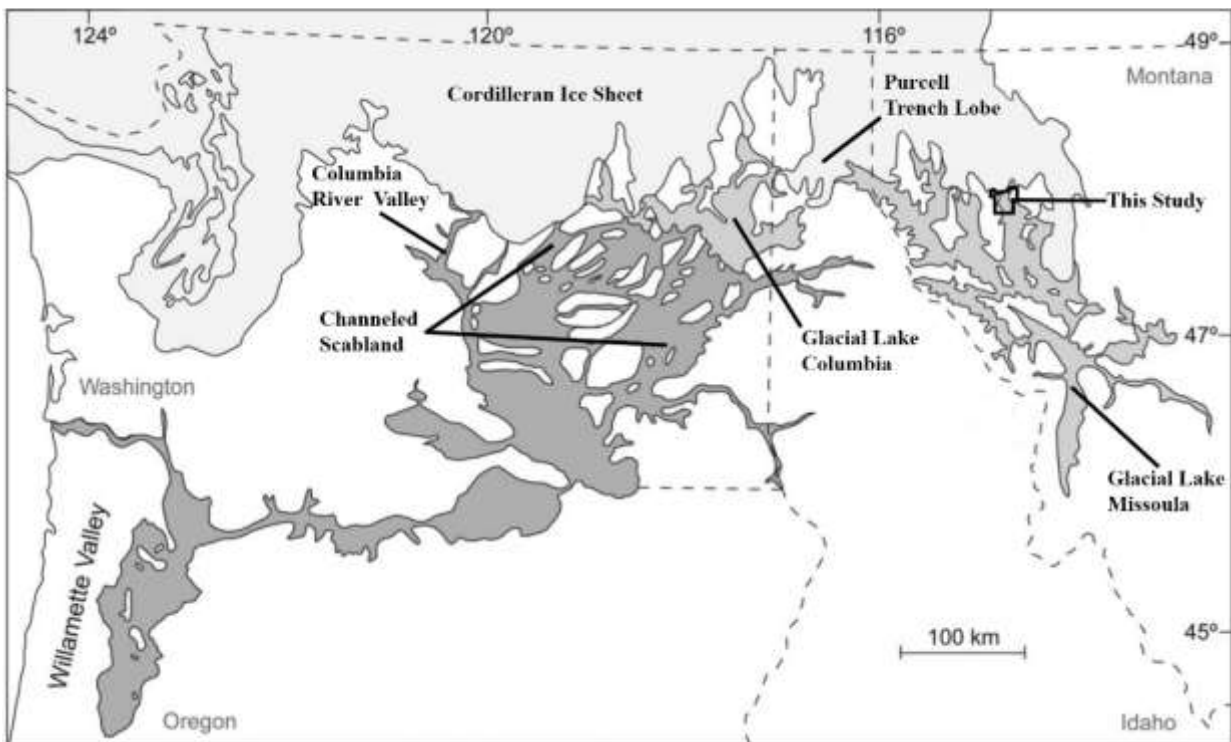


**Figure 1: Map showing the southern extent of the Cordilleran Ice Sheet (CIS), Glacial Lake Missoula, Glacial Lake Columbia, and the Channeled Scabland. When not blocked by a lobe of the CIS, the Columbia River valley was the main route for the Missoula floods. When the Columbia River valley was blocked by a lobe of the CIS, Glacial Lake Columbia was formed, and the Missoula floods were diverted south through the Channeled Scabland (Hanson and Clague, 2016; Balbas et al., 2017). Map modified from Hanson et al. (2012).**



## 1.1. Purpose

The unconsolidated surficial Quaternary deposits that cover the bedrock of northwestern Montana record the last glacial maximum (Alden, 1953), host significant aquifers in the region (LaFave, et al., 2004), and record the lake fluctuation history of Glacial Lake Missoula and other glacial lakes (Smith, 2004, 2006; Hofmann and Hendrix, 2010; Hanson et al., 2012; Smith, 2017). Holocene colluvial, alluvial, lacustrine, and fluvial deposits overlie and are inset into these glacial deposits (Pardee, 1910, 1942; Alden, 1953). It is therefore important to establish a stratigraphic framework for these extensive Quaternary units and differentiate between glacial and nonglacial Quaternary surficial deposits.

The relative timing of different lake stands, and the recessional history of the CIS is poorly constrained outside of the Flathead Valley in northwestern Montana due to lack of detailed mapping and geochronologic data. This project seeks to clarify the stratigraphy of glacial lake and glacial ice deposits near the southern terminus of the CIS, map Quaternary surficial deposits outside of the major lobes of the CIS in northwestern Montana, and determine the chronology of events that occurred during the last glacial maximum. Mapping for this study was in coordination with the Montana Bureau of Mines and Geology (MBMG) STATEMAP-funded geologic mapping. The Quaternary stratigraphic framework and geologic mapping completed in this project will be used by the MBMG in the future for completing the remaining unmapped quadrangles in northwestern Montana.

The study area corresponds with the southern terminus of the CIS and the northern basins previously thought to have been inundated by Glacial Lake Missoula. The Hubbart Reservoir, Murr Peak, McGregor Peak, and Marion 7.5' x 7.5', 1:24,000 USGS quadrangles (Figure 2) lie within an area occupied by both the CIS and Glacial Lake Missoula (Alden, 1953; Johns, 1970). The boundary of the study area was drawn to include the majority of the northwestern Hubbart

Reservoir quadrangle and portions of the three adjacent quadrangles mentioned above that contain significant areas of Quaternary surficial deposits. The study area also occupies portions of both the Kalispell and Polson 30' x 60' quadrangles which have yet to be mapped by the MBMG. Most maps in the area focused on the bedrock (Johns, 1970; Harrison et. al., 1986, 1992) and no detailed mapping at a scale of 1:24,000 has been conducted with a focus on the Quaternary deposits. For this study, the distribution, sedimentologic properties, and stratigraphic relationships between units were mapped over a 250 km<sup>2</sup> area that straddles the border of the Kalispell and Polson 30' x 60' quadrangles (Figure 2).

## **1.2. Physiography and Regional Setting**

The study area is located within the heavily forested Salish Mountains of the Northern Rocky Mountain Province. The Salish Mountains are part of the north- to northwest-trending mountain systems separated by intermontane drainage basins that characterize the topography of northwestern Montana (Johns, 1970). The Salish Mountains are bounded to the west by the Cabinet and Purcell Mountains and to the east by the Whitefish, Swan, and Mission Ranges. Mountain peaks of the Salish Mountains rise to elevations of 1500-2150 m above sea level.

The drainage system in the study area consists of the Little Bitterroot River and its tributaries. The Little Bitterroot River headwaters begin above Little Bitterroot Lake, west of the town of Marion (Figure 2). The Little Bitterroot River flows for about 105 km south-southeastward before it drains into the Flathead River. This drainage basin covers an area of about 1550 km<sup>2</sup> and consists of mountainous and lowland terrain (Meinzer, 1910). Much of the upper 40 km of the Little Bitterroot River is within the study area.

McGregor Lake is situated in a U-shaped valley in the northwest corner of the study area. This valley possesses an unnamed creek that drains into the Little Bitterroot River (Figure 2).

Lake Rogers is located approximately 1 km outside of the northeast corner of the study area in a valley that contains Sickler Creek (Figure 2). Sickler Creek drains northwestward through this valley into the Little Bitterroot River (Figure 2). The Little Bitterroot River then flows through a flat agricultural valley near Pine Prairie (Figure 2). At the south end of the valley, the Little Bitterroot River flows over a 24 m high knickpoint and continues to drain into a deep canyon containing a series of bedrock incised ribbon-shaped lakes called the Hidden Lakes (Figure 2). The canyon is up to 122 m deep and 150 m wide at its greatest width near the Hidden Lakes. This canyon will be referred to as the Hidden Lakes Canyon. After emerging from the Hidden Lakes Canyon, the Little Bitterroot River flows into the Hubbart Reservoir which is dammed by a concrete arch dam. A nameless artificial creek that diverts water from creeks south of the dam flows into the reservoir about 800 m west of the dam (Figure 2). After flowing out of the dam, the Little Bitterroot then flows out of the reservoir into another steep canyon where it flows across two other knickpoints, each roughly 21 m in height before exiting the study area near the Flathead Indian Reservation.

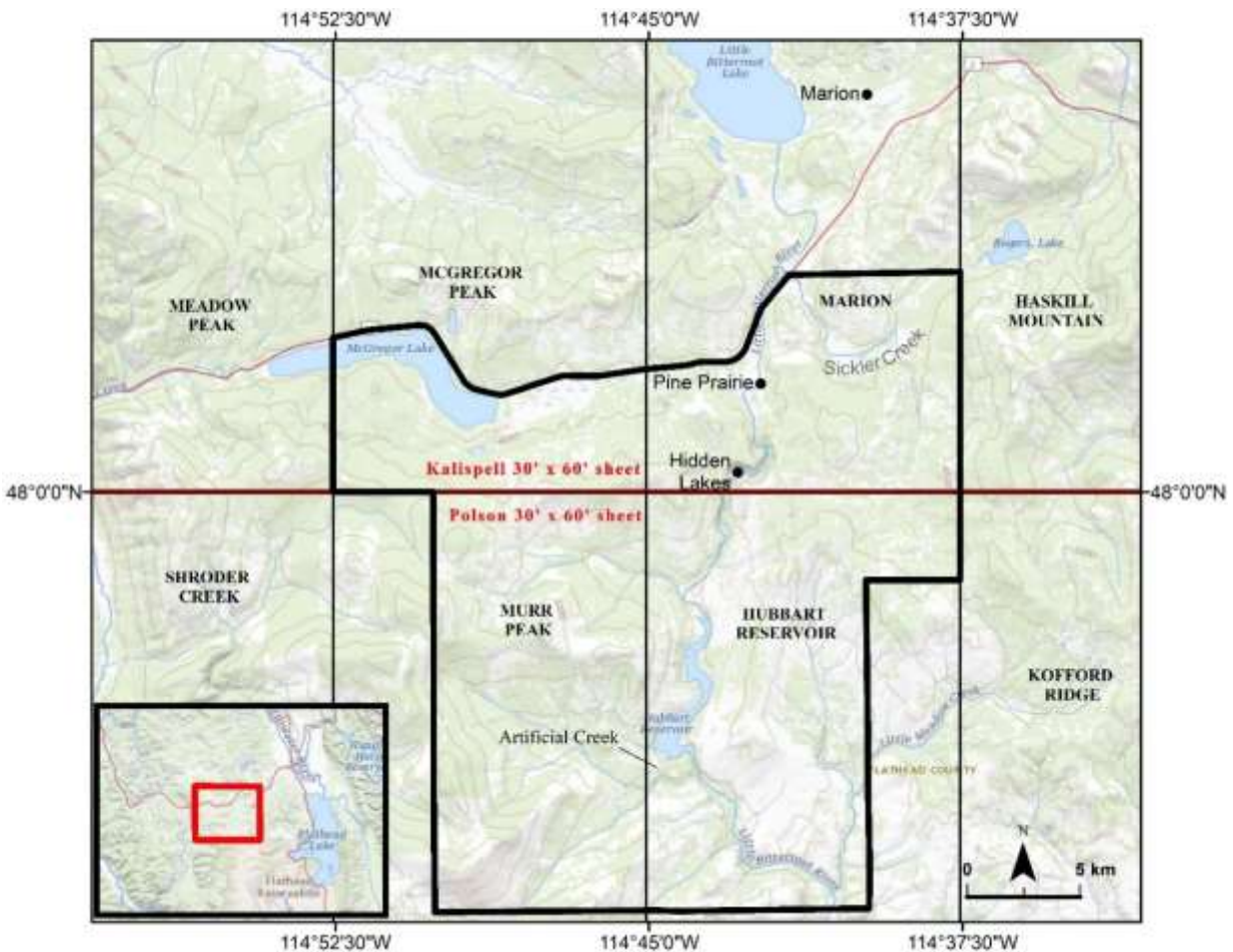


**Figure 2:** Study area is outlined in black and contains portions of the McGregor Lake, Marion, Murr Peak, and Hubbart Reservoir 7.5' quadrangles. McGregor Lake is located in the northwest corner of the study area. Lake Rogers is located approximately 1 km northeast of the study area. Sickler Creek is located in the northeast corner of the study area. The town of Marion is shown north of the study area to the right of Little Bitterroot Lake. The artificial creek is shown southwest of the Hubbart Reservoir.

The climate of the study area is determined by the Rocky Mountains, which extract moisture from Pacific maritime weather systems and act as a barrier for south moving arctic and Canadian storms (Johns, 1970; Martinson and Basko, 1998). Winters are generally cloudy, cool, and wet with the wettest months being November, December, and January. During the summer, days are warm and dry, and nights are cool. The mountains receive most of their precipitation as snow (Martinson and Basko, 1998).

### **1.3. Structural Setting**

The study area lies within the northern Rocky Mountains of Montana, an area that was deformed by multiple compressional and extensional tectonic events. Bedrock in the study area is primarily strata of the Mesoproterozoic Belt Supergroup. The study area is located near the crest of the Purcell Anticlinorium, a broad anticlinal feature formed during Cretaceous-Early Eocene eastward thrusting and folding associated with North American plate tectonic evolution and the formation of the Cordilleran thrust-belt (Harrison and Cressman, 1993; Price and Klavver, 1974; Fuentes et al., 2011). The fold and thrust structures are well expressed in the northern portion of the study area. Also present are multiple Eocene and younger listric high-angle normal faults that crosscut and reactivate thrust faults by back sliding (Harrison and Cressman, 1993; Lange et al., 1994; Constenius, 1996). This normal faulting is thought to be the result of crustal extension that occurred from the gravitational collapse of the Cordilleran fold-thrust belt's thickened crust (Harrison and Cressman, 1993; Lange et al., 1994; Constenius, 1996).

### **1.4. Previous Work**

Previous geologic mapping at a scale of 1:250,000 (Harrison et. al., 1986, 1992) and 1:126,720 (Johns, 1970) focused on bedrock and did not differentiate between Quaternary units. Most of the glacial deposits in these maps were mapped as Quaternary glacial deposits or Qg. Scarberry (in prep) mapped the Hubbart Reservoir quadrangle (Figure 3) but focused on bedrock and mapped all of the surficial deposits as one unit. The Kofford Ridge quadrangle east of the study (Figure 3) area was also mapped (Scarberry et al., in prep) and has glacial deposits mapped in the northern portion of the quadrangle. Lange and Zehner (1992) mapped the Hog Heaven volcanic field and the surrounding area (Figure 3) but focused on the volcanic rocks.

Geologic maps of surficial deposits for Glacier National Park and the Flathead Valley differentiated between subglacial and supraglacial deposits related to the last glacial maximum (Figure 3) (Carrara, 1990; Smith, 2004). Preliminary age control for deglaciation in the Flathead Valley is provided by the Glacier Peak tephra ( $13,180 \pm 120$  cal yr BP; Foit et al., 1993; Hofmann and Hendrix, 2010) found below (Konizeski et al., 1968; Hofmann and Hendrix, 2010) and within post-glacial eolian sand dunes (Smith, 2004) and a radiocarbon date of  $14,150 \pm 50$  cal yr BP from a pine needle recovered in a core containing varves near the southern end of Flathead Lake (Hofmann and Hendrix, 2010). These varves, the oldest being  $14,475 \pm 50$  cal yr BP, are overlain by silt interpreted to be deposited by floods from a proglacial lake on the margins of the Flathead Lobe (Hofmann and Hendrix, 2010). Downstream of the Flathead Lake outlet, geomorphic features and flood deposits inset into Glacial Lake Missoula deposits and a terrace containing the Glacier Peak tephra 2 m above the current Flathead River show that the flood events are younger than Glacial Lake Missoula deposits in the area and older than the Glacier Peak tephra (Hofmann and Hendrix, 2010). It is unclear whether the varves in the core were deposited by either Glacial Lake Missoula or ancestral Flathead Lake (Konizeski et al., 1968; Smith, 2004; Hofmann and Hendrix, 2010). Skudder and Hendrix (2010) mapped Quaternary deposits at the confluence of the Swan and Flathead Valleys (Figure 3).

Alden (1953) mapped the glacial geology of western Montana at a scale of 1:500,000 and discussed some glacial depositional and erosional landforms on the northern margins of the study area and in the valley containing McGregor Lake. Alden (1953) recognized there was ice near the town of Marion, at Lake Rogers, and in the valley containing McGregor Lake but did not give definitive limits for the ice. He attributed ice at Lake Rogers and near the town of Marion as being part of what he termed the Ashley Creek Lobe. The Ashley Creek Lobe was a

southwestward advancing sub-lobe of the glacier that occupied the Flathead Valley.

Alden (1953) does not state a definite ice source for the ice in the valley containing McGregor Lake. He states that ice in the valley containing McGregor Lake could have come from the north or west as part of what he termed the East Kootenai Glacier or from the east as part of the Ashley Creek Lobe. Alden (1953) also recognized that Glacial Lake Missoula extended as far north as Pine Prairie in the study area but does not give an extent or elevation for the lake.

Langer et al. (2011) reconstructed the glacial history of the Libby area (Figure 3) and determined several smaller valley lobes of the CIS impounded north flowing streams to form multiple proglacial lakes that later combined to form Glacial Lake Kootenai. Before the Kootenai River assumed its current drainage direction, Glacial Lake Kootenai drained through the Bull River into the Clark Fork River and through Elmira Idaho (Langer et al., 2011).

Northeast of the study area, (Figure 3) Capps (2004) focused on the glacial history of Ashley Lake, but did not produce a map. West of the study area near the Idaho-Montana border, Welk (2019) mapped Quaternary units in the Clark Fork River valley upstream from where the Purcell Lobe of the CIS impounded Glacial Lake Missoula (Figure 3). In this map, glaciolacustrine deposits overlie catastrophic flood gravels from earlier stands of Glacial Lake Missoula.

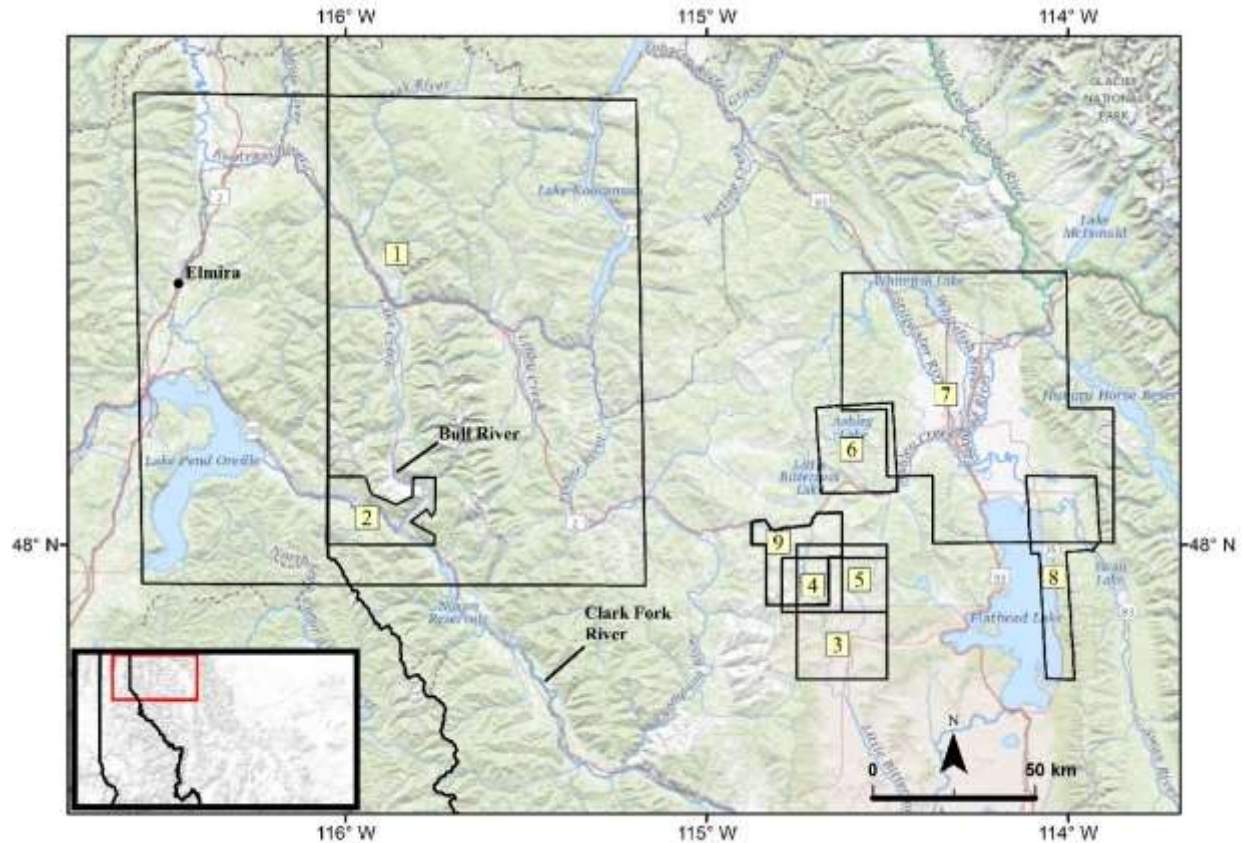


**Figure 3: Map showing location of relevant studies near the study area. 1) Langer et al. (2011); 2) Welk (2019); 3) Lange and Zehner (1992); 4) Scarberry (in prep); 5) Scarberry et al. (in prep); 6) Capps (2004); 7) Smith (2004); 8) Skudder and Hendrix (2010); 9) This study. The Bull River joins the Clark Fork River within the study area of Welk (2019). The Kootenai River drains north in the top left-hand corner of the map.**

Recent use of optical dating has provided some limited dates on the time since burial for Glacial Lake Missoula sediments. Hanson et al. (2012) reported three optical ages on quartz grains from Glacial Lake Missoula sediments at areas termed the Rail line and Ninemile sections (Figure 4). Their age for alluvial gravelly sand underlying the base of the glaciolacustrine sediments at the Ninemile section was  $15.1 \pm 0.6$  ka. Their two ages on sand within glaciolacustrine sediments at the Rail line section were  $14.8 \pm 0.7$  and  $12.6 \pm 0.6$  ka. Welk (2019) reported an optical age of  $16.02 \pm 1.08$  ka from feldspar grains sampled from a bed of silty sand 3.5 m above the base of glaciolacustrine sediments at an area termed the Elk Creek Road section (Figure 4). Smith et al. (2018) collected 17 samples in the Garden Gulch area



(Figure 4) and determined Glacial Lake Missoula deposits in the area were as old as  $20.9 \pm 1.3$  ka.

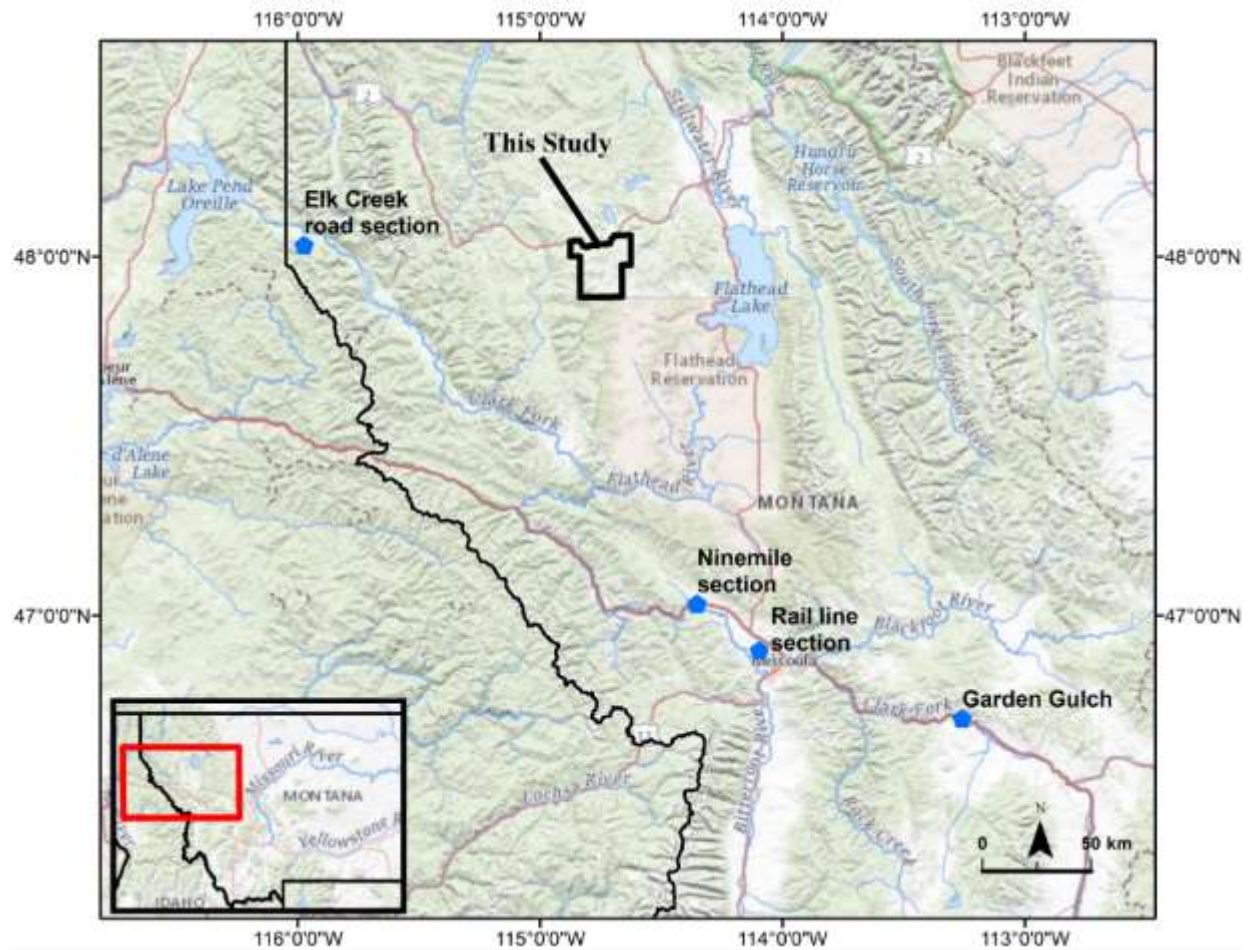


**Figure 4: Map showing the location of recent optical dates for Glacial Lake Missoula sediments in Montana.**

## 2. Methods

The study area contains geologic units that are older and younger than the glacial deposits, which are the primary focus of the current work. The bedrock units (Mesoproterozoic Belt Supergroup metasedimentary and Oligocene volcanic rocks) were differentiated from glacial deposits based on weathering and outcrop characteristics such as bedding orientations, unit thickness, and degree of consolidation. Some of the post-volcanic, pre-glacial and Holocene surficial sedimentary units were difficult to differentiate between each other because of similarities in composition, weathering, and distribution. Some of the post-volcanic sedimentary rocks are surficial and without close inspection resemble other glacial and Holocene deposits within the study area. The Holocene surficial deposits contain large amounts of silt and clasts from the pre-glacial and glacial deposits.

The Hubbart Reservoir, Marion, Murr Peak, and McGregor Peak quadrangles were all mapped at a 1:24,000 scale using standard geologic field mapping techniques, aerial images, and other smaller scale maps (Johns, 1970; Zehner, 1987; Harrison et al., 1986, 1992). Attitudes of tilted bedding and fault planes were measured using the Stereonet Mobile application for smartphones (Allmendinger, 2019). A large portion of the field area was traversed, and contacts walked out where possible, but the majority of the mapping was spent in the lower elevation areas where the glacial deposits are best preserved and exposed. The field mapping was conducted during the Summer of 2020 – Fall of 2020. OSL dating of sandy beds below and within glaciolacustrine sections was used to determine the ages of glaciolacustrine sediments and the relative ages of deglaciation.

The geologic map was created by tracing the unit contacts from a 1:24,000 scale field map onto mylar and scanning the map into ArcMap. The geologic map was then digitized in

ArcMap using the USGS FGDC digital cartographic standards for geologic maps. Topographic profiles were generated in ArcMap and the cross-sectional interpretations were filled in by hand. Final cross sections were scanned and edited in Illustrator then added to the map.

## **2.1. Mapping of Bedrock**

Bedrock contacts were mapped in the field based on lithology, outcrops, and topography. The two bedrock units in the study area include the Belt Supergroup rocks of the Ravalli Group (Johns, 1970; Winston, 1986; Zehner, 1987; Harrison et al., 1992; Ryan and Buckley, 1998) and Tertiary volcanic rocks (Zehner, 1987). Folds in the Belt rocks were mapped from changes in bedding orientations. Faults were mapped from fault plane exposures or the occurrence of multiple adjacent springs.

## **2.2. Mapping and Analysis of Quaternary Geology**

The differentiation of Quaternary deposits was one of the main goals of this project. Surficial Quaternary units were classified based on clast size, sorting, rounding, and morphostratigraphy. The relative ages of the deposits were determined from cross-cutting relationships. Different gravel units were differentiated by degree of weathering, stratigraphic position, elevations, and clast compositions. Pebble counts were conducted in selected areas to determine the clast lithologies of gravels. For each clast count location, 150 clasts were counted in outcrops with good exposure. Clasts in the gravels were categorized as local Belt metasedimentary (Ravalli Group) that make up the bedrock in the area, Belt metasedimentary that are not found within the boundaries of the study area, and other. The results were plotted on a ternary diagram. Other gravel units that were not evaluated in detail because of time constraints were mapped as Quaternary alluvial terraces.

The study area contains large areas of surficial fine-grained sediments, which made determination of glaciolacustrine deposits difficult. The glaciolacustrine deposits in the area were recognized by large percentages of silt and clay, rhythmic bedding, drop stones, dewatering structures, and load structures. A majority of the glaciolacustrine deposits were not well exposed and exposures had to be made by digging trenches with a shovel. Glaciolacustrine deposit distribution, erratics, and topographic features were used to map the northern extent and minimum elevations of Glacial Lake Missoula or other ice-marginal lakes in the area.

The CIS margin within the study area was mapped from the occurrence of glacial ice sheet deposits, glacial erosional features, moraines, lateral ice-marginal channels, and kettle depressions. Ice lobe extents, positions, and elevations were approximated in areas outside of the study area using topographic analysis with 1:24,000 scale topographic maps, aerial imagery, and the report of Alden (1953) in order to better understand the Quaternary geology in the area. Minimum thickness of ice within the study area was estimated from the elevations of ice sheet deposits and the glacial landforms mentioned above.

### **2.3. Analysis of Glaciolacustrine Deposits**

Measured stratigraphic sections of glaciolacustrine deposits were recorded at 3 outcrops. The first section was recorded on the property of a local rancher and is referred to as the Tripp section (Figure 5). The second section was recorded between the Hubbard Reservoir and the Hidden Lakes Canyon and is referred to as the Reservoir section (Figure 5). The third section was recorded near Highway 2 and is referred to as the Pine Prairie section (Figure 5).

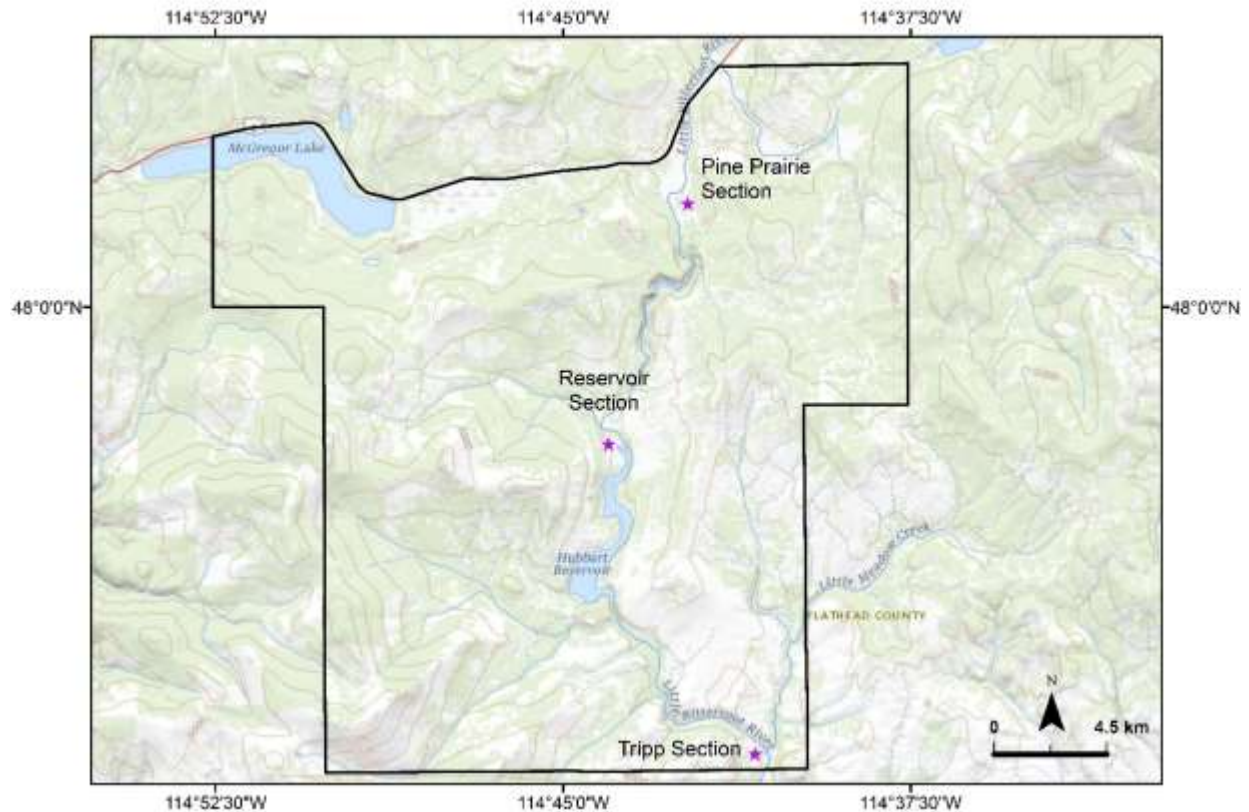


**Figure 5: Map showing locations of measured stratigraphic sections in glaciolacustrine deposits.**

The sections were exposed using shovels and then cleaned with trowels to produce clean, fresh, stair-stepped sections. Individual laminations and beds within the sections were measured with a ruler. The sections were measured in meters and individual laminations and beds were measured in centimeters. Sedimentary structures and other aspects of the sections were recorded in detail.

## **2.4. Geochronology of Glaciolacustrine Deposits**

Optical dating is used to date the time since quartz or feldspar grains were last exposed to light and is commonly used to date Quaternary sedimentary deposits (Hanson et al., 2012; Smith et al., 2018, Welk, 2019). The following discussion of techniques summarizes the logic and procedure of Lian and Roberts (2005). Natural crystals, specifically quartz and feldspar detrital

grains for this study, contain structural defects in their crystal structure that can trap free electrons. Free electrons are emitted by the surrounding sediments due to bombardment by alpha, beta, and gamma radiation. Samples are collected in the field in the dark and are not exposed to light until analysis in a laboratory. The mineral grains of interest are separated in the lab and stimulated with energy to produce the natural luminescence signal. This natural luminescence sample gives an estimate of the amount of radiation the sample has absorbed since burial. A subsample of the same material is used to measure the amount of radiation produced by the surrounding sediment that was absorbed by the mineral grains of interest. Water content of the sediment is also important because pore water can absorb or attenuate radiation. In this study, OSL dating was used to date the time since burial of quartz grains within or at the base of glaciolacustrine sections.

OSL samples were collected from the Reservoir and Tripp sections. These were labeled LT1, LT3, and R for two samples in the Tripp section and one sample at the Reservoir section, respectively. The samples were collected after the sections were excavated, cleaned, and documented. Samples were collected by pounding a 25-30 cm long, 4 cm internal diameter tube into basal sands below glaciolacustrine deposits and sand within glaciolacustrine deposits. LT1 was collected from laminated basal sands below glaciolacustrine clay and silt. LT3 was collected from sand within glaciolacustrine silt and clay. R was collected from climbing ripple cross-laminated sand bounded above by laminated glaciolacustrine sediments and below by alluvial gravels. Samples were packaged and sent to Dr. Sebastian Huot at the Illinois State Geological Survey OSL dating lab for analysis.

### 3. Results

Geologic mapping and detailed descriptions of Quaternary deposits along with important stratigraphic relationships were used to determine the chronology of events that occurred during the last glacial maximum, the southern limit of the CIS, and the northern limit of Glacial Lake Missoula in the study area. Although the main focus was on Quaternary deposits, some major pre-Quaternary geologic structures important to the Polson and Kalispell 1:100,000 scale USGS quadrangles were identified and mapped.

A geologic map at a scale of 1:24,000 was created (Plate 1). This map is the largest scale map for the area that includes bedrock and separate Quaternary surficial units. The map will be used by MBMG in the future for identification and differentiation of Holocene and Pleistocene surficial deposits in northwestern Montana. All the geologic map units mapped in this study are discussed below. Erratics, landforms, and other topographic features related to ice-sheets and glacial lakes in the study area are also discussed.

#### 3.1. Mesoproterozoic Belt Supergroup – Ravalli Undifferentiated (Yra)

The oldest bedrock in the area consists of Mesoproterozoic Belt Supergroup argillites, siltites and quartzites that are part of the Ravalli Group (Johns, 1970; Winston, 1986; Zehner, 1987; Harrison et al., 1992; Ryan and Buckley, 1998). In the study area, the Ravalli Group consists of the Burke, Revett, and St Regis Formations (Winston, 1986). The majority of the Ravalli Group rocks in the study area are of the Revett Formation (Zehner, 1987; Harrison et al., 1992; Ryan and Buckley, 1998; Scarberry, in prep), but some Burke Formation may be present in the McGregor Peak and Marion quadrangles (Harrison et al., 1986). Stratigraphically, the Revett Formation overlies the Burke Formation and underlies the St Regis Formation in the study area. Eastward near Glacier National Park, the Ravalli Group stratigraphy is different and

is not discussed here. Because this study focused on the Quaternary deposits, the bedrock was mapped as Ravalli Group undifferentiated. The terms “Belt rocks” and “Belt” are used here as a general term for Belt Supergroup rocks that cannot be definitively assigned to the Ravalli Group.

The Ravalli Group rocks are best exposed along the steep canyons of the Little Bitterroot River. The argillite is gray to medium bluish gray, laminated to thinly-bedded and contains mud cracks, ripples, and mud rip-up clasts. In some areas the argillite contains conspicuous amounts of magnetite and biotite (Figure 6A) that gives the rock a greenish-gray color. The siltite in the area is white to gray and thinly- to medium-bedded (Figure 6B). The quartzite in the area is not as abundant as the siltite and argillite. It is medium-bedded and commonly cross-bedded (Figure 6C). Magnetite is present throughout the siltite, argillite, and quartzite.



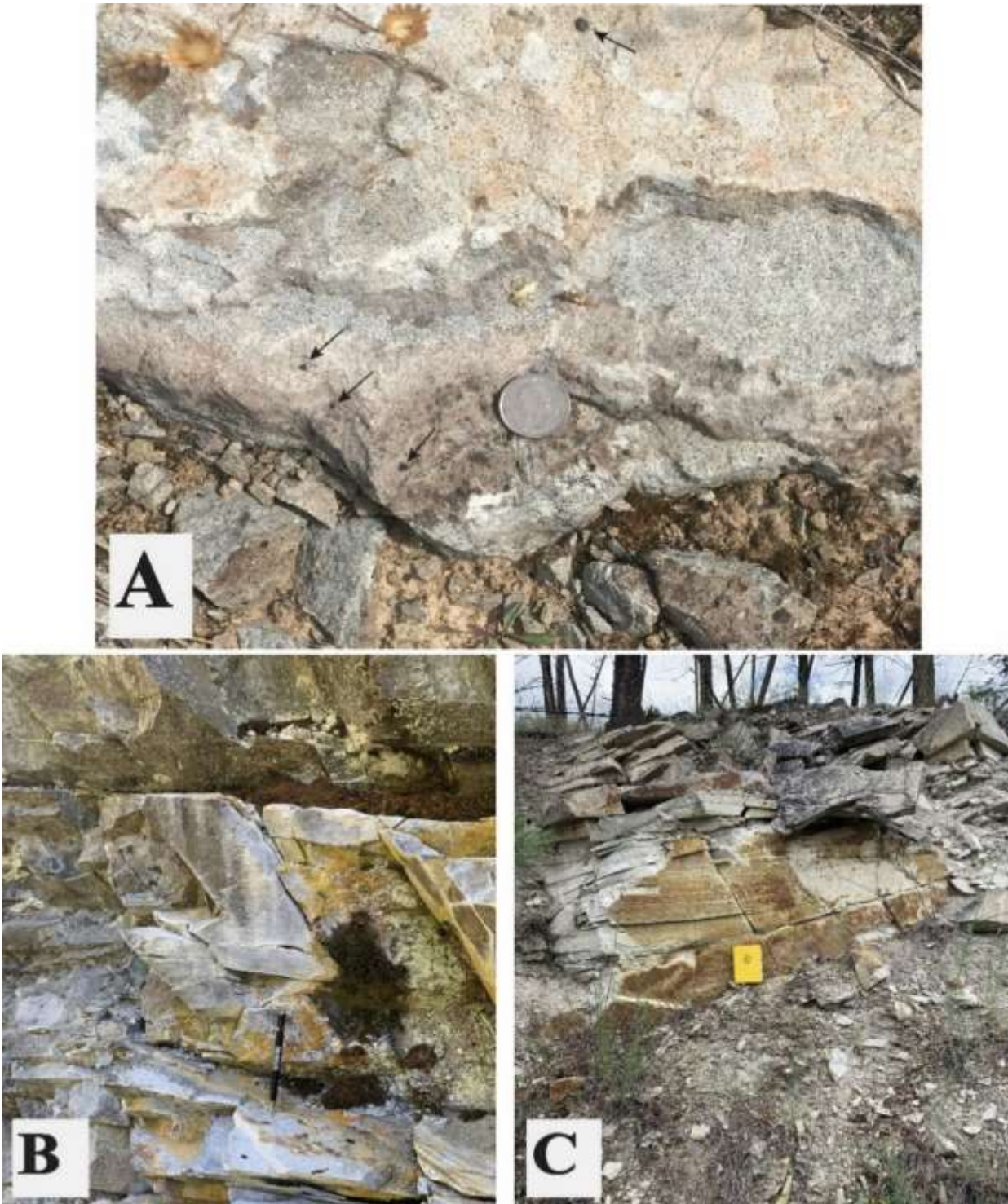


**Figure 6: Figure showing the Ravalli Group argillite, siltite and quartzite rocks. A) Magnetite and biotite rich argillite. Magnetite shown with black arrows and black speckles in rock are biotite. Quarter for scale has a diameter of 1.9 cm. Exposure occurs in SE  $\frac{1}{4}$ , sec. 20, T. 26 N., R. 24 W. B) Exposure of thinly-bedded siltite under medium-bedded siltite that occurs in SW  $\frac{1}{4}$ , sec. 16, T. 26 N., R. 24 W. Pencil for scale is 14 cm long. C) Cross-bedded quartzite. Yellow field book for scale with long dimension of 19 cm. Exposure occurs in SW  $\frac{1}{4}$ , sec. 27, T. 25 N., R. 24 W.**

One of the major problems encountered while mapping was differentiating the weathered Ravalli Group rocks from other surficial deposits. Differentiating this material from glacial till and other glacial deposits was important for constraining the extent of the CIS in the study area.

Weathering of Ravalli Group rocks produces angular poorly sorted argillite, siltite, and quartzite clasts surrounded by silt and sand. The silt and sand are primarily composed of quartz with lesser amounts of magnetite and biotite. The surficial material covers a large area, is less than a meter thick, unconsolidated, not stratified, and occurs adjacent to Ravalli Group outcrops. Outcrops of Ravalli Group in some areas show that the angular clasts in the material are derived directly from the underlying Ravalli Group and therefore have not been transported significant distances. In the northeast corner of sec. 28, T. 25 N., R. 24 W., outcrops show the gradation from bedrock to *in situ* unconsolidated angular fragments of the Ravalli Group (Figure 7B). Siltite derived saprolites (Figure 7c) near the southwest corner of the Hubbard Reservoir (NW ¼, sec. 18, T. 25 N., R. 24 W.) demonstrate the deep weathering and granular disintegration characteristic of the Ravalli Group in the study area.



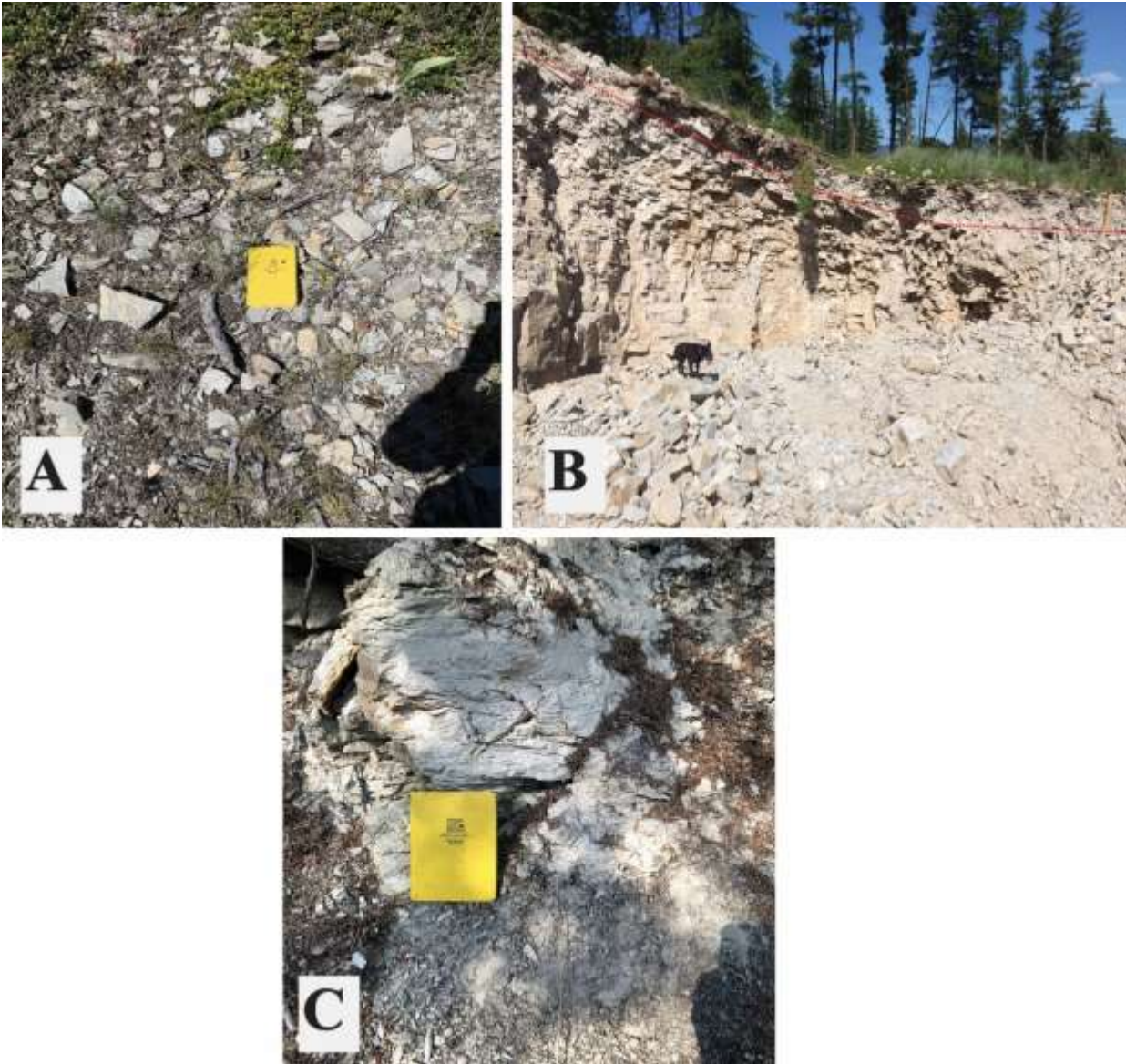


**Figure 7: A) Ravalli Group derived regolith that forms from weathering of the Ravalli Group below the land surface. Notebook for scale is 19 cm tall. Photo was taken in NE  $\frac{1}{4}$ , sec. 29, T. 26 N., R. 24 W. B) Quarry where gradation from Ravalli Group rocks to regolith is exposed. Approximate boundary of Ravalli Group rocks is shown by dashed red line. Dog for scale is approximately 70 cm long. Exposure occurs in NE  $\frac{1}{4}$ , sec. 28, T. 25 N., R. 24 W. C) Saprolite derived from Ravalli Group siltite with 19 cm long notebook for scale. Grainy surface is the result of granular disintegration. Notice the angular pebble sized siltite clasts surrounded by silt derived from the saprolite exposure. Saprolite occurs in NW  $\frac{1}{4}$ , sec. 18, T. 25 N., R. 24 W.**

The unconsolidated surficial material covering large areas within the study area was determined to be *in situ*-weathered bedrock, regolith, and saprolite. This material was therefore mapped as Ravalli Group undifferentiated. It is also likely that some of the finer grained material

is eolian and/or glaciolacustrine silt. Weathering of the Ravalli Group rocks was interpreted to be the result of periglacial processes and bioturbation. Till within the study area is differentiated from the *in situ*-weathered Ravalli Group by the presence of large subangular to subrounded boulders larger than 1 m. The till also forms landforms and occurs next to other landforms typical of glaciated areas.

Colluvium was differentiated from weathered Ravalli Group in many places within the study area. Colluvial deposits are several meters thick, crudely stratified parallel to slope, and do not contain *in situ* Ravalli Group outcrops with measurable bedding attitudes.

### **3.2. Geologic Structures**

The major structures found in the area include an east-directed thrust fault, a syncline-anticline pair related to the thrust fault, and a high angle fault interpreted to be a normal fault. The thrust fault plane was found in a quarry on private property in Sickler Creek (NE ¼, sec. 10, T. 26 N., R. 24 W.). This thrust fault is overlain by undisturbed stratified colluvium. The normal fault in the southeast corner of the study area was mapped from the occurrence of three adjacent springs. This normal fault is not well exposed, and it is difficult to observe offset.

### **3.3. Tertiary Deposits**

Several Tertiary deposits are present within the study area. Most of these deposits are Oligocene volcanic rocks related to the Hog Heaven volcanic field (Zehner, 1987). These units are the northwest extent of the Hog Heaven volcanic field and have been described in detail by Zehner (1987) and Lange and Zehner (1992).

#### **3.3.1. Ash Flow Tuff (Ta)**

Tan to yellowish-tan and poorly welded Oligocene ash-flow tuffs (Zehner, 1987) probably of rhyodacitic composition are poorly exposed directly south of the Hubbart Reservoir (Figure 8A)

(secs. 18, 19, 20, 21, 22, T. 25 N., R. 24 W.) and lie unconformably on Ravalli Group rocks.

Phenocrysts within the ash-flow tuff consist of quartz, plagioclase, sanidine, and biotite. Lithic clasts are commonly Belt rock fragments up to 10 cm long, rare granitic clasts, and other local volcanic rocks (Figure 8B). The contact between the ash-flow tuff and Ravalli Group rocks is not exposed which makes determination of thickness difficult. In the artificial creek that drains into the southern portion of the Hubbart Reservoir (NW ¼, sec. 18, T. 25 N., R. 24 W.), the ash-flow tuff is at least 15 m thick and is overlain by younger gravels.

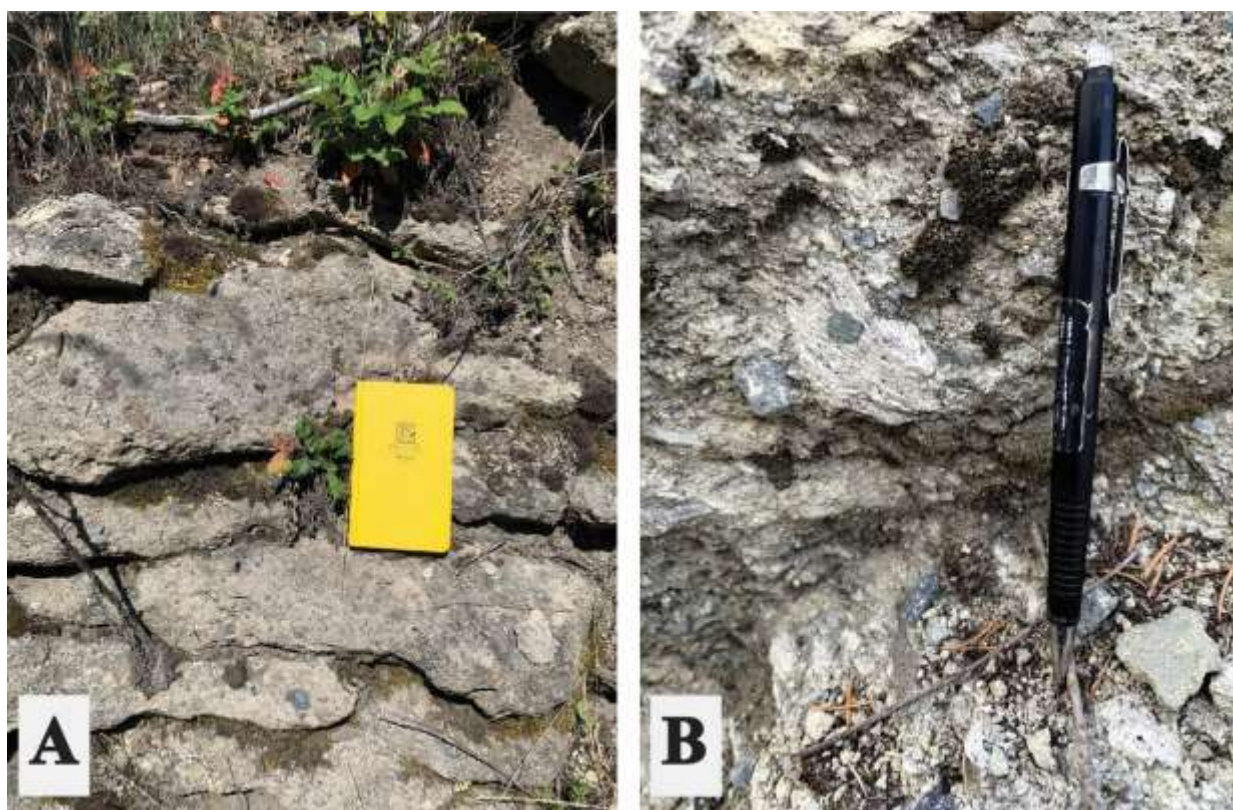


**Figure 8: A) Exposure of ash-flow tuff that occurs in NE ¼, sec. 20, T. 25 N., R. 24 W. Notebook is 19 cm long. B) Up close photo of the ash-flow tuff showing Belt and other volcanic rock clasts. Exposure occurs in NW ¼, sec. 20, T. 25 N., R. 24 W. Pencil for scale is 14 cm long.**

### **3.3.2. Tuffaceous Rock (Ttu)**

In the very southeast corner of the study area (SE ¼, sec. 27, T. 25 N., R. 24 W.), an orange-yellow, poorly welded, lithic rich, and crystal poor tuff is exposed. Lithic clasts are typically Belt Rock fragments. The contact between the Ravalli Group rocks and the tuff is not exposed which makes determination of thickness difficult. In the southeast corner of the study area, the tuff is at least 195 m thick assuming no faulting.

### **3.3.3. Weathered Volcanic Rock (Tts)**

An outcrop of gray weathered volcanic rock occurs in the northwest corner of sec. 27, T.25 N., R. 24 W. This outcrop of weathered volcanic rock is relatively small and shows a composition similar to the other volcanic rocks.

### **3.3.4. Diabase Intrusions (Ti)**

Black hypabyssal diabase intrusions with olivine and pyroxene phenocrysts occur in the northwest corner of sec. 13, T. 25 N., R. 25 W.

### **3.3.5. Tertiary Sediments (Ts)**

Buff to light-brown, medium-bedded to cross-bedded, weakly consolidated gravelly sandstone with interbedded sand and silt overlie the ash-flow tuff and Ravalli Group rocks in NE ¼, sec. 21, NW ¼, sec. 22, SE ¼, sec. 16, and SW ¼, sec. 15, T. 25 N., R. 24 W. (Figure 9A). The sand and silt consist of quartz, feldspar, biotite, magnetite, and Belt and ash-flow tuff lithic grains. The gravel is angular, poorly sorted, and consists of ash-flow tuff and Belt rock fragments. Silt beds show ball and pillow structures (Figure 9B). These sediments are derived mainly from erosion of the ash-flow tuff. Thickness is no more than 5 m.





**Figure 9:** A) Tertiary sediment exposure found in a pit. Tape measure is 2.4 m. Exposure occurs in NE  $\frac{1}{4}$ , sec. 21, T. 25 N., R. 24 W. B) Ball and pillow structures in a silt bed. Pencil length is 14 cm. Photo location is the same as 10A.

### 3.4. Tertiary or Quaternary Gravels (QTgr)

A red-orange to yellow, oxidized, unstratified, poorly consolidated conglomerate is present in the Hubbard Reservoir quadrangle (Figure 10A). The conglomerate consists of poorly sorted, subangular to rounded pebbles, cobbles, and boulders in a silty sand matrix. Pebble counts in an exposure south of the reservoir (NW  $\frac{1}{4}$ , sec. 20, T. 25 N., R. 24 W.) show that clasts within the conglomerate are nearly all locally derived argillite, siltite, and quartzite (Figure 11). The most abundant and distinct clast type is a white quartzite with purple laminations and cross-laminations, a common lithology of the Ravalli Group (Figure 10B). The gravels underlie terraces near Tamarack Creek and overlie the ash-flow tuff unit south of the Hubbard Reservoir. This unit is approximately 7 m thick at its maximum. The unit is best exposed where the artificial

creek flows into the Hubbard Reservoir (NW  $\frac{1}{4}$ , sec. 18, T. 25 N., R. 24 W.) (Figure 10C). This unit is older than the glacial outwash deposits and younger than the Tertiary volcanic deposits. The exact age of the deposit is unknown, but the weathering and the composition of the clasts distinguish it from other gravels in the study area.





**Figure 10: A) Exposure of QTgr in NW  $\frac{1}{4}$ , sec. 20, T. 25 N., R. 24 W. Yellow field book for scale is 19 cm long. B) Purple laminated quartzite clast that is common in QTgr. Glove for scale is approximately 19 cm long. Clast is from the exposure shown in 10A. C) Exposure in the artificial creek that shows the ash-flow tuff (gray) overlain by QTgr (orange). The creek flows through this area in NW  $\frac{1}{4}$ , sec. 18, T. 25 N., R. 24 W. Exposure is approximately 15 m thick.**

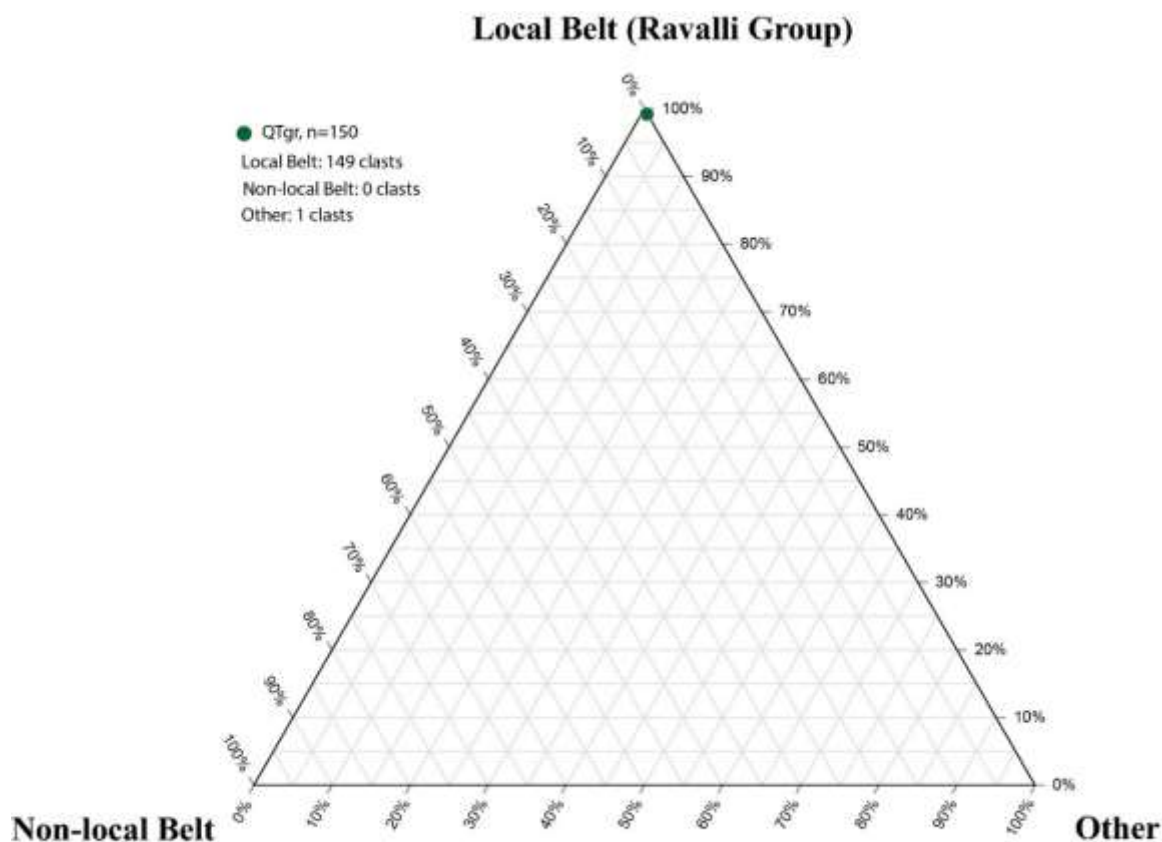


**Figure 11: Ternary diagram showing clast compositions for QTgr in an exposure south of the Hubbard Reservoir. Green circle shows that the clasts in QTgr are nearly all locally derived Ravalli Group clasts.**

### **3.5. Quaternary Deposits and Geology**

#### **3.5.1. Glacial Till (Qgt)**

Till deposits are exposed in the valley containing McGregor Lake. The deposits consist of locally derived, poorly sorted, angular to subrounded pebbles, cobbles, and boulders supported in a white-brownish loamy matrix (Figure 12A). The till forms hummocky topography and moraines in the valley east of McGregor Lake. Thickness of the till ranges from less than a meter for thin mantles on the valley sides to a maximum of 15 m for some of the moraines.

Glaciofluvial channels cut through the deposits in multiple places. The till is best characterized

by the presence of boulders larger than 1 m (Figure 12B). The till deposits end where the creek draining the valley containing McGregor Lake flows into the flat valley of Pine Prairie (NW  $\frac{1}{4}$  sec. 8, T. 26 N., R. 24 W.).



**Figure 12: A) Exposure of till along the moraine that borders the eastern edge of McGregor Lake (SW  $\frac{1}{4}$  sec. 8, T. 26 N., R. 25 W.). Notebook for scale is 19 cm tall. B) Large boulder found adjacent to moraine that occurs in NW  $\frac{1}{4}$  sec. 14, T. 26 N., R. 25 W. Notebook for scale is the same as in 12A.**

### **3.5.2. Outwash and Glaciofluvial Deposits (Qgo)**

Glacial outwash deposits underlie plains and terraces in the valley east of McGregor Lake, in Sickler Creek, and in Pine Prairie (Figure 13A). Other gravels thought to be glaciofluvial, underlie glaciolacustrine deposits in the Reservoir and Tripp sections (Figure 13B). The outwash is inset into glacial till in the valley adjacent to McGregor Lake and lies unconformably on bedrock elsewhere. The gravel deposits that underlie the glaciolacustrine



deposits were deposited on bedrock. The outwash and glaciofluvial deposits contain moderately sorted, subangular to rounded pebble and cobble sized clasts in a sandy silty matrix. The deposits are crudely bedded in some exposures, and some clasts are imbricated. Rare boulders indicate ice rafting (Figure 13C).

Pebble counts in gravels at the base of the Tripp section (Qgo1) and in a terrace near Pine Prairie (Qgo2) show that the clasts consist of locally derived Ravalli Group rocks and other Belt rock clasts that are not found in the study area (Figure 14). The nonlocal Belt rock clasts are distinct and consist of a laminated greenish-gray (5 G 6/1) argillite, laminated to cross-laminated pale-purple (5 P 6/2) argillite, moderate-reddish-orange (10 R 6/6) quartzite, and an oxidized moderate-reddish-brown (10 R 4/6) fine grained metasedimentary rock. The presence of these clasts distinguishes the deposits from other gravels. The pebble counts also support correlation of the outwash terraces to the gravels underlying the glaciolacustrine sediments. Maximum thickness of the unit is 10 m, with the best exposures being near the Tripp section and a quarry in Pine Prairie.



**Figure 13: A)** View of quarry in a Pine Prairie outwash terrace (SE  $\frac{1}{4}$  sec. 8, T. 26 N., R. 25 W.). Tree for scale is approximately 4 m tall. **B)** Exposure of gravels near the Tripp section (SW  $\frac{1}{4}$ , sec. 27, T. 25 N., R.

24 W.). Exposure is approximately 5 m thick. C) Large boulder found in the Pine Prairie outwash terrace indicating ice rafting. Boulder found in the quarry shown in 13A. Map board for scale is 32 cm long.

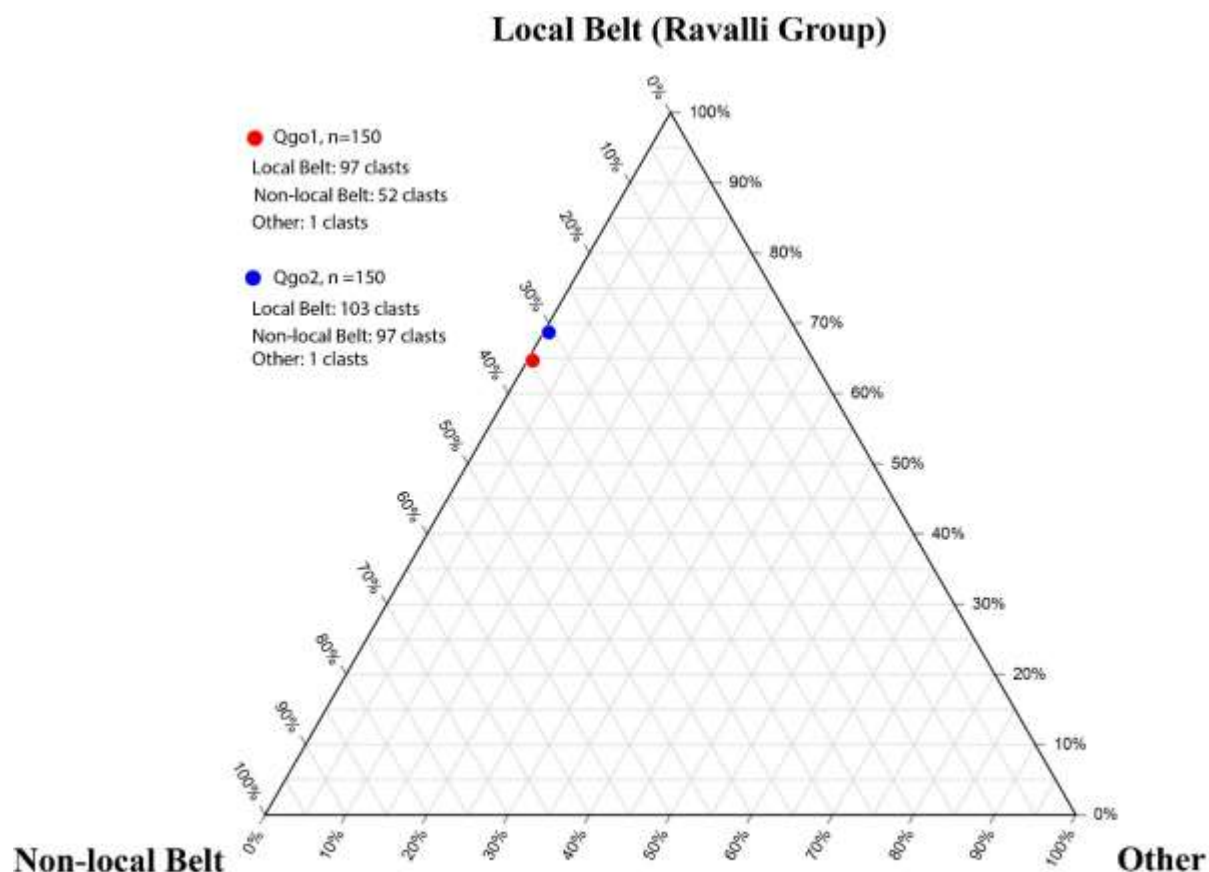


**Figure 14: Ternary diagram showing clast compositions for the Tripp section (Qgo1) and Pine Prairie terrace (Qgo2). Blue and red circles show that the clasts in Qgo are nearly all locally derived Ravalli Group and non-local Belt.**

### 3.5.3. Kame Terrace Deposits (Qkt)

Margins of the valley containing McGregor Lake contain ice-marginal alluvial terraces, or kame terraces. These terraces consist of subangular to rounded, moderately sorted pebbles and cobbles in a brown sandy silty matrix. These deposits are inset into glacial till in some areas. The

kame terraces are differentiated from the till by flat surfaces, better sorting, and lack of outsized boulders.

### **3.5.4. Glaciolacustrine Deposits (Qgl)**

The glaciolacustrine sediments within the study area consist of stratified clay, silt, very fine sand, and fine sand showing rhythmic bedding, soft sediment deformation, dewatering structures, and evidence of ice-rafting. In some places the deposits are underlain by glacial outwash and glaciofluvial deposits. Glaciolacustrine sediments were recorded in detail in measured stratigraphic sections at the Pine Prairie, Reservoir, and Tripp sections. These sections are discussed below.

#### **3.5.4.1. Pine Prairie Section**

The Pine Prairie section is 3.3 m thick and was excavated along a north-south oriented road cut (Figures 15 and 16A). The top of the section is located at an elevation of 1192 m, with the upper meter of the section being too bioturbated and weathered to describe. The base of the outcrop was not excavated or exposed but, it is assumed that the glaciolacustrine sediments lie on glacial outwash deposits immediately west of the section. The Pine Prairie section consists of a silt-clay facies and a silt facies. Extensive soft sediment deformation is present in the section.

##### **3.5.4.1.1. Silt-Clay Facies**

The Pine Prairie section consists almost entirely of rhythmically bedded couplets consisting of a basal silt overlain by clay (Figures 15 and 16A). The couplets range in thickness from 2-7 cm. The silt portion of the couplets is massive to laminated with thin clay laminae and is generally thicker than the clay portion (Figure 16B). The basal contact of the silt is sharp while the silt-to-clay contacts are gradational (Figure 16B). The clay beds in the couplets range in

thickness from 4 to 0.5 cm whereas the silt beds in the couplets range from 12 to 1 cm, showing that the clay beds are more consistent in thickness than the silt beds.

One portion of the section is severely disturbed and contains dish structures, flame structures, clastic dikes, small scale faults, and two overturned folds with axial planes oriented to the southwest (Figure 16C and 16D). Flat bedded clay and silt couplets directly overlie the disturbed bedding (Figure 16C and 16D). Characteristics of the clastic dikes vary. Many of the dikes are less than 1 cm thick, downward tapering, and are infilled mostly with massive silt. These clastic dikes are tilted to the southwest and offset and disrupt the couplets (Figure 16D). Other 1-2 cm thick clastic dikes are channel-shaped with straight to undulating boundaries, are infilled with massive silt, contain sinuous laminae parallel to the edges, contain floating clay clasts, and offset the couplets. The upper flat-bedded silt and clay couplets are infiltrated by dendritic modern-day rootlets and have two clastic dikes extending into the section from the convoluted section below. The couplets that appear lower in the section are not convoluted but contain small-scale normal and reverse faults (Figure 15).

#### **3.5.4.1.2. Silt Facies**

The Pine Prairie section contains three distinct massive to laminated silt beds that range in thickness from 5-12 cm (Figures 15 and 16E). Each silt bed is separated by the silt-clay facies. The lowermost silt bed has a planar erosive and loaded lower contact with the rhythmites below. The upper contact with the overlying clay is gradational and faulted. The second lowermost silt bed contains an erosive undulatory contact with rhythmites below and a gradational contact with the clay above (Figure 16E). The top silt bed contains an erosive lower faulted contact with the rhythmites below (Figure 16E). The upper contact separates the silt bed from the convoluted sediments above and is severely disturbed and irregular (Figure 16E). Flame structures from the



underlying clay are present in the lowermost silt bed. Clay rip-ups and lenses are found in the top and lower silt beds.

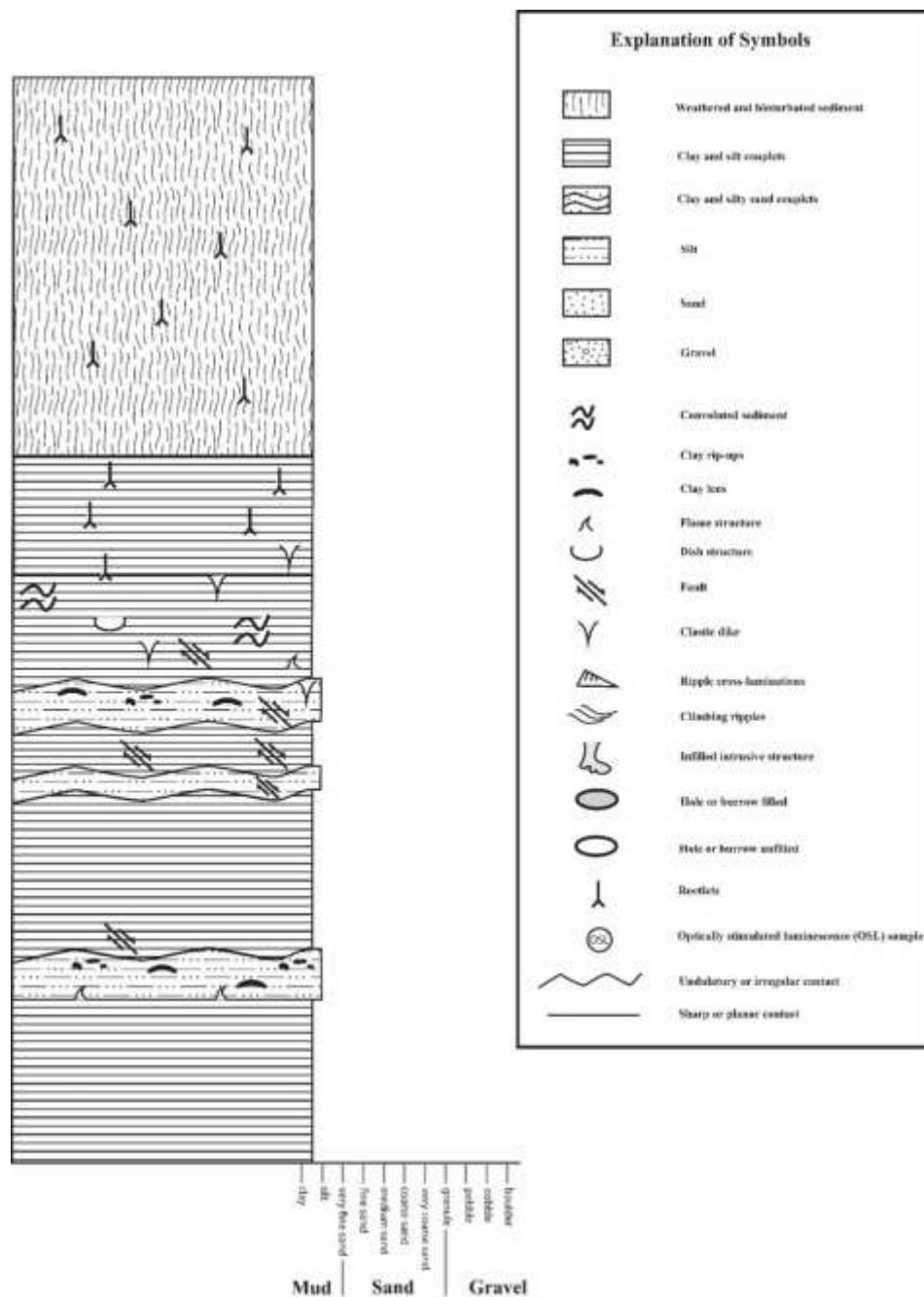
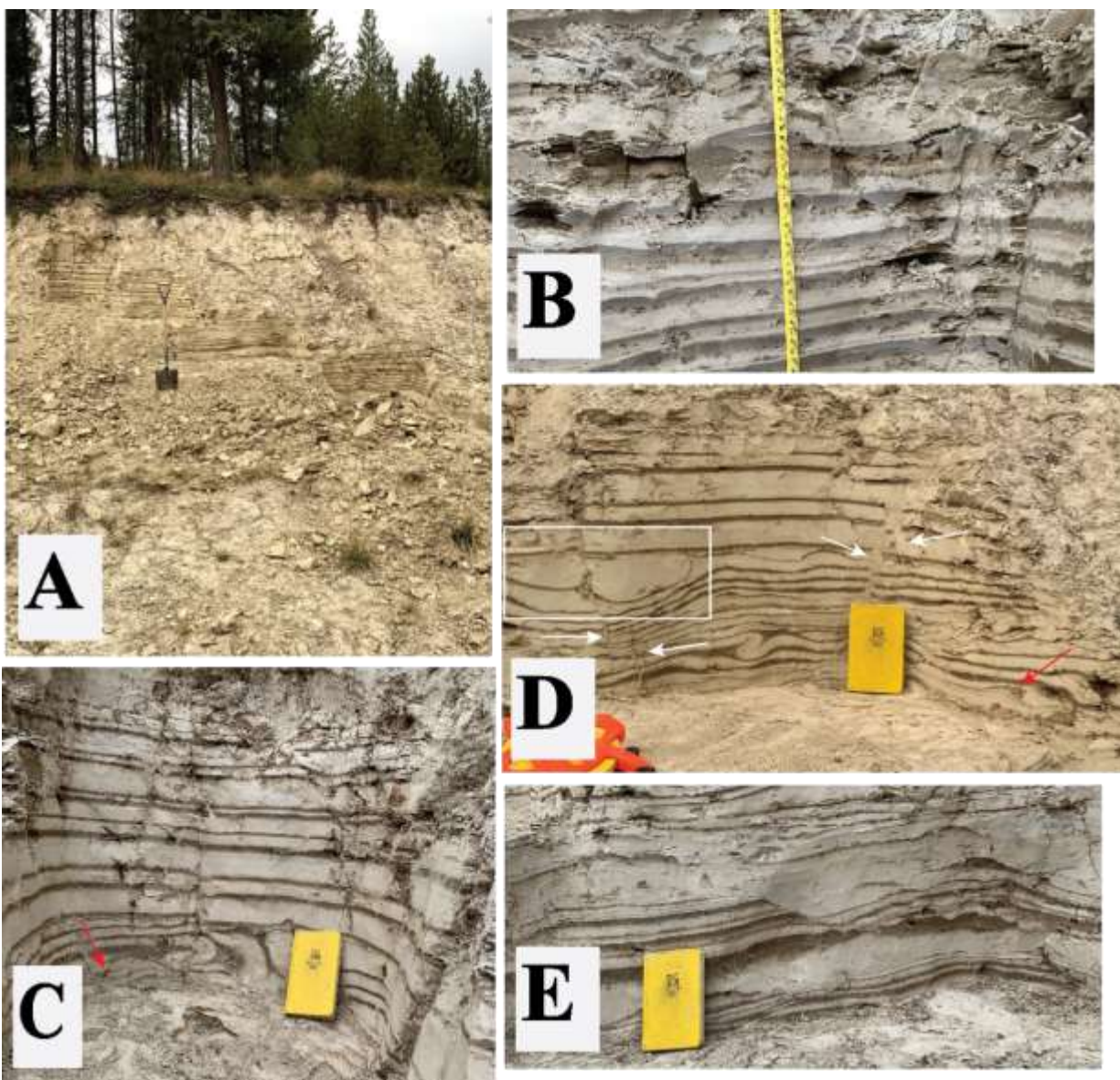


Figure 15: Measured stratigraphic column of the Pine Prairie section with key for all measured sections.



**Figure 16:** A) Excavated exposure of the Pine Prairie section (SW  $\frac{1}{4}$  sec. 9, T. 26 N., R. 25 W.). Shovel is approximately 1 m long. B) Rhythmic silt and clay couplets with sharp contacts between couplets. Contacts between the silt and clay are gradational. Tape measure shows 17 cm. C) Convolute rhythmites overlain by undisturbed rhythmites. Red arrow points to flame structure. Fold to the left of the notebook. Notebook for scale is 19 cm long. D) Convolute rhythmites overlain by undeformed rhythmites. White arrows point to clastic dikes. Clastic dikes to the left are downward tapering, tilted to the southwest, and offset the rhythmites. Clastic dikes to the right are thicker, channel-shaped, tilted in opposing directions, and offset the rhythmites. Red arrow points to flame structure. White box outlines dish structures. Fold occurs to the left of notebook. E) Upper two silt beds in the section. Lower silt bed has an erosive lower contact and gradational upper contact. Upper silt bed has an erosive and faulted lower contact and a deformed upper contact.

### **3.5.4.2. Reservoir Section**

The Reservoir section is 1.2 m thick with the top of the section located at an elevation of 1068 m. The section overlies glaciofluvial gravels of Qgo at the base (Figures 17 and 18A). The upper 40 cm of the section was too weathered and bioturbated to analyze. Two lithofacies are present in the section: a gravel-sand facies and a silty sand-clay facies.

#### **3.5.4.2.1. Gravel-Sand Facies**

The gravel-sand facies comprises the basal section of the Reservoir section and consists of glaciofluvial gravels mapped as Qgo overlain by massive, well sorted very fine sand (Figures 17 and 18A). The contact between the gravel and sand appears to be conformable. The massive sand at the top of this facies is differentiated from the overlying silty sand-clay facies by lack of rhythmic bedding and a distinct color change.

#### **3.5.4.2.2. Silty Sand-Clay Facies**

The Reservoir section is composed mostly of rhythmically bedded couplets consisting of a basal fine sand or silty very fine sand bed overlain by a thin ( $< 1$  cm) clay lamina or drape. The lowermost couplet is 20 cm thick and contains horizontally laminated, ripple, and climbing ripple cross-laminated fine sand. The transition from ripple laminae in-phase to ripple laminae in-drift can be observed in this couplet (Figure 18B). Ripples turn into horizontal laminations near the top of the bed that are then overlain by a clay lamina. The ripples show a northeast flow direction (Figure 18B). The second lowermost couplet is 18 cm thick and consists of laminated silty very fine sand with approximately 3 cm of ripple cross-laminations having an erosive lower boundary and a southwest flow direction (Figure 18C). These ripples are overlain by horizontally laminated silty very fine sand and a clay lamina. The remaining overlying couplets are thinner and consist of massive to laminated silty very fine sand with a thin overlying clay lamina. The

silty sand-to-clay contacts in the couplets are gradational and undulatory and the basal contact of the silty sand that separates the couplets is sharp and undulatory. Modern day rootlets disturb the entire section but are mostly concentrated in the clay laminae. The OSL sample R was taken from the lowermost rippled sand for optical dating.

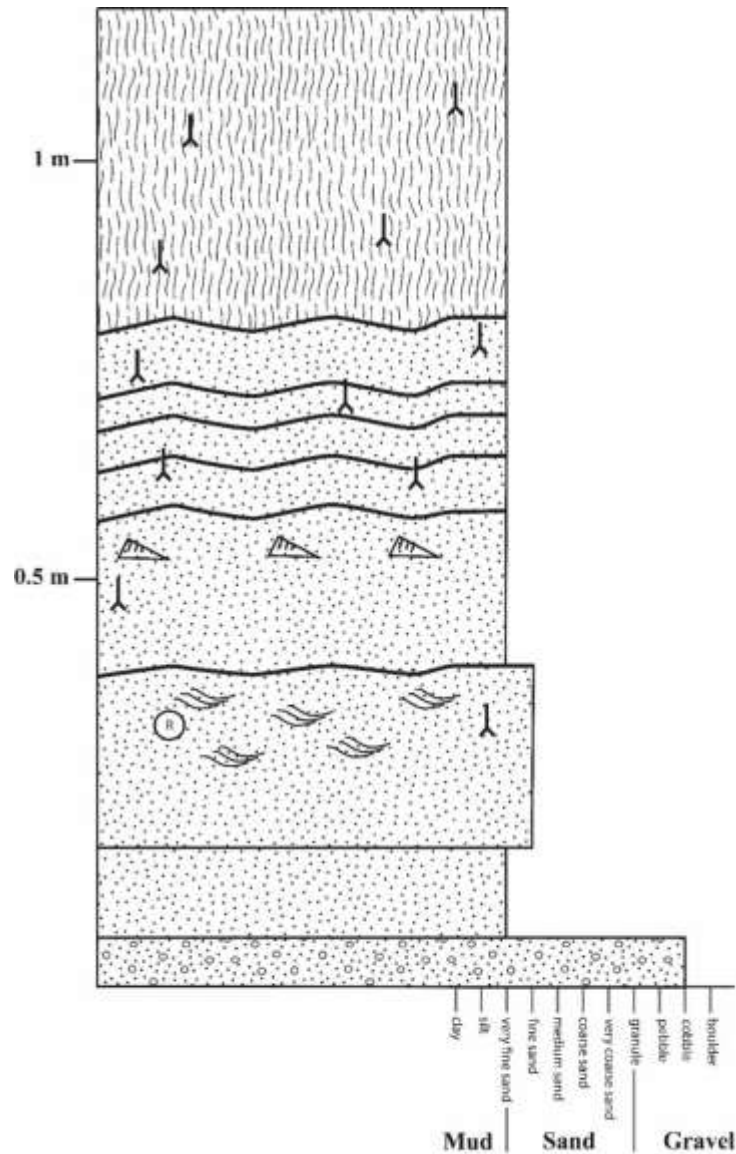


**Figure 17: Stratigraphic column of the Reservoir section. See figure 15 for key. OSL sample R was taken from the climbing ripple cross-laminated fine sand in the lowermost couplet.**



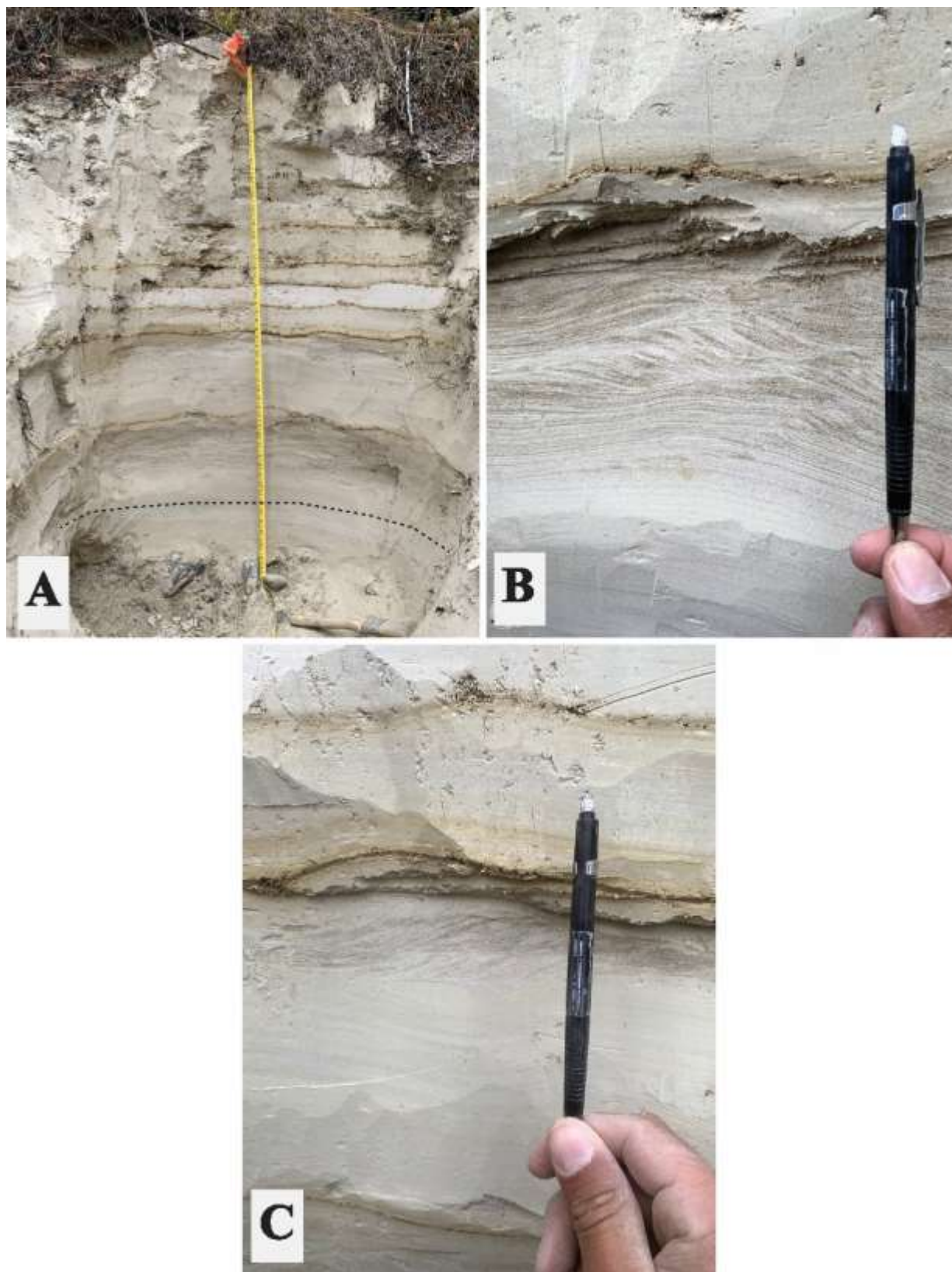


**Figure 18: A) Exposure of the Reservoir section (SE ¼ sec. 31, T. 26 N., R. 24 W.). Dashed black line shows the contact between the gravel-sand and silty sand-clay facies. B) Transition from in-phase to in-drift ripple laminae in the lowermost silty sand-clay couplet. Flow direction is from left to right (to the northeast). Pen for scale is 14 cm long. C) Second lowermost couplet with ripple cross-laminations. Flow is from right to left (to the southwest).**

### **3.5.4.3. Tripp Section**

The Tripp section is 2 m thick with the top of the section located at an elevation of 989 m. The section is underlain by glaciofluvial gravels of Qgo (Figure 19). The uppermost meter of the section was too weathered and bioturbated to analyze. The section consists of three lithofacies: a gravel facies, a sand facies, and a sand-silt facies.

A large sedimentary structure intrudes and disturbs the majority of the section (Figures 19 and 20A). It is assumed the structure extends to the upper weathered and bioturbated portion of the section. This structure has vertical sides near the top of the section and is lobate near the bottom of the section. The sand-silt and sand facies are folded near the top of the section, with the fold being crosscut by the intrusive structure (Figure 20C). Two large holes crosscut the large intrusive structure with the upper hole being unfilled and the lower hole being filled with stratified sand and silt (Figures 19 and 20A). Analysis of the sediments in the mid and upper portion of the section was difficult due to the large intrusive structure. Limited exposure of the sediments on the sides of the section were used to analyze the stratigraphy.

#### **3.5.4.3.1. Gravel Facies**

The gravel-sand facies comprises the basal portion of the Tripp section and consists of glaciofluvial gravels of Qgo. The gravel occurs at the base of the section and is overlain by the sand facies (Figures 19 and 20A).

#### **3.5.4.3.2. Sand Facies**

The sand facies consists of two sand beds above the gravels and a sand bed above the sand-silt facies near the top of the section. The contact between the lowermost sand bed and gravel is marked by a change from a cobble conglomerate to medium sand. The sand is moderately sorted and laminated. A darker moderately sorted coarse sand bed overlies the medium sand bed across a sharp planar contact (Figure 20A). This bed contains laminations and grades into fine sand with ripple cross-laminations at the top of the bed. The sand appears to fine up into the sand-silt facies above. A separate moderately sorted laminated medium sand bed occurs over the sand-silt facies across a planar contact near the top of the section. The OSL sample LT1 was taken from the first sandy bed for optical dating. The sample LT3 was taken from the uppermost sand (Figure 19).

#### **3.5.4.3.3. Sand-Silt Facies**

The sand-silt facies overlies the sand facies near the bottom of the section and underlies another bed of the sand facies near the top of the section. This facies consists of fine sand, very fine sand, silt, and clayey silt. Wavy and horizontal silt laminae are present throughout the facies (Figure 20B). This facies fines upward from very fine sand to rhythmically laminated clayey silt. A wedge-shaped clastic dike that is infilled with laminated sand is present in the lower portion of this facies (Figure 20B).

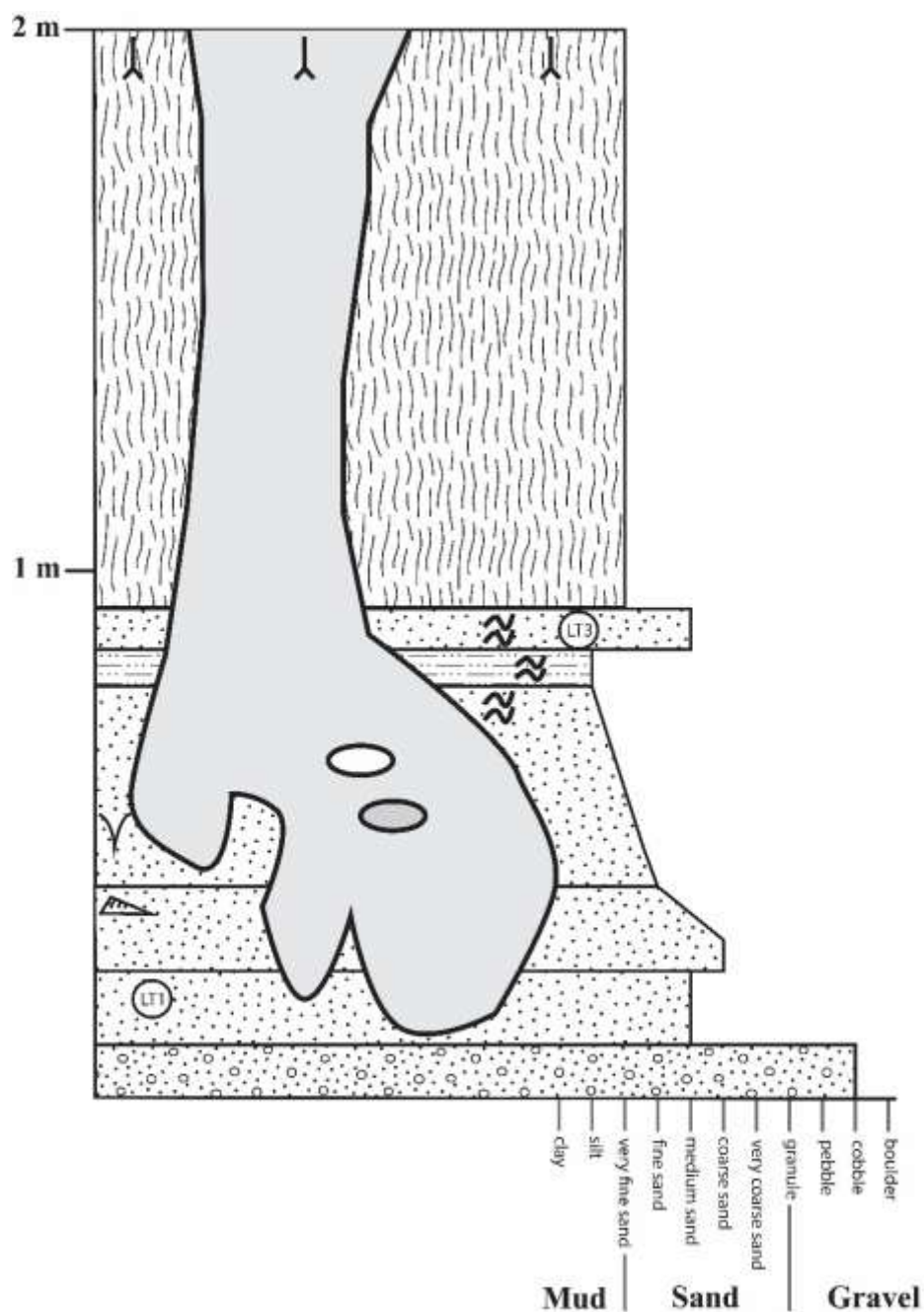


**Figure 19: Stratigraphic column of the Tripp section. See figure 15 for key. OSL sample LT1 was taken from the medium sand overlying the gravels. OSL sample LT3 was taken from the uppermost medium sand bed.**



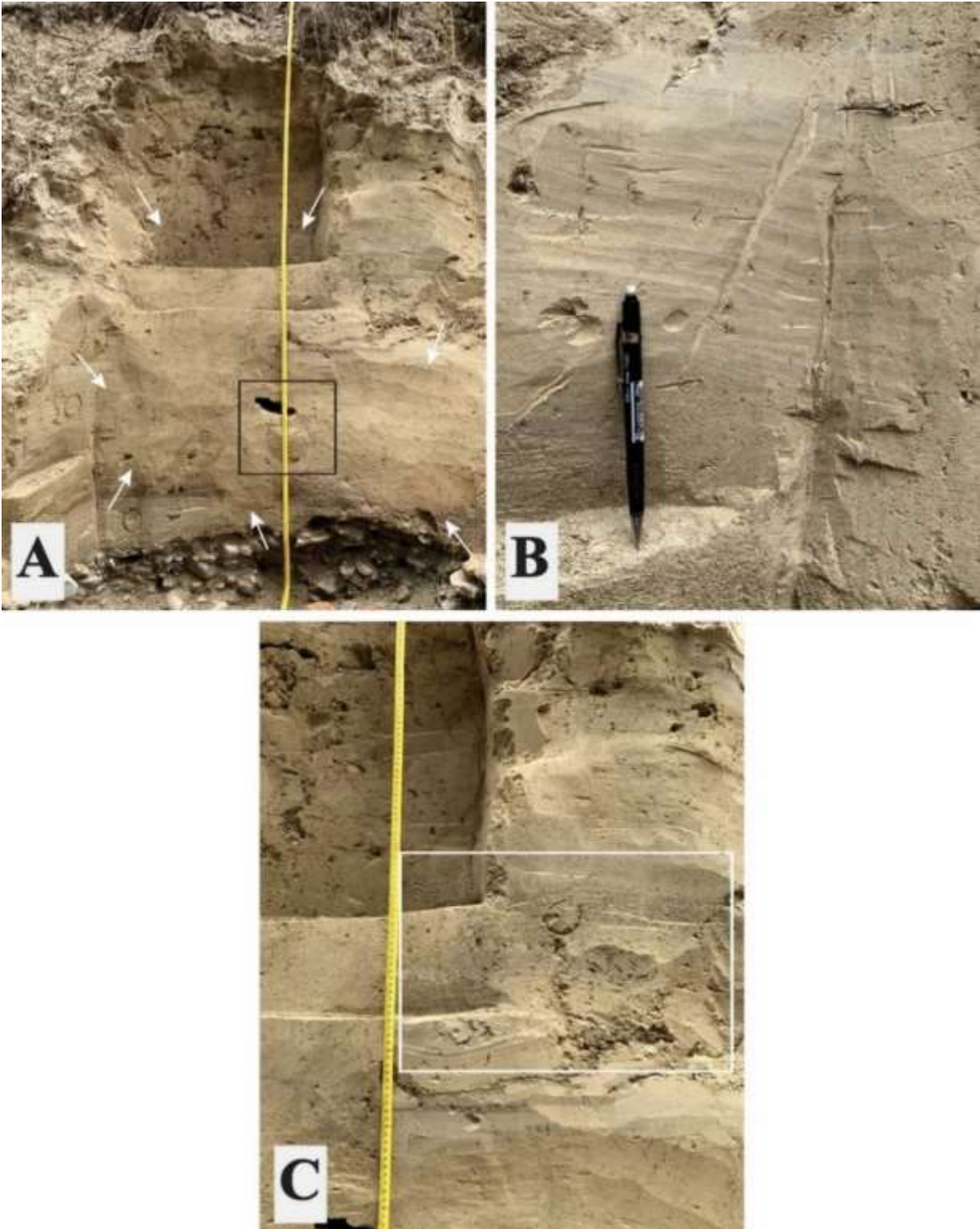


**Figure 20: A) Exposure of the Tripp section (SW  $\frac{1}{4}$  sec. 27, T. 25 N., R. 24 W.). Length of tape measure is 2 m. White arrows show the edges of the intrusive feature and the black box contains the two holes that crosscut the intrusive feature. Lower hole is infilled with stratified sediment. Two sand beds occur above the gravel. B) Contact between sand and sand-silt facies occurs near the lower tip of the wedge-shaped**

clastic dike to the left of the pencil. Notice the subtle ripple cross-laminations near the top of the sand and the wavy laminations in the sand-silt facies. C) White box contains a fold that is crosscut by the intrusive structure. Tape measure shows 90 cm.

### **3.5.5. Colluvium Deposits (Qc)**

Colluvial deposits are present on the bottom of slopes along the Little Bitterroot River and some of its tributaries. These colluvial deposits are unconsolidated and consist of crudely bedded, poorly sorted, angular to rounded pebbles, cobbles, and boulders in a clayey, silty, and sandy matrix (Figures 21A and 21B). Clasts consist of mostly local angular Belt rock clasts, but clasts from older Quaternary and Tertiary deposits are present. Thickness where exposed ranges from 3-6 m.

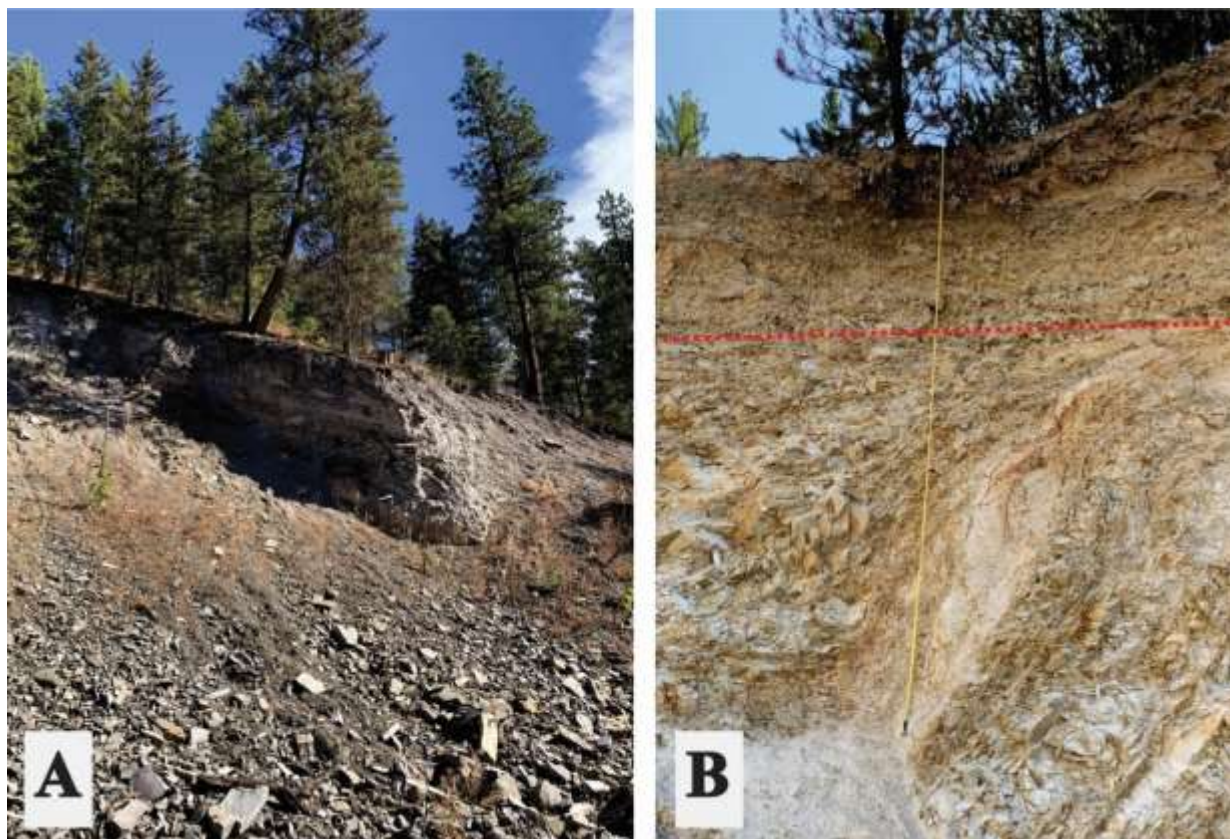


**Figure 21: A) Crudely bedded colluvium exposure on a steep slope near the Hubbard Reservoir dam (SE  $\frac{1}{4}$  sec. 18, T. 25 N., R. 24 W.). Outcrop is approximately 5 m thick. B) Undisturbed stratified colluvium overlying a thrust fault in Sickler Creek (SW  $\frac{1}{4}$  sec. 11, T. 26 N., R. 24 W.). Dashed red line shows contact between faulted Ravalli Group rock and colluvium. Tape measure shows 6 m.**

### **3.5.6. Boulder Fan Deposit**

A large fan-shaped gravel deposit containing boulders up to 7 m in size is located where the Hidden Lakes Canyon opens up into the wider plain above the Hubbard Reservoir (NE  $\frac{1}{4}$  sec. 31, T. 26 N., R. 24 W.). The deposit is poorly sorted, unconsolidated, not stratified, and consists of angular to rounded pebbles, cobbles, and boulders in a silty sand matrix. The majority of the clasts are angular Ravalli Group boulders similar to the rock forming the canyon walls. Some of the clasts within the deposit are subrounded to rounded pebbles and cobbles. The deposit extends further downstream into the reservoir and is exposed when the water level in the reservoir is low (Figure 22B). The largest boulders are found near the mouth of the canyon, with boulder size

decreasing farther away from the canyon mouth (Figures 22A and 22B). The boulder fan deposit is inset into glaciolacustrine sediments that overlie glaciofluvial gravels.





**Figure 22: A) Boulder with long dimension of 7 m found near the upper portion of the boulder fan deposit (NE  $\frac{1}{4}$  sec. 31, T. 26 N., R. 24 W.). Field book for scale is 19 cm long. B) Distal portion of the boulder fan deposit extending into the Hubbard Reservoir (NE  $\frac{1}{4}$  sec. 6, T. 25 N., R. 24 W.). Pocket knife for scale on boulder to the right is 6 cm long.**

### **3.5.7. Quaternary Landslide deposits (Qls)**

A large landslide or slump block is located at the southern end of the Hubbard Reservoir, where the artificial creek drains into the reservoir (NW ¼ sec. 18, T. 25 N., R. 24 W.). The deposit consists of unconsolidated, poorly sorted, angular to rounded pebbles, cobbles, and boulders in an orange-reddish-brown matrix. Material in the deposit is derived from the adjacent Quaternary-Tertiary conglomerate and ash-flow tuff. The landslide has a distinct crescentic head scarp and hummocky topography.

### **3.5.8. Talus Deposits (Qta)**

The bottoms of the steep canyons incised by the Little Bitterroot River contain piles of poorly sorted, unconsolidated, blocky, and tabular local Belt rock fragments. These deposits typically have no soil development and have moved downslope due to gravity. Thickness of these deposits is unknown but is probably less than 10 m.

### **3.5.9. Holocene Alluvium (Qal)**

Holocene unconsolidated, stratified clay, silt, sand, and gravel is deposited along the banks of the Little Bitterroot River and some of its tributaries. This alluvium has a distinct grassy vegetation that covers the deposit. The alluvium overlies and is inset into almost all of the geologic units in the study area.

## **3.6. Glacial Landforms and Features**

Several landforms and topographic features in the valley that contains McGregor Lake show evidence for glaciation in the valley. These landforms and features also provide evidence for ice flow direction, minimum thickness, and maximum position of the ice sheet.

### **3.6.1. Depositional Landforms**

There are several moraines composed of till in the U-shaped valley containing McGregor Lake that range in size from a few meters to several hundreds of meters in length and width. Lateral moraines with crest oriented NE-SW are present in the southern half of the valley east of McGregor Lake. These moraines suggest that ice-flow direction was to the east or northeast. Two other moraines are also distinct in the valley. A recessional moraine borders the eastern edge of McGregor Lake and most likely is the cause for McGregor Creek draining westward into the Thompson River. The other moraine is a terminal moraine. It is the easternmost moraine in the area and extends into the northwest corner of sec. 8, T. 26. N., R. 24 W. This moraine marks the farthest advance of the ice in the study area.

Multiple kettle lakes and kettle depressions are located around McGregor Lake and on the valley floor east of McGregor Lake. Some of the kettle lakes and depressions have an inlet and outlet while others are isolated. These landforms end near the easternmost end moraine and can also be used to mark the farthest extent of the ice in the valley. Other depositional landforms are the outwash plains and terraces and kame terraces which are discussed in section 3.5.2 and 3.5.4 respectively.

### **3.6.2. Erosional Landforms and Features**

Just north of the study area and Highway 2 in the valley containing McGregor Lake, the bedrock shows northwest-southeast trending large-scale glacial grooves (Figure 23). Also present at elevations of 1345 m within the same scoured bedrock are multiple boggy depressions and deeply incised, north-south trending channels. (Figure 23). Some of these channels connect the valley containing McGregor Lake to the valley to the north. From aerial photographs and topographic maps, scouring of the bedrock appears to occur around the highest peaks in the

valley. These landforms and features show evidence for ice overtopping the bedrock ridge from the north and flowing south into the valley containing McGregor Lake.

The valley containing McGregor Lake contains ice-marginal channels on the valley walls and other glaciofluvial channels on the valley floor. Channels east of the moraine bordering McGregor Lake show drainage to the east or northeast and are incised into till and bedrock. Other channels drain into McGregor Lake and are also incised into till and bedrock. Some of the channels enter and exit kettle depressions. Most of these channels contain modern day discharge. Due to poor exposures in the field, the channels are best seen in aerial photographs and in digital elevation models.

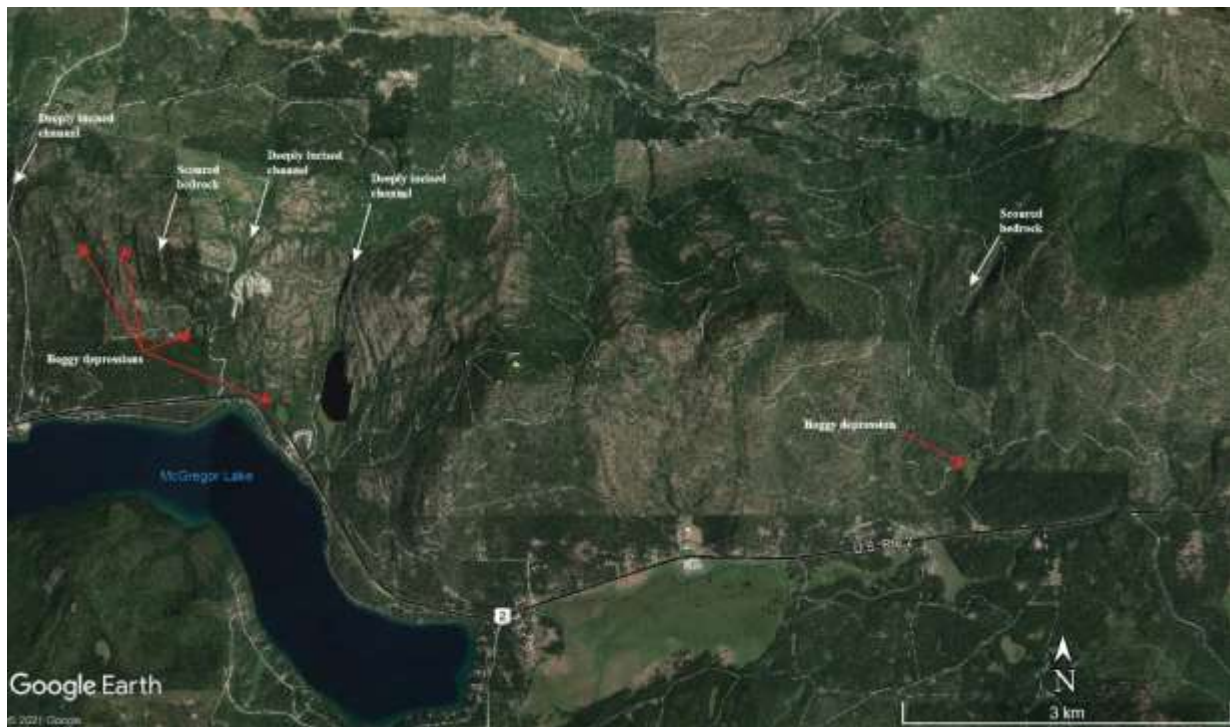


**Figure 23: Figure showing the scoured bedrock just north of the study area. Boggy depressions and channels that are deeply incised into bedrock shown by white arrows. Study area boundary is shown in black and borders Highway 2.**



### **3.7. Erratics and Overflow Channels**

Solitary outsized boulders interpreted to be ice-carried erratics are found throughout the study area. Where associated with till, the erratics were likely deposited by the ice sheet. Erratics outside of the ice limit were most likely deposited by icebergs carried in areas of outwash or floating in a proglacial lake. Three erratics are of particular interest because of their location and elevation. Two erratics (E1) of interest are located within 3 m of each other and are found along the edges of the Hidden Lakes Canyon (Figure 24). These erratics are Belt rock boulders with long dimensions of approximately 2 m and are at an elevation of 1256 m. The other erratic (E2) of interest is located in Granger Creek, a tributary to Sickler Creek (Figure 24). This erratic has a long dimension greater than 1 m and has a granitic lithology. This erratic is located at an elevation of 1243 m. Due to lack of ice-sheet geomorphic evidence and till deposits at these locations, the boulders were probably deposited by icebergs in the same lake that deposited the glaciolacustrine sediments.

A channel connects the valley of Sickler Creek to Pine Prairie (Figure 24) and forms a pass between the two valleys. The elevation of the channel at the pass is 1220 m. The channel contains boggy scours and depressions near the pass. More erosion on the Pine Prairie side of the pass shows flow was into Pine Prairie from the valley of Sickler Creek. Lack of ice-sheet deposits and ice-sheet landforms near the channel indicates the channel is most likely not an ice-marginal or glaciofluvial channel. Instead, the elevation of the feature, its close position to the Pine Prairie section, and its location close to the erratics indicates the feature is most likely an overflow channel related to a proglacial lake.

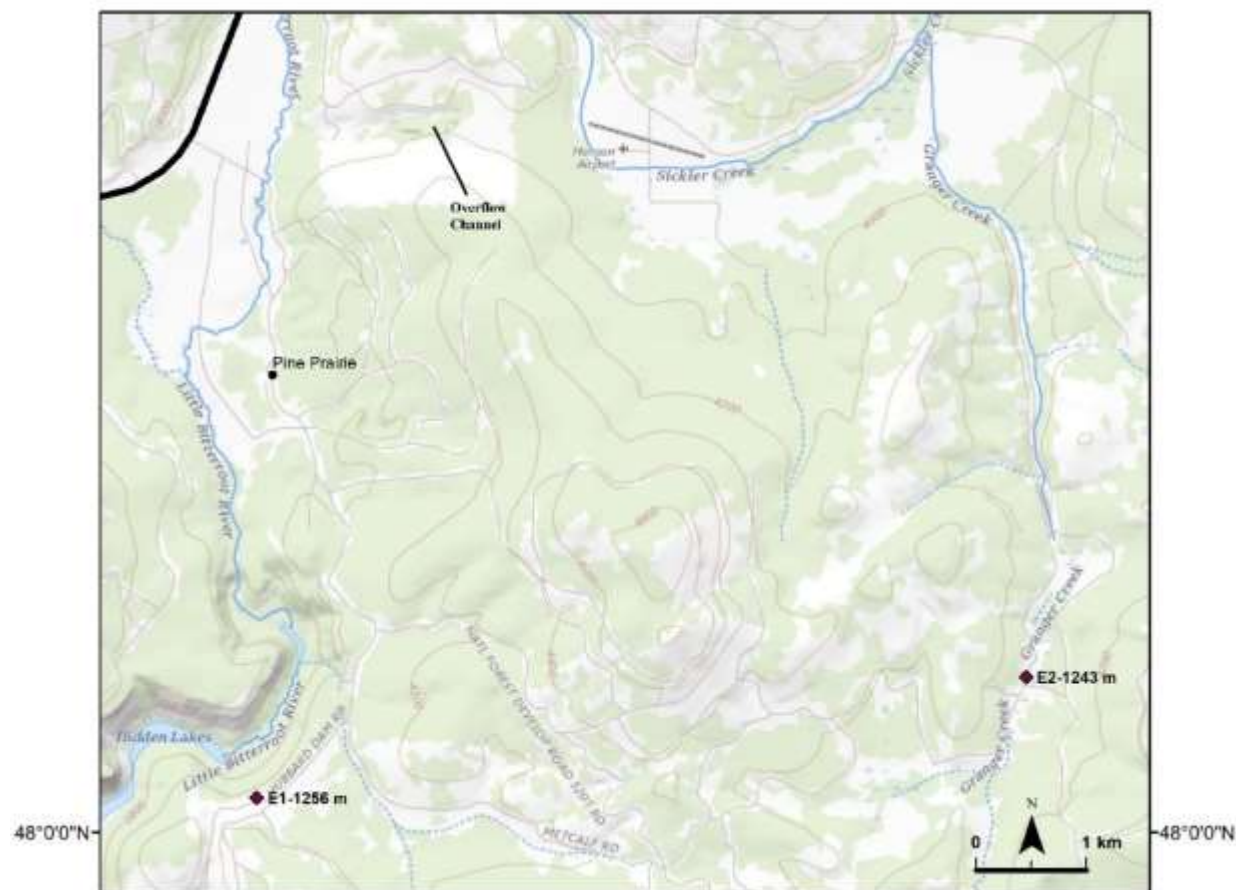


**Figure 24:** Figure showing location of three important erratics. Two of the erratics are labeled as E1 and are located at an elevation of 1256 m. The other erratic E2, is located in Granger Creek at an elevation of 1243 m. Overflow channel labeled near the top of the figure.

### 3.8. Optical Ages

Estimation of the time since burial using OSL is dependent on the environmental dose rate and the equivalent dose. The equivalent dose is the natural radiation dose that the mineral grain has received since burial, as measured in the laboratory. Determination of the equivalent dose for this study was carried out using the single-aliquot regenerative method (Murray and Wintle, 2000, 2003) (Appendix A). The equivalent dose rate for the three samples is shown in Table I. The environmental dose rate is an estimate of the amount of radiation the mineral grain has received from U, Th, Ra, Pb, K, and cosmic rays. The contribution to radiation from U, Th,

Ra, Pb, K, and cosmic rays is shown in Table II. These dose rates are reduced by estimates of the water-content history of the samples. The estimated burial age is calculated by dividing the equivalent dose by the environmental dose rate.

OSL dates on 150-250  $\mu\text{m}$  quartz grains for the samples LT1, LT3, and R are shown in Table I along with the number of aliquots accepted for the samples and burial depth. It should be noted that due to some of the characteristics of the samples observed in the laboratory, Dr. Sebastian Huot determined the ages of the samples may be underestimated. For detailed information on the exact procedures and data for the OSL samples see Appendix A.

**Table I: Small-Aliquot OSL age information.**

Sample	Depth	Number of Aliquots (accepted/total)	Dose Rate (Gy/ka)	Equivalent Dose (Gy)	OSL Age $\pm 1\sigma$ (ka)
<b>LT1</b>	1.80 m	40/230	$2.62 \pm 0.10$	$53 \pm 2$	$20.3 \pm 1.2$
<b>LT3</b>	1.10 m	36/240	$2.25 \pm 0.08$	$39 \pm 2$	$17.4 \pm 1.1$
<b>R</b>	0.92 m	57/240	$2.33 \pm 0.08$	$51 \pm 2$	$21.8 \pm 1.4$

**Table II: Presumed water content and contribution to radiation from U, Ra, Pb, Th, K, and cosmic rays.**

Sample	water content (%)	$^{238}\text{U}$ (Bq/kg)	$^{226}\text{Ra}$ (Bq/kg)	$^{210}\text{Pb}$ (Bq/kg)	$^{232}\text{Th}$ (Bq/kg)	$^{40}\text{K}$ (Bq/kg)	Cosmic rays (Gy/ka)
<b>LT1</b>	$20 \pm 5$	$32.1 \pm 2.0$	$34.2 \pm 0.5$	$33.3 \pm 2.2$	$37.8 \pm 0.7$	$536 \pm 11$	$0.21 \pm 0.01$
<b>LT3</b>	$20 \pm 5$	$29.6 \pm 2.1$	$33.6 \pm 0.5$	$32.7 \pm 2.3$	$35.1 \pm 0.8$	$443 \pm 11$	$0.23 \pm 0.01$
<b>R</b>	$20 \pm 5$	$20.3 \pm 1.2$	$37.5 \pm 0.5$	$35.0 \pm 1.9$	$33.2 \pm 0.5$	$422 \pm 08$	$0.23 \pm 0.01$

## 4. Discussion

### 4.1. Defining the Cordilleran Ice Sheet Margin

Glacial ice-sheet deposits, kettle depressions, moraines, large-scale glacial grooves, and ice-marginal channels in the valley containing McGregor Lake record the advance and retreat of CIS in this valley. Nowhere else in the study area were ice-sheet deposits and landforms found similar to those in the valley of McGregor Lake. The eastern most moraine in the valley of McGregor Lake is interpreted to mark the maximum advance of the ice in the valley.

Ice-marginal channels and kettle lakes on the southern walls of the valley containing McGregor Lake are used here to define the minimum elevation of ice on the southern valley walls. Large scale glacial grooves, boggy depressions, and deeply incised channels on the bedrock ridges north of the valley containing McGregor Lake show ice advanced from the north and overtopped these ridges. The maximum elevation of the glacial grooves on the edges of the highest peaks (~1540 m) are used here to interpret the minimum elevation of the ice that flowed in from the north. With this interpretation, the two highest points on the ridge to the north of the valley containing McGregor Lake would be nunataks. Lateral moraines on the valley floors show the ice flowed east once it had reached the valley bottom. It is unclear whether or not ice advanced from the west and contributed to the ice that advanced from the north. More work to the west of McGregor Lake is needed to verify this.

A moraine located on the eastern side of Lake Rogers that is responsible for damming the lake (Alden, 1953) and a lake-filled depression on the valley wall adjacent to Lake Rogers at an elevation of 1307 m are evidence for ice advancing at least up to Lake Rogers. The exact thickness of the ice at Lake Rogers is unknown, but the small lake on the valley wall suggests the ice was at least to an elevation of 1307 m.

Kettle lakes and depressions in the outwash plain approximately 6 km southwest of Marion and approximately 3 km north of Pine Prairie suggest the ice advanced to at least this position. The elevation and thickness of this ice is unknown, but the ice most likely overtopped the divide at an elevation of 1348 m that separates the valley to the north of McGregor Lake and the valley containing the town of Marion. After topping the divide, the ice would have connected with the ice in the valley to the north of McGregor Lake.

Based on the field mapping done in this study, topographic analysis, aerial imagery, and the work of Alden (1953), the CIS margin was defined for the valley containing McGregor Lake and approximated for areas bordering the northern portion of the study area (Figure 25).

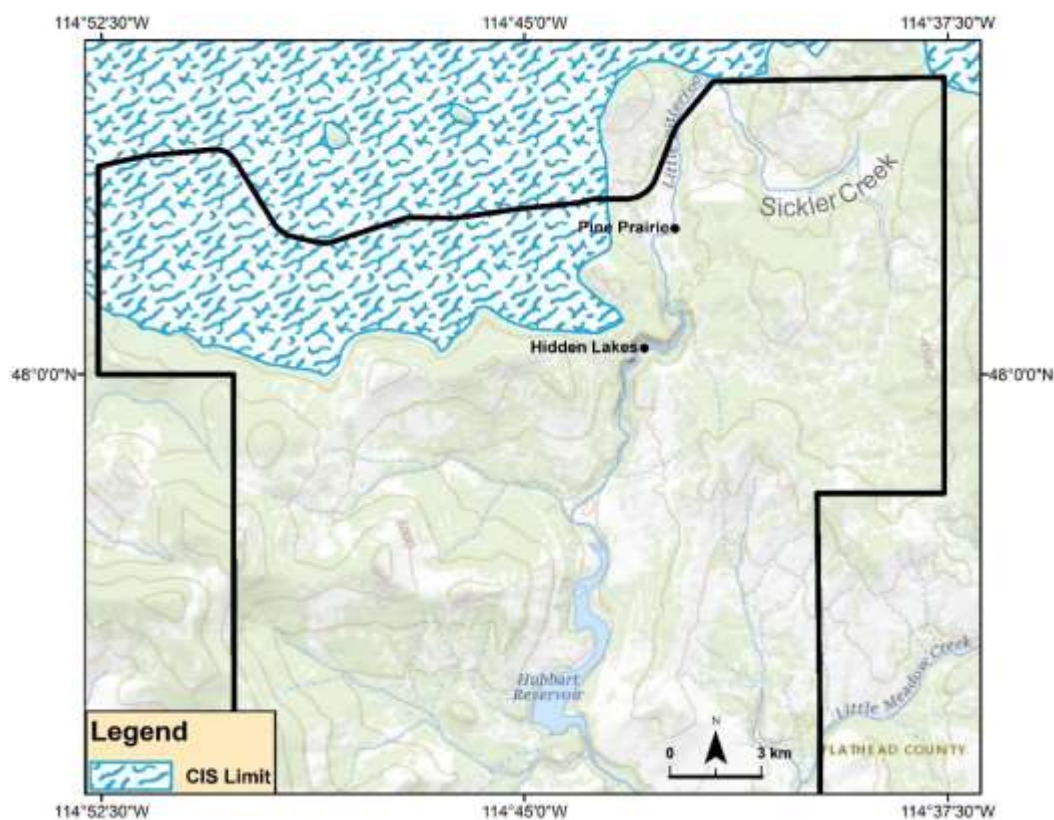


**Figure 25: Interpreted CIS limit within and to the north of the study area. Ice margin modified from Locke and Smith (2004).**

## 4.2. Glacial Lake Extent and Elevation

Extensive glaciolacustrine sediments attributed to Glacial Lake Missoula have been mapped in the Mill Pocket Creek and Niarada quadrangles which border the southeastern corner of the study area (Harrison et al., 1986; Lange and Zehner, 1992). Based on this mapping, the distribution of glaciolacustrine deposits within the study area, and the observations of Alden (1953) and Johns (1970), the glaciolacustrine deposits within the study area are interpreted to be deposited by a northern arm of Glacial Lake Missoula.

Glacial Lake Missoula extended as far north as Pine Prairie as shown by the Pine Prairie section. The ice-rafted erratics (E1) on the walls of the Hidden Lakes Canyon show that the lake was at least at an elevation of 1256 m. This elevation does not account for glacial isostatic rebound and the erratics indicate the absolute minimum extent of the lake as the keels of the icebergs that rafted in the erratics tend to be 10's of meters below the lake surface. The overflow channel that connects Pine Prairie and the valley of Sickler Creek is located at an elevation of 1225 m. This pass would have been overtopped by water and the valley of Sickler Creek would have been submerged to an elevation of at least 1256 m or more. The granitic ice-rafted erratic in Granger Creek is further evidence for the lake extending in the valley of Sickler Creek.

The overflow channel shows flow towards Pine Prairie from the valley of Sickler Creek. Flow of water from the valley of Sickler Creek could have occurred in a couple of ways. One scenario is that the CIS blocked the drainage route for glacial meltwater flowing west through the valley of Sickler Creek from the melting glacier at Lake Rogers. The valley of Sickler Creek would have filled up with water until it spilled over into Pine Prairie. The other scenario is that when the lake drained, the water in Pine Prairie would have drained before the water in Sickler

Creek. The difference in water level gradient would cause the water in the valley of Sickler Creek to pour into Pine Prairie.

No glaciolacustrine deposits were found in the valley of McGregor Lake and thus it is interpreted that the lake did not enter the valley. The lake was most likely in contact with the ice margin shown above. This would account for the ice-rafted erratics. The interpreted minimum lake elevation, maximum extent, and ice margin relationship for Glacial Lake Missoula is shown in Figure 26. It is likely that Glacial Lake Missoula reached its maximum elevation of ~1280 m based on the evidence listed above. The lake at an elevation of 1280 m is shown in Figure 26.



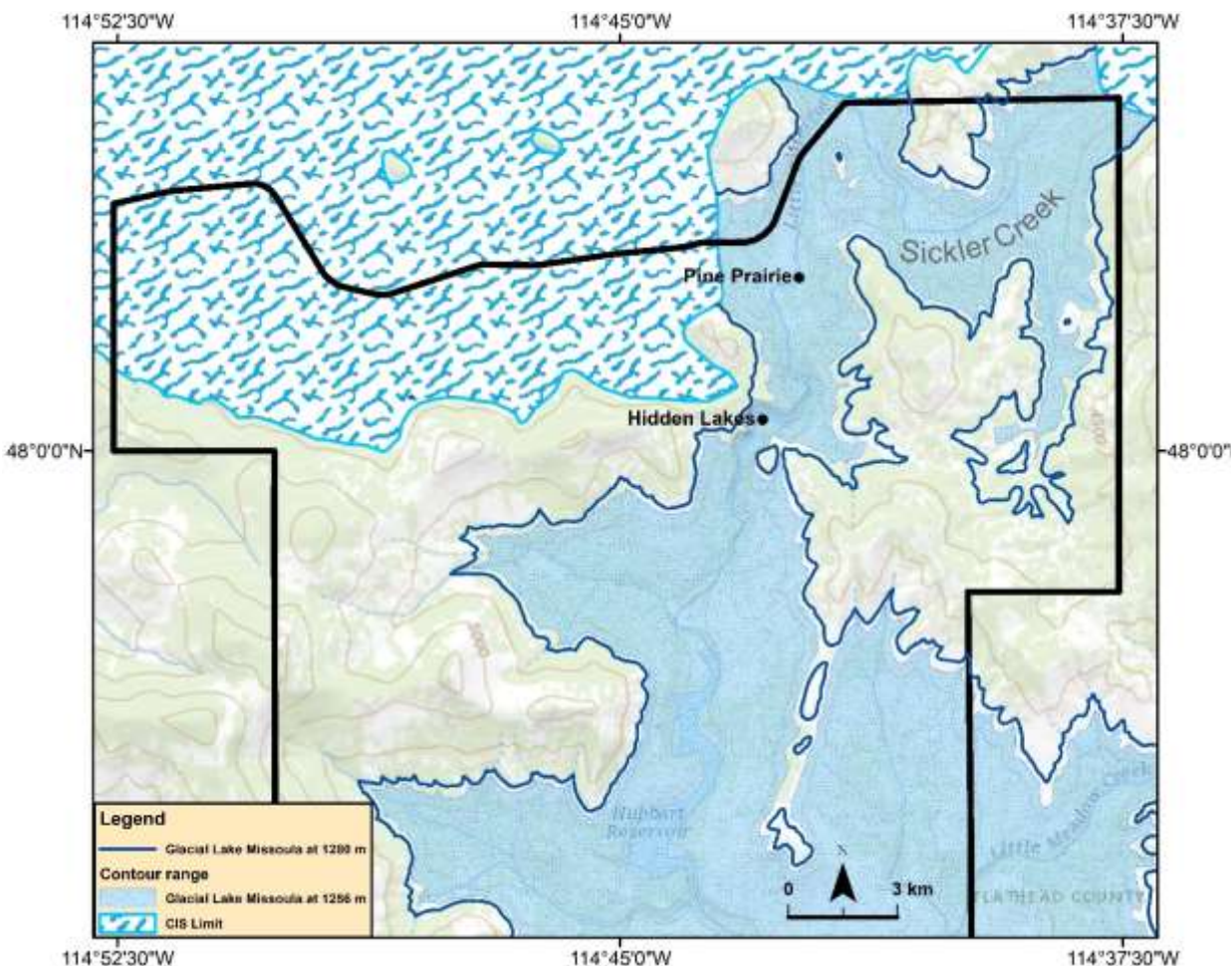


**Figure 26: Interpreted northern extent of Glacial Lake Missoula in the study area at an elevation of 1256 m (light blue polygon) and at 1280 m (dark blue line). The relationship between the interpreted CIS limit and Glacial Lake Missoula is shown.**

### 4.3. Sedimentology and Optical Ages of Glaciolacustrine Sediments

Rhythmically bedded clay and silt couplets in the Pine Prairie section contain no current structures, have gradational contacts between clay and silt in the couplets, have sharp contacts between couplets, and the clay thickness within the couplets is relatively constant. These characteristics fulfill the criteria for being classified as seasonally controlled lake bottom sediments or varves (Reineck and Singh, 1980). The silt in the couplets is deposited by hyperpycnal flow into the lake during seasonal peak glacial meltwater runoff and the clay is deposited during annual winter low-flow conditions (Hofmann and Hendrix, 2010). A

gradational change from silt to clay shows a gradual decrease in flow and the onset of winter (Hofmann and Hendrix, 2010). Relatively constant thickness of the clay beds in the couplets shows consistent winter sedimentation from year to year (Ashley, 1975). A sharp contact below the basal silt suggests a rapid onset of high-flow conditions (Ashley, 1975).

Convoluted laminae, small-scale faults, dewatering structures, and clastic dikes like those in the Pine Prairie section have been interpreted in Glacial Lake Missoula sediments at the Ninemile, Rail line (Hanson et al., 2012), and Garden Gulch sections (Smith, 2017) as evidence for desiccation and periglacial modification after lake level fluctuations or lake drainages left the sediments subaerially exposed. Unlike the Pine Prairie section, the three sections mentioned above consist of multiple fining upward cycles where sand and silt commonly containing ripples grade into silt and clay rhythmites similar to those in the Pine Prairie section. These fining upward sequences are also interpreted as evidence for multiple cycles of lake regression and transgression (Hanson et al., 2012; Smith, 2017).

The Pine Prairie section does not contain these fining upward cycles and consists entirely of deep lake bottom varves with three distinct silt beds. Gradational contacts between the silt beds and the overlying clay suggest the same depositional processes as the other rhythmites. Erosive lower contacts and clay rip-ups in the silt beds suggest higher energy flows, but not high enough to produce ripple structures as they are not present in the silt beds. These silt beds were probably deposited during higher meltwater years or during high discharge events that were followed by normal seasonal sedimentation. The severely disturbed section of varves is also overlain by flat-lying varves. This is indicative of continued deposition under the same deep lake bottom conditions. If the deformation present in the Pine Prairie section was caused by subaerial exposure, then it would be expected that deposits related to transgression would overlie the

varves as seen in the Rail line, Ninemile, and Garden Gulch sections. This is not the case here, and the interpretation of desiccation and periglacial modification following subaerial exposure in the Pine Prairie section is not accepted.

The overturned soft sediment folds that are found in the Pine Prairie section are classic examples of soft sediment folds associated with slope failures in varved lacustrine deposits (Alsop and Marco, 2013). Clastic dikes tilted to the southwest are most likely infilled fractures that formed perpendicular to the direction of slope movement (Cruden and Varnes, 1996). This interpretation does not apply to all the clastic dikes because many of the dikes are tilted to the northwest and extend into the upper flat-bedded varves. Sinuous laminae on the boundaries of the dikes and floating clay clasts within the sediment suggest these dikes are the result of fluidization (Lowe, 1975). Flame and dish structures found within the Pine Prairie section are further evidence for dewatering. The soft sediment deformation structures within the Pine Prairie section are evidence for rapid deposition causing differential loading and dewatering. The interpretation of penecontemporaneous soft-sediment deformation structures is favored. It is also possible that the slope failure and other fluidization in the Pine Prairie section could be formed by seismic events related to Quaternary faults to the east (Stickney et al., 2000), but determination of this is beyond the scope of this study.

The Reservoir section rhythmites do not show the characteristics of deep lake bottom varves like those in the Pine Prairie section. The thickness of the silty very fine sand beds to the clay laminations, and the climbing ripple and ripple cross-laminations in the lower two couplets is evidence for deposition close to an inflowing current source (Ashley, 1975). Thinning of the couplets up section and the lack of higher flow velocity structures in the upper four couplets is evidence for reduced sedimentation and deposition less proximal to the inflowing current source

(Ashley, 1975). This thinning of the couplets and lower flow conditions up-section is interpreted to record a lake transgression. The ripple and climbing ripple cross-laminations in the lower two couplets most likely formed from lake-bottom currents during initial filling of the lake.

Sediment-laden meltwater streams near a delta (Jopling and Walker, 1968; Ashley, 1975; Gustavson et al., 1975), subaqueous river plumes, and turbidity currents caused by sediment surges near a delta front (Pharo and Carmack, 1979) could all deposit climbing ripple and ripple cross-laminations. The interpretation of turbidites for these couplets is not accepted because none of the couplets appear to contain erosive bottoms and the upper couplets do not contain ripple structures common in turbidites. The rhythmites here are interpreted to be deposited near a delta prograding to the south along the Little Bitterroot River. The silty sand was deposited during seasonal high meltwater discharge and the clay drapes were deposited during the winter in times of limited sedimentation (Ashley, 1975; Gustavson et al., 1975).

This interpretation classifies the rhythmites as seasonal rhythmites or varves. Varves found in Pine Prairie are distal equivalents to the varves in the Reservoir section. Both sections are controlled by seasonal sedimentation, but the Reservoir section sediments were deposited closer to a sedimentation source (Ashley, 1975). This accounts for the variation in silt and clay thickness between the two locations. The Reservoir section is found close to where the Little Bitterroot River flows out of the high gradient Hidden Lakes Canyon into the flat plain that the Hubbart Reservoir currently occupies. Tamarack Creek also joins the Little Bitterroot River in this area. Hydrodynamically the area near the Reservoir section would be an ideal location for a glaciofluvial stream flowing down the Little Bitterroot River to enter a lake inundating the flat area to form a delta.

The OSL date of the R sample from the lowermost couplet of the Reservoir section yielded an age of  $21.8 \pm 1.4$  ka and is consistent with the initial formation of Glacial Lake Missoula ( $22 - 13$  ka; O'Connor et al., 2020). Thus, the age agrees with the interpretation of the sediments recording an early lake transgression.

In the Tripp section, the upward fining sequence from coarse-grained laminated and rippled sand to rhythmically laminated clayey silt is evidence for transgression and deepening of Glacial Lake Missoula. This interpretation is further supported by the OSL sample LT1 age of  $20.3 \pm 1.2$  ka bounding the sequence from below and the OSL sample LT3 age of  $17.4 \pm 1.1$  ka that bounds the sequence from above. The age of  $20.3 \pm 1.2$  ka is consistent with the initial impoundment of Glacial Lake Missoula (O'Connor et al., 2020). Based on the age, the lowermost basal sand at the Tripp section is tentatively interpreted to be deposited during lake transgression possibly in a shallow lake or near the lake shore. The sandy bed in the top of the section from which LT3 was taken from could have been deposited subaqueously or subaerially, but the folding of the sand and underlying clayey silt and the weathering of the sediments above this horizon makes determination difficult. Regardless, it is possible to place the initial transgression of the lake between the ages of  $20.3 \pm 1.2$  and  $17.4 \pm 1.1$  ka based on the two OSL dates bounding the fining upward sequence.

A large intrusive structure cuts through most of this section and shows disturbance of well-bedded glaciolacustrine sediments. Interpretation of this structure is difficult due to limited exposure. The structure has vertical upper boundaries and lobate lower boundaries that flare out and disturb the surrounding sediment. The axial plane of the fold that is crosscut by the intrusive structure suggest the structure originated near the top of the section and subsequently spread downward and out near its base. This indicates that the feature is not caused by vertical upward

movement of fluidized sediment and is most likely caused by collapse or injection of the sediment from above. This structure may be related to the grounding and subsequent *in situ* decay of an iceberg. The weight of the grounded iceberg could cause deformation in the underlying sediment, thus creating the observed fold (Thomas and Connell, 1985). Subsequent melting of the iceberg could cause collapse and consolidation of the sediment below the iceberg (Thomas and Connell, 1985). It would also be expected that debris from the iceberg would be incorporated in the deformed sediment (Thomas and Connell, 1985) which is not conclusively seen here. It is also possible that the feature is a filled in or collapsed burrow that was formed by a Holocene mammal. If the structure was created by a grounded iceberg, then this would be evidence for a complete or partial draining of the lake, but it cannot conclusively be said that the structure was formed by the grounding of an iceberg. Origin of the structure is unclear, but it is certain that the structure is younger than the OSL sample LT3, as the structure cross cuts the sand bed from which the sample was taken.

The small clastic dike in the Tripp section is tentatively interpreted to be a fluidization structure because the structure is infilled with sand similar to the sand below, the structure occurs in a fining upward sequence, and there are no other soft sediment deformation structures that would indicate subaerial exposure. The clastic dike could be related to the large intrusive structure that disturbs the whole section.

There is no conclusive evidence for subaerial exposure of the sediments detailed above. It can be conclusively stated from three OSL ages and the sedimentology in the sections discussed above that Glacial Lake Missoula transgressed up the valley of the Little Bitterroot River between  $21.8 \pm 1.4$  and  $20.3 \pm 1.2$  ka and existed for several thousands of years to, or beyond,  $17.4 \pm 1.1$  ka.

#### **4.4. Evidence for a Lake Drainage**

One hypothesis evaluated in this study is that the 120 m-deep Hidden Lakes Canyon was formed or modified from outflow of floodwater caused by a draining of Glacial Lake Missoula. The bedrock scours forming the Hidden Lakes in the Hidden Lakes Canyon are geomorphic evidence for bedrock scouring and incision. The position of the glaciofluvial gravels at the Reservoir section approximately 10 m above the valley floor shows that the Hidden Lakes Canyon existed during deposition of the gravels and before deposition of the glaciolacustrine sediments. Meltwater coming down from Pine Prairie had to have flowed down the Hidden Lakes Canyon in order to deposit the glaciofluvial gravels. This shows the Hidden Lakes Canyon was not created through one single catastrophic flood related to a drainage of Glacial Lake Missoula. Initial formation of the canyon must have predated the last glacial maximum and was modified but not created through the events recorded in the glacial deposits here.

A large boulder fan deposit at the mouth of the Hidden Lakes Canyon where it opens into the flat area above the Hubbart Reservoir is inset into the Reservoir section glaciolacustrine deposits and into the underlying glaciofluvial deposits. This indicates the boulder fan deposit is younger than the Reservoir glaciolacustrine and glaciofluvial sediments. Nowhere were glaciolacustrine deposits found overlying this deposit. The boulder fan deposit here is interpreted to be deposited by rapid flood waters draining through the Hidden Lakes Canyon. This interpretation is further supported by the bedrock incision and scouring that forms the Hidden Lakes.

When the ice dam forming Glacial Lake Missoula failed, areas down-stream and closer to the ice dam would have drained almost immediately while areas further upstream and confined by narrow canyons lagged behind and were left with a high hydraulic gradient that would induce a large current (Pardee, 1942; O'Conner et al., 2020). Floodwater draining through the Hidden



Lakes Canyon likely scoured the canyon bottom and walls picking up boulder-sized clasts. When the floodwater exited the Hidden Lakes Canyon and entered the wide low relief area above the Hubbard Reservoir, the floodwater velocity decreased, and the largest boulders were deposited near the mouth of the canyon. Smaller boulders continued to be deposited downstream forming a fan-shaped deposit.

It is interesting that the floodwater entering the flat area above the Hubbard Reservoir did not completely erode the exposed Reservoir section sediments. Detailed hydrodynamic analysis of the floodwater could determine exact discharges and volumes of the floodwater, but such analysis is beyond the scope of this study. Other such deposits related to floodwaters depositing large boulders at the mouths of canyons have been described south of the Flathead Valley (Hofmann and Hendrix, 2010) and in the Channeled Scabland (O'Connor et al., 2020).

#### **4.5. Relation to Regional Chronology of Glacial Lake Missoula**

Regional chronology of Glacial Lake Missoula constrains the age that the lake could have existed to between 22 and 13 ka (O'Connor et al., 2020). Stratigraphic analysis from inside the lake basin (Chambers, 1971, 1984; Smith, 2006; Hanson et al., 2012; Smith et al., 2018) and from downstream of the basin (Waite, 1980, 1985; Atwater, 1986; Benito and O'Connor, 2003; Clague et al., 2003; Normark and Reid, 2003; Waite, 2016; Balbas et al., 2017) has showed the lake drained multiple times. Other studies have determined that the oldest floods were the largest, with later floods being smaller (Benito and O'Connor, 2003; Waite, 2016; Balbas et al., 2017).

The  $21.8 \pm 1.4$  and  $20.3 \pm 1.2$  ka OSL dates from basal units in the glaciolacustrine deposits are on the older end of the range that Glacial Lake Missoula could have existed and most likely record the initial transgression of the lake. The measured sections from this study are

all at elevations above the Ninemile (936 – 959 m) and Rail line (963 – 975 m) sections. The Garden Gulch section is at elevations of 1173 – 1186 m which is above the Reservoir and Tripp sections but below the elevation of Pine Prairie section. It would be expected that the sediments from this study would be subaerially exposed if the lower elevation sediments from the Ninemile, Rail line, and Garden Gulch sections were subaerially exposed during a lake drainage. The measured sections here are much thinner than the Ninemile, Rail line, and Garden Gulch sections. It could be possible that the measured sections from this study are simply too thin and incomplete to record multiple lake draining cycles. The deep lake bottom varves with the occasional thicker silt bed in Pine Prairie could have been deposited in later stages of Glacial Lake Missoula when the lake emptied less catastrophically. The boulder fan deposit at the mouth of the Hidden Lakes Canyon and the bedrock scoured Hidden Lakes support evidence for at least one large drainage of Glacial Lake Missoula. However, lack of glaciolacustrine deposits across the fan indicates the lake did not inundate elevations above about 1070 m in the area after the fan was deposited.

## 5. Conclusions

During the last late Pleistocene glaciation the CIS advanced to its maximum position in the valley containing McGregor Lake, at Lake Rogers, and approximately 4 km north of Pine Prairie. Ice advanced from the north and possibly from the west into the valley containing McGregor Lake. Once the ice had reached the valley floor, the ice advanced eastward to its terminal position just to the west of Pine Prairie. Ice in the valley of McGregor Lake was at least 200 m thick. The ice at Lake Rogers and to the north of Pine Prairie advanced from the east as a smaller lobe of the glacier that occupied the Flathead Valley (Alden, 1953).

Glacial Lake Missoula deposits distributed throughout the area extend up into Pine Prairie. Ice-rafted erratics in the study area show that Glacial Lake Missoula reached an elevation of at least 1256 m, if not 10's of meters higher and extended into the valley of Sickler Creek. Stratigraphic analysis of three glaciolacustrine sequences show the lake transgressed between  $21.8 \pm 1.4$  and  $20.3 \pm 1.2$  ka which is consistent with other regional chronology. Glaciolacustrine deposits from this part of the Glacial Lake Missoula basin do not show conclusive evidence for subaerial exposure and multiple lake level fluctuations. A large fan-shaped deposit containing boulders with long dimensions greater than 5 m at the mouth of the Hidden Lakes Canyon and the bedrock scoured Hidden Lakes are evidence for at least one catastrophic drainage of Glacial Lake Missoula.

## 6. References Cited

- Alden, W.C., 1953, Physiography and glacial geology of western Montana and adjacent areas: U.S. Geological Survey Professional Paper 231, 200 p., doi:10.3133/pp231.
- Allmendinger, R.W., 2019, Stereonet Mobile (Version 3.4.1) [Mobile application software]. Retrieved from <http://apple.com/app-store/>
- Alsop, G., and Marco, S., 2013, Seismogenic slump folds formed by gravity-driven tectonics down a negligible subaqueous slope: *Tectonophysics*, v. 605, p. 48-69, doi:10.1016/j.tecto.2013.04.004.
- Arnold, L.J., and Roberts, R.G., 2009, Stochastic modelling of multi-grain equivalent dose (De) distributions: Implications for OSL dating of sediment mixtures: *Quaternary Geochronology*, v. 4, p. 204-230, doi:10.1016/j.quageo.2008.12.001.
- Ashley, G.M., 1975, Rhythmic sedimentation in Glacial Lake Hitchcock, Massachusetts-Connecticut, *in* Jopling, A.V., and McDonald, B.C., eds., *Glaciofluvial and Glaciolacustrine Sedimentation*: Tulsa, Oklahoma, The Society of Economic Paleontologists and Mineralogists, p. 304-320, doi:10.2110/pec.75.23.0304.
- Atwater, B.F., 1986, Pleistocene glacial lake deposits of the Sanpoil River Valley, northeastern Washington: U.S. Geological Survey Bulletin 1661, 39 p., doi:10.3133/b1661.
- Baker, V.R., 1973, Paleohydrology and sedimentology of Lake Missoula flooding in eastern Washington: Geological Society of America Special Paper 144, 79 p., doi:10.1130/SPE144-p1.
- Balbas, A.M., Barth, A.M., Clark, P.U., Clark, J., Caffee, M., O'Connor, J.E., Baker, V.R., Konrad, K., and Bjornstad, B., 2017,  $^{10}\text{Be}$  dating of late Pleistocene megafloods and Cordilleran Ice Sheet retreat in the northwestern United States: *Geology*, v. 45, p. 583-586, doi:10.1130/G38956.1.
- Benito, G., and O'Connor, J.E., 2003, Number and size of last-glacial Missoula floods in the Columbia River Valley between the Pasco Basin, Washington, and Portland, Oregon: *Geological Society of America Bulletin*, v. 115, p. 624-638, doi:10.1130/0016-7606(2003)115%3C0624:NASOLM%3E2.0.CO;2.

- Brooks, C., Hart, S.R., and Wendt, I., 1972, Realistic use of two-error regression treatments as applied to rubidium-strontium data: *Reviews of Geophysics*, v. 10, p. 551-577, doi:10.1029/RG010i002p00551.
- Bretz, J.H., 1923, Glacial drainage on the Columbia Plateau: *Geological Society of America Bulletin*, v. 34, p. 573-608, doi:10.1130/GSAB-34-573.
- Bretz, J.H., 1969, The lake Missoula floods and the Channeled Scabland: *The Journal of Geology*, v. 77, p. 505-543, doi:10.1086/627452.
- Capps, D.L., 2004, The Quaternary history of the Cordilleran Ice Sheet fringe: Ashley Lake area, Montana [M.S. thesis]: Montana State University, 117 p.
- Carrara, P.E., 1990, Surficial geologic map of Glacier National Park, Montana: U.S. Geological Survey Miscellaneous Publications - IMAP 1508-D, scale 1:100,000, doi:10.3133/i1508D.
- Chambers, R.L., 1971, Sedimentation in glacial Lake Missoula [M.S. thesis]: University of Montana, 97 p.
- Chambers, R.L., 1984, Sedimentary evidence for multiple glacial lakes Missoula, *in* McBane, J.D., and Garrison, P.B., eds., northwest Montana and adjacent Canada: Billings, Montana, Montana Geological Society, p. 189-199.
- Clark, P.U., Clague, J.J., Curry, B.B., Dreimanis, A., Hicock, S.R., Miller, G.H., Berger, G.W., Eyles, N., Lamothe, M., Miller, B.B., Mott, R.J., Oldale, R.N., Stea, R.R., Szabo, J.P., Thorleifson, L.H., and Vincent, J.-S., 1993, Initiation and development of the Laurentide and Cordilleran Ice Sheets following the last interglaciation: *Quaternary Science Reviews*, v. 12, p. 79-114, doi:10.1016/0277-3791(93)90011-A.
- Clague, J.J., Barendregt, R., Enkin, R.J., and Foit, F.F., 2003, Paleomagnetic and tephra evidence for tens of Missoula floods in southern Washington: *Geology*, v. 31, p. 247-250, doi:10.1130/0091-7613(2003)031%3C0247:PATEFT%3E2.0.CO;2.
- Constenius, K.N., 1996, Late Paleogene extensional collapse of the Cordilleran foreland fold and thrust belt: *Geological Society of America Bulletin*, v. 108, p. 20-39, doi:10.1130/0016-7606(1996)108%3C0020:LPECOT%3E2.3.CO;2.

- Cruden, D.M., and Varnes, D.J., 1996, Landslide types and processes, *in* Turner, A.K., and Schuster, R.L., eds., *Landslides: Investigation and Mitigation*: Washington D.C, Transportation Research Board, Special Publication 247, p. 36-75.
- Foit Jr., F.F., Mehringer Jr., P.J., and Shepard, J.C., 1993, Age, distribution, and stratigraphy of Glacier Peak tephra in Eastern Washington and Western Montana, United States: *Canadian Journal of Earth Science*, v. 30, p. 535–552, doi:10.1139/e93-042.
- Fuentes, F., DeCelles, P.G., Constenius, K.N., and Gehrels, G.E., 2011, Evolution of the Cordilleran foreland basin system in northwestern Montana, USA: *Geological Society of America Bulletin*, v. 123, p. 507-533, doi:10.1130/B30204.1.
- Galbraith, R.F., Roberts, R.G., Laslett, G.M., Yoshida, H., and Olley, J.M., 1999, Optical dating of single and multiple grains of quartz from Jinmium rock shelter, northern Australia: Part I, experimental design and statistical models: *Archaeometry*, v. 41, p. 339-364, doi:10.1111/j.1475-4754.1999.tb00987.x.
- Gilmore, G.R., 2008, *Practical Gamma-ray Spectrometry* (2nd ed): Chichester, UK, John Wiley & Sons, Ltd, 381 p., doi:10.1002/9780470861981.
- Gustavson, T.C., Ashley, G.M., and Boothroyd, J.C., 1975, Depositional sequences in glaciolacustrine deltas, *in* Jopling, A.V., and McDonald, B.C., eds., *Glaciofluvial and Glaciolacustrine Sedimentation*: Tulsa, Oklahoma, The Society of Economic Paleontologists and Mineralogists, p. 264-280, doi:10.2110/pec.75.23.0264.
- Hanson, M.A., Lian, O.B., and Clague, J.J., 2012, The sequence and timing of large late Pleistocene floods from glacial Lake Missoula: *Quaternary Science Reviews*, v. 31, p. 67-81, doi:10.1016/j.quascirev.2011.11.009.
- Hanson, M.A., and Clague, J.J., 2016, Record of glacial Lake Missoula floods in glacial Lake Columbia, Washington: *Quaternary Science Reviews*, v. 133, p. 62–76, doi:10.1016/j.quascirev.2015.12.009.
- Harrison, J.E., Griggs, A.B., and Wells, J.D., 1986, *Geologic and Structure Maps of the Wallace 1° × 2° Quadrangle, Montana and Idaho*: U.S. Geological Survey Miscellaneous Investigations Map I-1509, scale 1:250,000, doi:10.3133/i1509A.

- Harrison, J.E., Cressman, E.R., and Whipple, J.W., 1992, Geologic and Structure Maps of the Kalispell 1° × 2° Quadrangle, Montana, and Alberta and British Columbia: U.S. Geological Survey Miscellaneous Investigations Series Map I-2267, scale 1:250,000, doi:10.3133/i2267.
- Harrison, J.E., and Cressman, E.R., 1993, Geology of the Libby thrust belt of northwestern Montana and its implications to regional tectonics: U.S. Geological Survey, Professional Paper 1524, 42 p., doi:10.3133/pp1524.
- Hofmann, M.H., and Hendrix, M.S., 2010, Depositional processes and the inferred history of ice-margin retreat associated with the deglaciation of the Cordilleran Ice Sheet: The sedimentary record from Flathead Lake, northwest Montana, USA: *Sedimentary Geology*, v. 223, p. 61–74, doi:10.1016/j.sedgeo.2009.10.004.
- Huntley, D.J., and Baril, M.R., 1997, The K content of the K-feldspars being measured in optical dating or in thermoluminescence dating: *Ancient TL*, v. 15, p. 11-13.
- Huntley, D.J., and Hancock, R.G.V., 2001, The Rb contents of the K-feldspar grains being measured in optical dating: *Ancient TL*, v. 19, p. 43-46.
- Huot, S., and Lamothe, M., 2003, Variability of infrared stimulated luminescence properties from fractured feldspar grains: *Radiation Measurements*, v. 37, p. 499-503, doi:10.1016/S1350-4487(03)00014-3.
- Johns, W.M., 1970, Geology and mineral deposits of Lincoln and Flathead Counties, Montana: Montana Bureau of Mines and Geology Bulletin 79, 182 p.
- Jopling, A.V., and Walker, R.G., 1968, Morphology and origin of ripple-drift cross-lamination, with examples from the Pleistocene of Massachusetts: *Journal of Sedimentary Petrology*, v. 38, p. 971-984, doi:10.1306/74D71ADC-2B21-11D7-8648000102C1865D.
- Kolb, T., and Fuchs, M., 2018, Luminescence dating of pre-Eemian (pre-MIS 5e) fluvial terraces in Northern Bavaria (Germany) – Benefits and limitations of applying a pIRIR225-approach: *Geomorphology*, v. 321, p. 16-32, doi:10.1016/j.geomorph.2018.08.009.



- Konizeski, R.L., Brietkrietz, A., and McMurtrey, R.G., 1968, Geology and groundwater resources of the Kalispell valley, northwestern Montana: Montana Bureau of Mines and Geology Bulletin 68, 42 p.
- LaFave, J.I., Smith, L.N., and Patton, T.W., 2004, Ground-water resources of the Flathead Lake area: Flathead, Lake, and parts of Missoula and Sanders Counties, Montana. Part A- Descriptive overview: Montana Bureau of Mines and Geology Ground-Water Assessment Atlas 2-A, 144 p.
- Lange, I.M., and Zehner, R.E., 1992, Geologic map of the Hog Heaven volcanic field, northwestern Montana: Montana Bureau of Mines and Geology Geologic Map 53, scale 1:24,000.
- Lange, I.M., Zehner, R., and Hahn, A., 1994, Geology, geochemistry, and ore deposits of the Oligocene Hog Heaven volcanic field, northwestern Montana: *Economic Geology*, v. 89, p. 1939–1963, doi:10.2113/gsecongeo.89.8.1939.
- Langer, W.H., Van Gosen, B.S., Meeker, G.P., Adams, D.T., and Hoefen, T.M., 2011, The dispersion of fibrous amphiboles by glacial processes in the area surrounding Libby, Montana, USA: *Environmental Earth Science*, v. 65, p. 157-168, doi:10.1007/s12665-010-0832-8.
- Lian, O.B., and Roberts, R.G., 2005, Dating the Quaternary: Progress in luminescence dating of sediments: *Quaternary Science Reviews*, v. 25, p. 2449-2468, doi:10.1016/j.quascirev.2005.11.013.
- Locke, W., and Smith, L.N., 2004, Pleistocene mountain glaciation in the state of Montana, USA, *in* Ehlers, J., and Gibbard, P.L., eds, *Quaternary Glaciations - Extent and Chronology, Part II: North America*: Amsterdam, The Netherlands, Elsevier, p. 117-121, doi:10.1016/S1571-0866(04)80193-3.
- Lowe, D.R., 1975, Water escape structures in coarse-grained sediments: *Sedimentology*, v. 22, p. 157-204, doi:10.1111/j.1365-3091.1975.tb00290.x.

- Ludwig, K.R., 2003, Mathematical-statistical treatment of data and errors for Th-230/U geochronology, 52, *in* Bourdon, B., Henderson, G.M., Lundstrom, C.C., and Turner, S.P., eds, Uranium-Series Geochemistry: Washington, D.C., Mineralogical Society of America, p. 631-656, doi:10.2113/0520631.
- Martinson, A.H., and Basko, W.J., 1998, Soil Survey of Flathead National Forest Area, Montana: U.S. Department of Agriculture, 100 p.
- Meinzer, O.E., 1910, Artesian water for irrigation in the Little Bitterroot Valley, Montana: U.S. Geological Survey Water Supply Paper 400-B, 37 p, doi:10.3133/wsp400B.
- Murray, A.S., and Funder, S., 2003, Optically stimulated luminescence dating of a Danish Eemian coastal marine deposit: a test of accuracy: Quaternary Science Reviews, v. 22, p. 1177-1183, doi:10.1016/S0277-3791(03)00048-9.
- Murray, A.S., and Wintle, A.G., 2000, Luminescence dating of quartz using an improved single-aliquot regenerative-dose protocol: Radiation Measurements, v. 32, p. 57-73, doi:10.1016/S1350-4487(99)00253-X.
- Murray, A.S., and Wintle, A.G., 2003, The single aliquot regenerative dose protocol: Potential for improvements in reliability: Radiation Measurements, v. 37, p. 377-381, doi:10.1016/S1350-4487(03)00053-2.
- Olley, J.M., Caitcheon, G.G., and Roberts, R.G., 1999, The origin of dose distributions in fluvial sediments, and the prospect of dating single grains from fluvial deposits using optically stimulated luminescence: Radiation Measurements, v. 30, p. 207-217, doi:10.1016/S1350-4487(99)00040-2.
- O'Connor, J.E., Baker, V.R., Waitt, R.B., Smith, L.N., Cannon, C.M., George, D.L., and Denlinger, R.P., 2020, The Missoula and Bonneville floods-A review of ice-age megafloods in the Columbia River basin: Earth-Science Reviews, v. 208, 103181, 51 p, doi:10.1016/j.earscirev.2020.103181
- Normark, W.R., and Reid, J.A., 2003, Extensive deposits on the Pacific plate from Late Pleistocene North American glacial lake outbursts: Journal of Geology, v. 111, p. 617-637, doi:10.1086/378334.
- Pardee, J.T., 1910, The Glacial Lake Missoula: Journal of Geology, v. 18, p. 376-386.

- Pardee, J.T., 1942, Unusual currents in glacial Lake Missoula: Geological Society of American Bulletin, v. 53, p. 1569-1600.
- Pharo, C.H., and Carmack, E.C., 1979, Sedimentation processes in a short residence-time intermontane lake, Kamloops Lake, British Columbia: Sedimentology, v. 26, p. 523-541, doi:10.1111/j.1365-3091.1979.tb00927.x.
- Price, R.A., and Kluver, M.H., 1974, Structure of the Rocky Mountains of the Glacier-Waterton Lakes National Park Area, *in* Voight, B., Voight, M.A., and International Congress on Rock Mechanics, Rock mechanics, the American northwest: An advance expedition report including a glimpse at the structure of the North Cascade, and Rainier Yellowstone, Grant Teton, Glacier, national park regions, with special reference and full descriptions concerning the mechanical problems of landslides, for citizens, emigrant and tourist: University Park, Pennsylvania, College of Earth and Mineral Science, Pennsylvania State University, p. 213-216.
- Reinick, H., and Singh, I., 1980, Depositional sedimentary environments, with reference to terrigenous clastics: Berlin, New York, Springer-Verlag, p. 127-128.
- Ryan, P.C., and Buckley, S.N., 1998, Sedimentation, strata-bound Cu-Ag mineralization, and syndepositional tectonics in the Revett Formation, Flathead Indian Reservation, western Montana, *in* Berg, R.B., ed., Belt Symposium III: Montana Bureau of Mines and Geology Special Publication 112, p. 278–289.
- Scarberry, K.C., in preparation, Geologic map of the Hubbart Reservoir 7.5' quadrangle, Flathead and Sanders Counties, Montana: Montana Bureau of Mines and Geology Open-File Report XXX, scale 1:24,000.
- Scarberry, K.C., McDonald C., and Coppage, E.L., in preparation, Geologic map of the Kofford Ridge 7.5' quadrangle, Flathead County, Montana: Montana Bureau of Mines and Geology Open-File Report XXX, scale 1:24,000.
- Skudder, P.A. and Hendrix, M.C., 2010, Surface geologic map of the confluence of the Swan and Flathead valleys, western Montana: Montana Bureau of Mines and Geology EDMAP portion of the National Geologic Mapping Program 3, scale 1:24,000.

- Smith, L.N., 2000, Surficial Geologic Map of the upper Flathead River valley (Kalispell valley) Area, Flathead County, Northwestern Montana: Montana Bureau of Mines and Geology Montana Ground-Water Assessment Atlas GWAA-02B-6, p. Scale 1:48,000.
- Smith, L.N., 2004, Late Pleistocene stratigraphy and implications for deglaciation and subglacial processes of the Flathead Lobe of the Cordilleran Ice Sheet, Flathead Valley, Montana, USA: *Sedimentary Geology*, v. 165, p. 295–332, doi:10.1016/j.sedgeo.2003.11.013.
- Smith, L.N., 2006, Stratigraphic evidence for multiple drainings of glacial Lake Missoula along the Clark Fork River, Montana, USA: *Quaternary Research*, v. 66, p. 311–322, doi:10.1016/j.yqres.2006.05.009.
- Smith, L.N., 2017, Repeated sedimentation and exposure of glacial Lake Missoula sediments: A lake-level history at Garden Gulch, Montana, USA: *Quaternary Science Reviews*, v. 155, p. 114–126, doi:10.1016/j.quascirev.2016.11.018.
- Smith, L.N., Sohbati, R., Buylaert, J-P., Lian, O.B., Murray, A., and Jain, M., 2018, Timing of lake-level changes for a deep last-glacial Lake Missoula: Optical dating of the Garden Gulch area, Montana, USA: *Quaternary Science Reviews*, v. 183, p. 23–35, doi:10.1016/j.quascirev.2018.01.009.
- Stickney, M.C., Haller, K.M., and Machette, M.N., 2000, Quaternary faults and seismicity in Western Montana: Montana Bureau of Mines and Geology Special Publication 114, scale 1:750,000.
- Thomas, G.S.P, and Connell, J., 1985, Iceberg drop, dump, and grounding structures from Pleistocene glacio-lacustrine sediments, Scotland: *Journal of Sedimentary Research*, v. 55, p. 243–249, doi:10.1306/212F8689-2B24-11D7-8648000102C1865D.
- Vandenberghe, D., De Corte, F., Buylaert, J.P., Kučera, J., and Van den haute, P., 2008, On the internal radioactivity in quartz: *Radiation Measurements*, v. 43, p. 771–775, doi:10.1016/j.radmeas.2008.01.016.
- Waite, R.B., 1980, About forty last-glacial Lake Missoula jokulhlaups through southern Washington: *The Journal of Geology*, v. 88, p. 653–679.

- Waitt, R.B., and Thorson, R.M., 1983, The Cordilleran Ice Sheet in Washington, Idaho, and Montana, *in*, Porter, S.P., and Wright, H.E., eds., Late Quaternary Environments of the United States, v. 1: Minneapolis, Minnesota, University of Minnesota Press, p. 53-70.
- Waitt R.B., 1985, Case for periodic, colossal jokulhlaups from Pleistocene glacial Lake Missoula: Geological Society of America Bulletin, v. 96, p. 1271-1286, doi:10.1130/0016-7606(1985)96<3C1271:CFPCJF>3E2.0.CO;2.
- Welk, E., 2019, Quaternary geology of the Cabinet, Heron and Smeads Bench 7.5' quadrangles, with emphasis on glacial Lake Missoula sediments [M.S. thesis]: Montana Technological University, 79 p.
- Winston, D., 1986, Stratigraphic correlation and nomenclature of the Middle Proterozoic Belt Supergroup, Montana, Idaho, and Washington, *in* Roberts, S.M., ed., Belt Supergroup: a guide to Proterozoic rocks of western Montana and adjacent areas: Montana Bureau of Mines and Geology Special Paper 94, p. 69–84.
- Zehner, R.E., 1987, Petrology, structure, and tectonic setting of the Hog Heaven volcanics, and their relationship to mineralization [M.S. thesis]: University of Montana, 132 p.

## 7. Appendix A: Final Luminescence Report



Prairie Research Institute

Illinois State Geological Survey  
615 E. Peabody Drive, MC-650  
Champaign, IL 61820-6615

May 26, 2021

Luminescence dating report for Carlos Montejo and Dr. Larry Smith, from the Montana Technological University

ISGS code	Sample	Equivalent dose (Gy) <sup>1</sup>	Dose rate (Gy/ka)	Age (ka) <sup>1</sup>	Overdispersion (%)	n (accepted/total)
775	LT1	53 ± 2	2.62 ± 0.10	20.3 ± 1.2	45 ± 7	40/230
776	LT3	39 ± 2	2.25 ± 0.08	17.4 ± 1.1	47 ± 7	36/240
777	R	51 ± 2	2.33 ± 0.08	21.8 ± 1.4	36 ± 4	57/240

<sup>1</sup> minimum age model (Galbraith et al., 1999)

Optically stimulated luminescence (OSL) dating was measured on quartz (150 – 250 µm), on small aliquots. These samples showed a large age distribution, expected for such sedimentary environment. We opted to derive the best age from the minimum age model. Uncertainties are reported at a 1σ significance, providing a level of confidence of approximately 67%. The uncertainties combine random and systematic errors, added in quadrature. Further details can be found in the report.

Sebastien Huot, Ph.D.

Illinois State Geological Survey

Champaign, Illinois

shuot@illinois.edu

+1-217-300-2579 (office)

UNIVERSITY OF ILLINOIS URBANA-CHAMPAIGN

217.333.4747 • isgs.illinois.edu

This is a report on the optically stimulated luminescence (OSL) dating of three samples delivered to us by Carlos Montejó and Dr. Larry Smith, in October 2020. The samples were retrieved in opaque tubes, from natural outcrops. The depositional environment is interpreted as glaciolacustrine. As it is expected to be partial bleached. For the purposes of internal identification, we labeled these samples ISGS 775 to 777.

## 1. Sample preparation and equipment

The tubes were opened and the mineral extraction was conducted in a subdued orange light environment. One inch of sediment was removed from both ends of the tube because these might have been partially exposed to light during sampling. Sediment from the external portions was used to measure the in situ water content and its radioactive content (uranium, thorium, and potassium), both for dose rate calculation. K-feldspar and quartz minerals for IRSL/OSL dating were extracted from the remainder (inner portion) of each tube.

These minerals were wet sieved to retrieve the 150- to 250- $\mu\text{m}$  grain size. A hydrochloric acid attack (HCl, 10%) was applied to dissolve any carbonate minerals that might be present. Using a heavy liquid solution (2.58 g/mL) of lithium heteropolytungstate (LST), we separated K-feldspar (<2.58) from the quartz and Na-feldspar minerals (>2.58). For quartz, further purification was done with a hydrofluoric acid (HF) attack (40% for 1 hour) to dissolve any remaining impurities. A second HCl attack was performed to dissolve calcium fluorite minerals, a potential by-product of HF dissolution of Ca-rich silicates. Finally, the purified quartz extracts were again sieved, at 150  $\mu\text{m}$ , to remove partially dissolved impurities. A purity check was performed by doing an Infrared over blue OSL stimulation. These quartz samples showed no significant contamination from feldspar.

To obtain the dose rate, sediments from the external portion of each sampling tube were dried, and a representative portion was encapsulated in thin disk-shaped containers (~20 g) and sealed with 2 layers of epoxy gel. A minimum waiting time of 21 days after sealing is recommended to restore the radioactive equilibrium of radon-222 daughter products (Gilmore, 2008). The specific activities (Bq/kg) were measured with a broad-energy high-purity germanium detector (BEGe), in a planar configuration, shielded by 15 cm of lead. Efficiency calibration of the detector was obtained with a set of six certified standards (IAEA-RGU-1, IAEA-RGTh-1, IAEA-RGK-1, IAEA-385, NIST 4350b, and NIST 4355).

## 2. Equivalent dose (De) measurements

For the equivalent doses (De) measurements, we relied on an automated Risø TL-DA-20 system, equipped with a set of blue (470 nm) and infrared (870 nm) LEDs, for light stimulation. Detection was made in the UV (Hoya U340 filter) for quartz. For each samples, we dispensed quartz grains over a small area (2 mm), onto a silicon oil covered stainless disk (10 mm diameter). Around 20 - 40



grains were dispensed on each disks' center. A total of 240 aliquots were measured, for each quartz samples.

OSL measurements were carried out with a single-aliquot regenerative dose (SAR) protocol (Table 1; Murray and Wintle, 2000; Murray and Wintle, 2003). The optimal measurement parameters were selected by a dose recovery test (latent dose bleached twice with blue LEDs, at 125 °C), for quartz. An initial dose was given at first (that was a close match to the measured equivalent dose for each sample; 67 Gy) and it was subsequently recovered by measuring its equivalent dose with the SAR protocol. The samples responded reasonably well to the treatment. The optimal measurement treatment was verified for each sample. From this we selected a preheat temperature (Lx) of 260 °C (held for 10 seconds). The preheat temperature for the test dose (Tx) was 240 °C. The dose recovery test gave an average measured-to-given dose ratios of  $0.95 \pm 0.02$  (9 aliquots). This outcome is positive. Considering this result, we opted to select the parameters in Table 1.

**Table 1. Measurement steps for the single-aliquot regenerative protocol**

Step	Procedure (quartz)
1	Regeneration <sup>1</sup> /natural dose
2	Preheat (260 °C), hold for 10 seconds
3	OSL stimulation with blue LEDs at 100 °C for 40 seconds (Lx)
4	Test dose beta irradiation (20 Gy)
5	Cut heat (240 °C) for 0 seconds
6	OSL stimulation with blue LEDs at 100 °C for 40 seconds (Tx)
7	Repeat Steps 1–6 with further regeneration doses

<sup>1</sup>For equivalent dose measurements, we gave a range of laboratory-induced doses that would properly encompass the variability of the observed natural luminescence.

In addition, limited measurements of the equivalent dose (De) was attempted with K-feldspar, on sample 775 (LT1). For this, we relied on an automated Lexsyg Smart system equipped with a set of green (525-nm) and infrared (850-nm) LEDs for light stimulation. Detection was done in UV-blue light (combination of Schott BG3 glass and Delta BP 365/50 EX Interference filters) for quartz. For K-feldspar minerals, the detection was done in blue light (combination of Schott BG39 glass and Semrock 414/46 Brightline HC Interference filters). For K-feldspar, grains were dispensed on a small area, 2 mm in diameter; around 20 - 40 grains were dispensed on each cup.

IRSL measurements were carried out with a single-aliquot regenerative dose (SAR) protocol (Table 2; Murray and Wintle, 2000; Huot and Lamothe, 2003). The optimal measurement parameters were selected by a dose recovery test (latent dose bleached with sunlight for 1 day). An initial dose was given at first (that was a close match to the measured equivalent dose for each sample: 78 Gy) and it was subsequently recovered by measuring its equivalent dose with the SAR protocol. The sample responded reasonably well to the treatment. From this we selected a preheat temperature (Lx and Tx) of 220 °C (held for 60 seconds; Huot and Lamothe, 2003). The dose recovery test was performed for one sample using the most appropriate temperature. It yielded an average measured-to-given dose ratio of  $1.02 \pm 0.03$ . This outcome is positive. Considering this result, we opted to select the parameters in Table 2.

**Table 2. Measurement steps for the single-aliquot regenerative protocol**

Step	Procedure (K-feldspar)
1	Regeneration <sup>1</sup> /natural dose
2	Preheat (220 °C), hold for 60 seconds
3	Pause <sup>2</sup>
4	IRSL stimulation with IR LEDs at 50 °C for 100 seconds (L <sub>x</sub> )
5	Test dose beta irradiation (13 Gy)
6	Preheat (220 °C) for 60 seconds
7	IRSL stimulation with IR LEDs at 50 °C for 100 seconds (T <sub>x</sub> )
8	Repeat Steps 1–7 with further regeneration doses

<sup>1</sup> For equivalent dose measurements, we gave a range of laboratory-induced doses that would properly encompass the variability of the observed natural luminescence.

<sup>2</sup> There was no pause here for equivalent dose measurements. A pause was observed here for anomalous fading measurements.

## 2.1 Equivalent dose calculation

For the equivalent dose, all calculations were made using the “late light” approach for background subtractions, by taking the initial 5 data channels (0.8 second) from the OSL decay curve and removing the background from the end of the stimulation curve for quartz (50 data channels, 8 seconds; Figure 1). For the equivalent dose of K-feldspar, the channel data settings were: initial 5 (5 seconds) from the IRSL decay curve along with the end of the stimulation curve (30 data channels, 30 seconds; Figure 1).

Uncertainties relied on Poisson statistics. For curve fitting, we also propagated the uncertainties from the optimized luminescence growth curve parameters. In addition, when the observed scatter about the best fit regression line was too high, the uncertainties were increased (Figure 2). For this, we relied on the one-tailed probability  $\chi^2$  distribution, with  $N - 3$  degrees of freedom (where  $N$  is the number of measured data points). When the probability was lower than 15% (i.e., the data points

scattered above and beyond the best fit line), the uncertainties for the optimized parameters were expanded by Student's  $t$  values for  $N - 3$  degrees of freedom (Brooks et al., 1972; Ludwig, 2003).

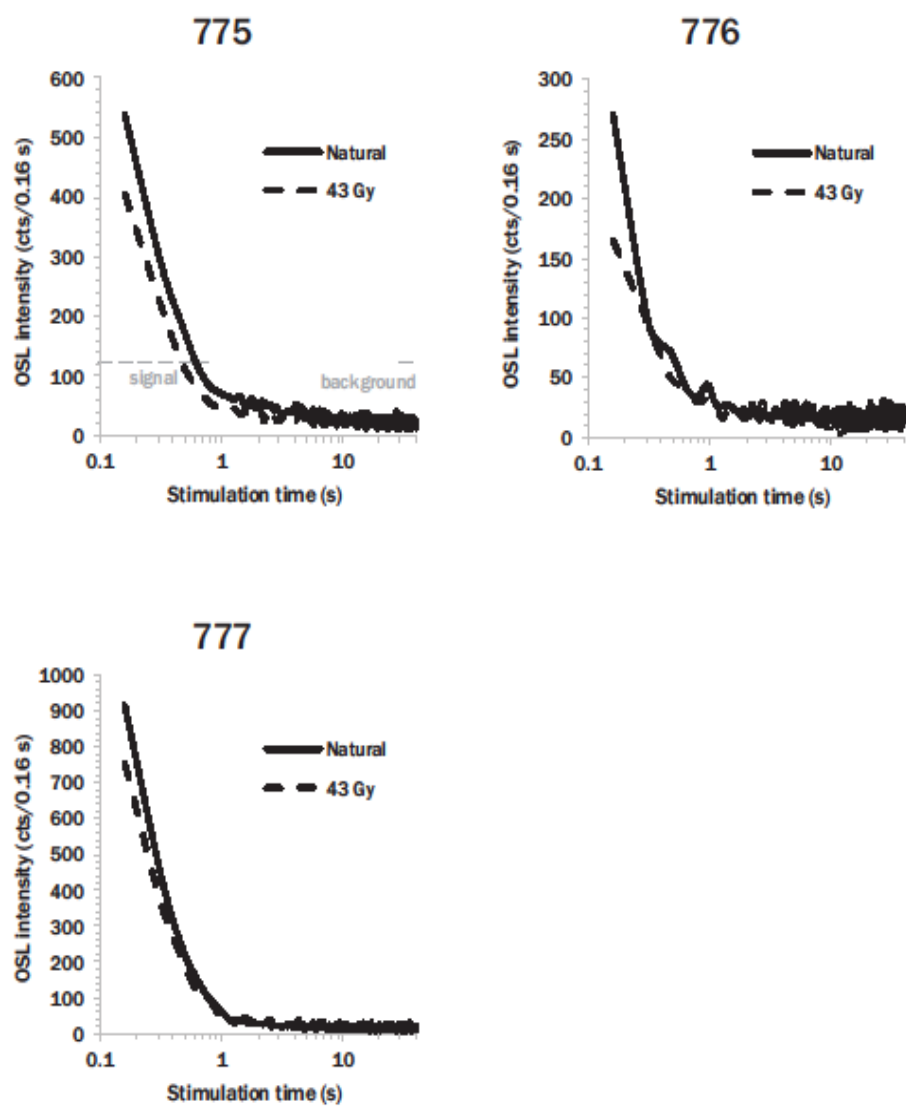


Figure 1. Typical OSL decay curve, for a naturally dose aliquot (solid curve) or laboratory-induced dose (dashed curve, in Gy). The area under the curve is proportional to the dose of radiation stored within the mineral. Their luminescence growth curve are shown in Figure 2.

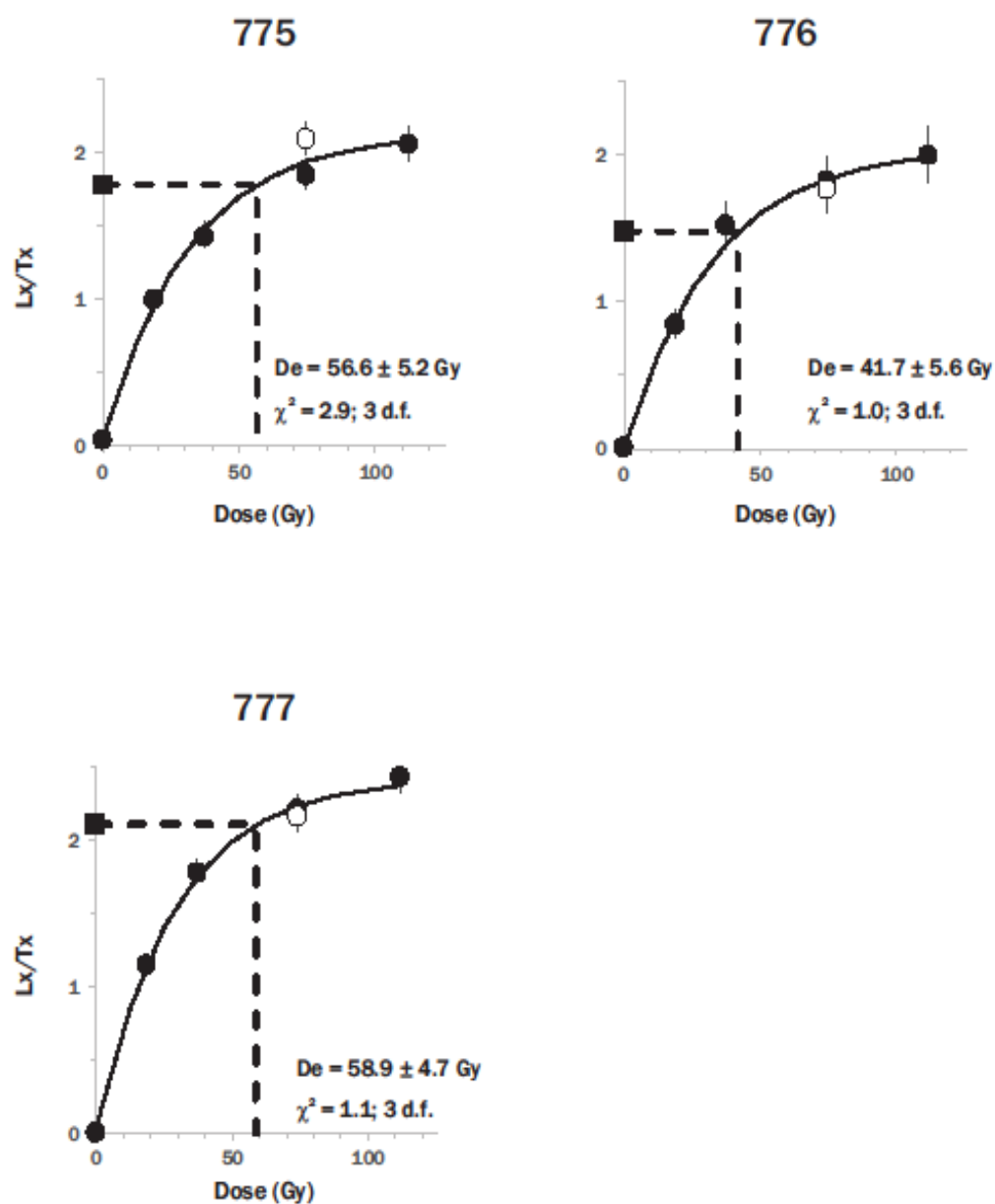


Figure 2. Luminescence dose response curve for the same aliquots shown in Figure 1. Each point corresponds to the OSL ( $L_x$ ; measurement step 3) of a natural (red square) or laboratory-induced dose (filled circles), normalized by the luminescence response to a fixed test dose ( $T_x$ ; measurement step 6). A repeat measurement (the recycling test; open circles) was performed at the end. The equivalent dose is obtained by interpolation. For the aliquots shown here, the observed measurements scatter well around the predicted best-fit curve.



## 2.2 Age distribution

A weighted average (using the central age model; Galbraith et al., 1999) was used in all calculations, except when noted otherwise. The central age model provides an overdispersion parameter. This parameter characterizes the degree to which the observed weighted distribution is consistent with the predicted weighted distribution from the observed data. At 0%, the observed distribution is equal to the statistical prediction. In luminescence dating, it is common for the observed distribution to be slightly larger than the expected distribution by a value of approximately 20%. This means that the calculated uncertainties tend to underestimate the "real" uncertainties because of intrinsic (e.g., instrumental uncertainties, luminescence characteristics of quartz and K-feldspar) or extrinsic (e.g., partial bleaching, external beta microdosimetry) factors. The central age model expands the age uncertainty in an attempt to account for this discrepancy. Here, the overdispersions are moderately large! (Table 3). It indicates a larger scatter in the calculated age distribution (Figure 3).

Table 3. Age overdispersion parameters<sup>1</sup>

ISGS code	Sample	Overdispersion (%)
775	LT1	45 ± 7
776	LT3	47 ± 7
777	R	36 ± 4

<sup>1</sup>A value of 20% is typical in luminescence

To document the shape of the age distribution more clearly, we must reduce the number of quartz (or K-feldspar) grains dispensed on each aliquot. Otherwise, in the presence of a multitude of grains on one aliquot (some being well bleached and others not; alternatively, from two distinct events, of different ages), each emitting a luminescence light signal, all these would add up to give an average, overestimated age compared to the most recent geological event that brought these quartz grains inside the sand wedge (Arnold and Roberts, 2009). The only recourse here is to reduce the number of grains dispensed on the aliquot (Olley et al., 1999). At the extreme limit, we would measure the luminescence from a single grain.

Usually, the best age estimate should rely on the average value from a repeated set of observations. We can think of instances when this might be inappropriate. A positive skewness, such as is noted here for most samples (Figure 3), is a clear sign of partial bleaching. In other words, during the last sedimentary cycle (erosion, transport, deposition, and burial), not all sedimentary grains of sand were sufficiently exposed to sunlight to completely reset the "dosimetric clock" that they had accumulated in their previous burial setting. Alternatively, it could reflect a population mixture of different events, formed at different ages, but with the most predominant population coming from the more recent event.

Although the mean is the scientist's best friend, it might prove to be an inappropriate estimator in this situation. Here, we opted to rely on the minimum age model (Galbraith et al., 1999). We chose to add an additional uncertainty ( $\sigma_b$ ; 10%), in quadrature, to each individual aliquot before inserting

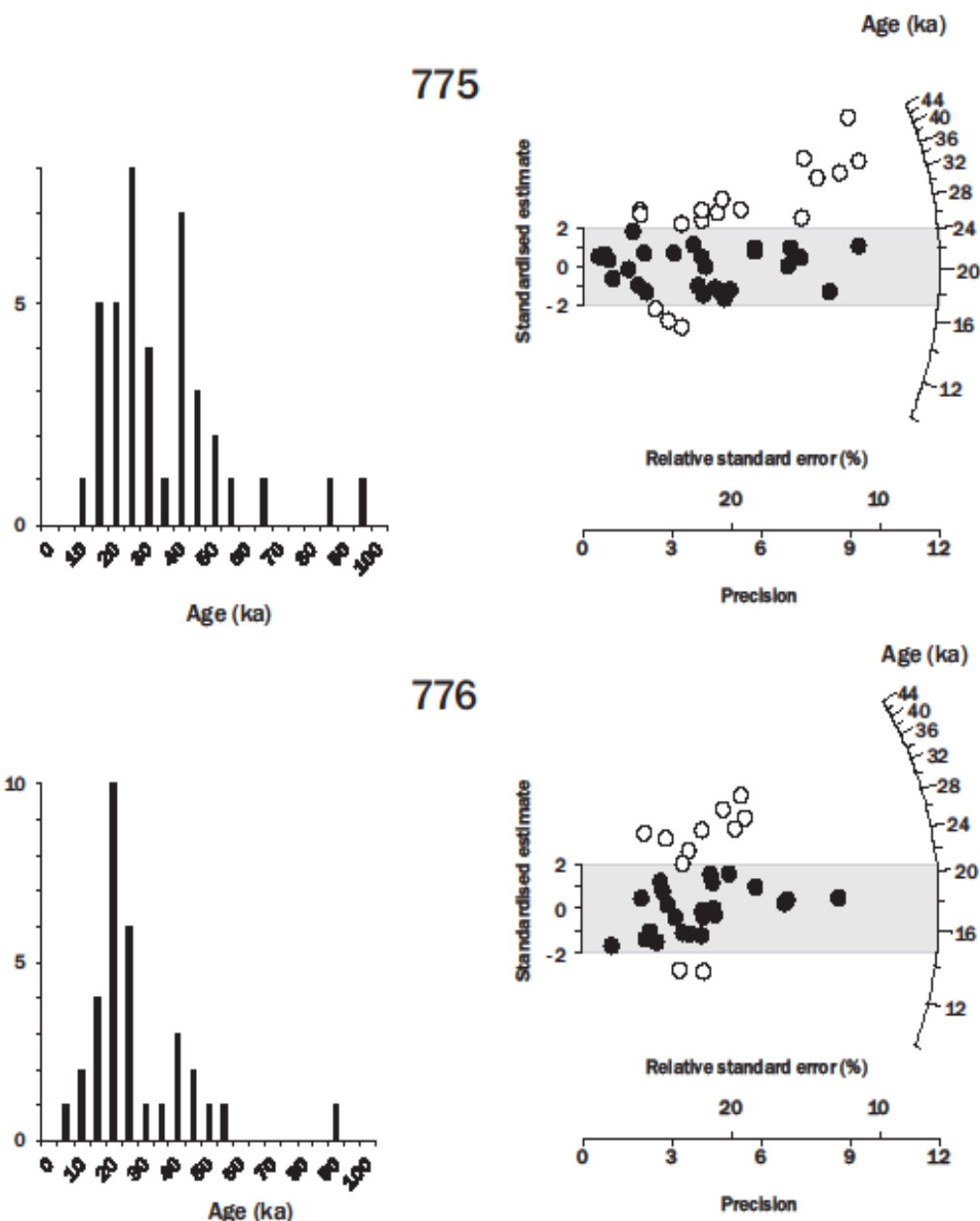


Figure 3. Age distributions, as a histogram and a radial plot, for all samples. Each circle on the radial plot represents the age and uncertainty, for a single aliquot. The age is read on the arc axis, by drawing a straight line from (0, 0), passing through a circle and intersecting the radial axis (log scale). The (0, 0) coordinate corresponds to a 0 standardised estimate (y-axis) and 0 precision (x-axis). The uncertainty is read on the horizontal axis, by drawing a perpendicular line reaching a circle. Hence, two aliquots, having the same age, but with different uncertainty, will lay on the same straight line (from (0, 0) to the radial axis). The aliquot with the smaller uncertainty (higher precision) will be closer to the arc. Values (filled circles) within the light grey shaded band are consistent (at  $2\sigma$ ) with the weighted mean (Central Age Model). A cluster of aliquots within this shaded band expresses confidence that we have a population of grains consistent with a single age.

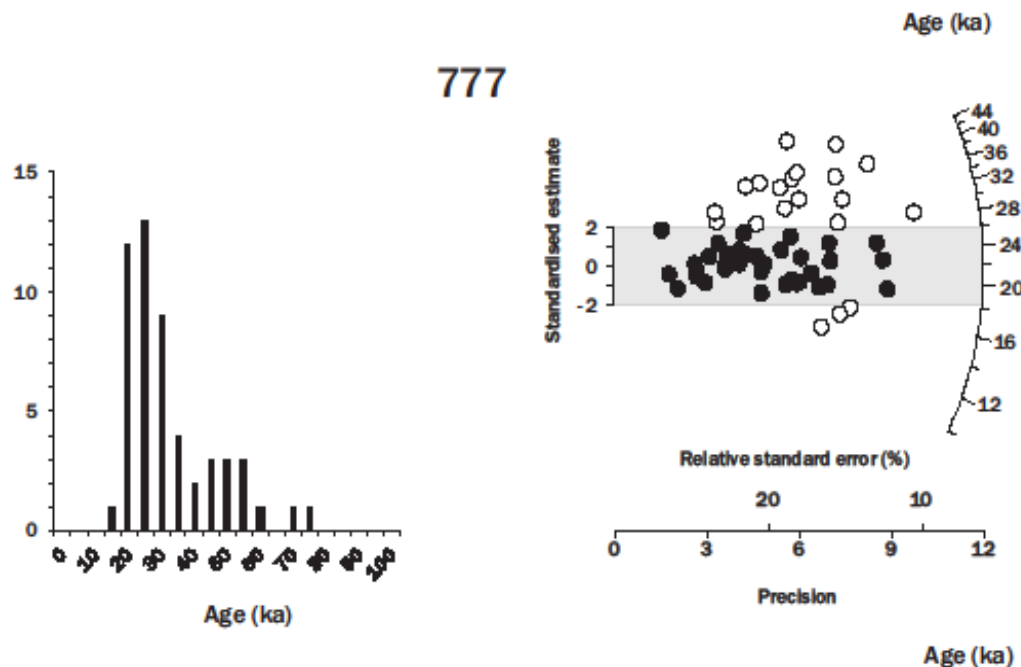


Figure 3. Age distributions, as a histogram and a radial plot, for all samples. Each circle on the radial plot represents the age and uncertainty, for a single aliquot. The age is read on the arc axis, by drawing a straight line from (0, 0), passing through a circle and intersecting the radial axis (log scale). The (0, 0) coordinate corresponds to a 0 standardised estimate (y-axis) and 0 precision (x-axis). The uncertainty is read on the horizontal axis, by drawing a perpendicular line reaching a circle. Hence, two aliquots, having the same age, but with different uncertainty, will lay on the same straight line (from (0, 0) to the radial axis). The aliquot with the smaller uncertainty (higher precision) will be closer to the arc. Values (filled circles) within the light grey shaded band are consistent (at  $2\sigma$ ) with the weighted mean (Central Age Model). A cluster of aliquots within this shaded band expresses confidence that we have a population of grains consistent with a single age.

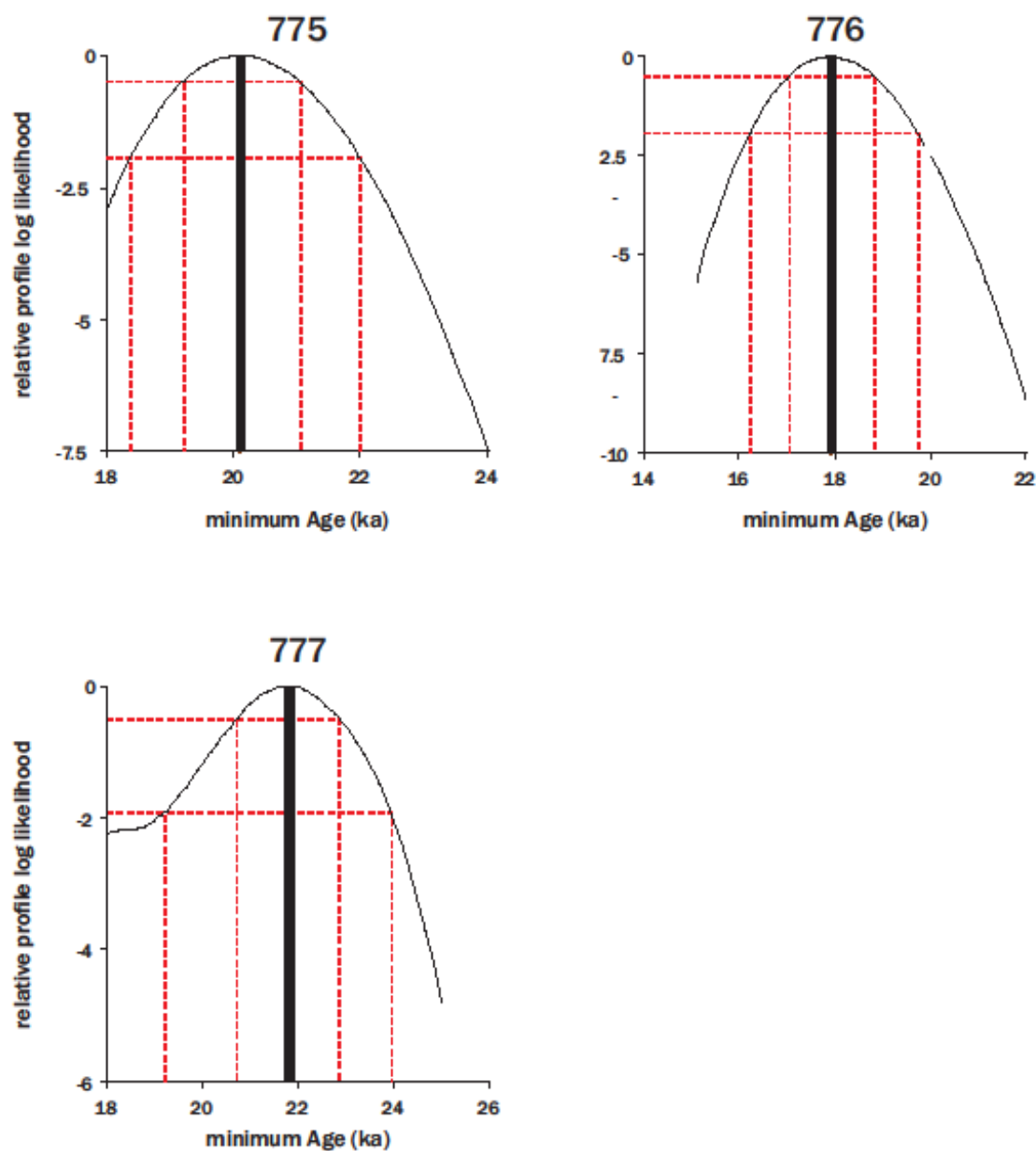


Figure 4. Relative profile log likelihood. The minimum age is found at the maximum value of the profile (solid vertical line). The  $1\sigma$  and  $2\sigma$  age uncertainties are shown by the dashed lines intersecting the profile, at a 0.5 and 1.92 relative likelihood.



The preliminary IRSL age is  $24 \pm 2$  ka. However, K-feldspar suffers from anomalous fading, meaning the real, fading corrected IRSL age, would lie around 33 ka. Fading was not measured. Older, too old, here, and most likely due to partial bleaching.

K-feldspar, compared to quartz, requires appreciably longer exposure to sunlight, to fully reset its latent luminescence age during the last sedimentary cycle (erosion, transport, deposition). The IRSL is old, but not overwhelming older than quartz. Thus, even if the equivalent dose from these quartz minerals is high, they should still be reliable. In addition, since quartz minerals are more likely to be fully bleached, we opted to measure all three ages with quartz.

### 3. Dose rate

The water content was measured for each sample. The as-received water content was very humid or bone dry (Table 5). Given the sedimentary context, and conversation with Larry and Carlos, in the past these samples would have been wetter than currently observed *in situ*. Hence, we opted for the values presented here. We assigned a water content uncertainty of 5 % to account for possible variation during the entire length of burial. The bulk density was measured for each samples.

Table 5. Water content, measured and presumed from the sample, along with bulk density

ISGS code	Sample	In situ (%)	presumed (%)	density (g/cm <sup>3</sup> )
775	LT1	17	$20 \pm 5$	1.36
776	LT3	25	$25 \pm 5$	1.40
777	R	1	$20 \pm 5$	1.74

Waiting times of around 30 days were observed before measuring the radioactive activities of uranium, thorium, and potassium, from which we can derive contributions from alpha, beta, and gamma energy decay (Table 6). There is a slightly excess in <sup>226</sup>Ra, relative to its direct parent, <sup>238</sup>U for sample ISGS 777 ( $1.16 \pm 0.06$ ). It is not a cause for concern, here, given the large activity of <sup>40</sup>K.

Table 6. Specific activity (Bq/kg)

ISGS code	Sample	<sup>238</sup> U	<sup>226</sup> Ra	<sup>210</sup> Pb	<sup>232</sup> Th	<sup>40</sup> K
775	LT1	$32.1 \pm 2.0$	$34.2 \pm 0.5$	$33.3 \pm 2.2$	$37.8 \pm 0.7$	$536 \pm 11$
776	LT3	$29.6 \pm 2.1$	$33.6 \pm 0.5$	$32.7 \pm 2.3$	$35.1 \pm 0.8$	$443 \pm 11$
777	R	$32.3 \pm 1.8$	$37.5 \pm 0.5$	$35.0 \pm 1.9$	$33.2 \pm 0.5$	$422 \pm 8$

For quartz, we assumed an internal content of  $0.08 \pm 0.02$  ppm and  $0.18 \pm 0.03$  ppm, for uranium and thorium, respectively (Vandenbergh et al., 2008). A conservative  $0.04 \pm 0.02$  "a value"

the aliquots into the minimum age model to account for intrinsic and extrinsic uncertainties which cannot be properly quantified (Figure 4; Table 4).

Table 4. Burial age comparison between the weighted mean (central age model) and minimum age model (MAM)

ISGS code	Sample	Weighted mean (ka)	MAM (ka)
775	LT1	28 ± 3	20.3 ± 1.2
776	LT3	20 ± 2	17.4 ± 1.1
777	R	26.6 ± 1.8	21.8 ± 1.4

As a clarification, the model is thus named: minimum age model. It is not a lower "boundary age". It should be considered instead as the best age estimate, reflective of the geological burial age for the last sedimentary event.

### 2.3 K-feldspar measurements

Limited equivalent dose measurements were performed with K-feldspar minerals, with sample ISGS 775 (LT1). The initial justification was a concern that quartz ages might underestimate the true burial age, here.

The concern was centered on the unusually low saturation level of the luminescence growth curve (Figure 2). The saturation level dictates the maximum equivalent dose that can be measured. It is a variable characteristic. It is often described by the < characteristic dose >, a parameter expressing the single saturation exponential curve. The characteristic dose lies around 66 % of the luminescence saturation level.

A typical, average, quartz mineral has a characteristic dose ranging from 50 – 100 Gy. Equivalent doses above the characteristic dose are harder to measure, precisely. Precisely, because the luminescence growth curve is curving, and rapidly approaching a flat level (c.f. Figure 4 of Murray and Funder, 2003). Also, when the equivalent dose is so large, well above this characteristic dose, we often notice the OSL age underestimate the expected age (for example, see Kolb and Fuchs, 2018). It is not an absolute behavior and there are very old luminescence ages derived from quartz in the literature. The cause remains undetermined, hence we have yet to devise a laboratory test that would alert us of this potential danger. Other, that is, than knowing the age, independently!

Here, these three samples have low characteristic doses, ranging from 24 to 32 Gy, in average. The equivalent doses ranges from 40 to 53 Gy (i.e. from the minimum age model). It is a cause of concern.

In that light, we opted to perform a preliminary age measurement with K-feldspar, on sample LT1. The characteristic dose of K-feldspar is consistently higher. Here, for LT1, it is approximately 300 Gy.



(efficiency of alpha particles compared with beta particles upon inducing a trapped charge in quartz and feldspar; i.e., alpha is only 4% as effective as beta) was retained. The external alpha dose rate contribution was assumed to be negligible here because we etched the quartz grains (Table 7). For K-feldspar, we assumed an internal content of  $12.5 \pm 0.5\%$  and  $400 \pm 100$  ppm, for potassium and rubidium, respectively (Huntley and Baril, 1997; Huntley and Hancock, 2001). A conservative  $0.10 \pm 0.05$  "a value" was retained.

Table 7. Contribution to the dose rate, expressed in Gy/ka

ISGS code mineral		beta external (Gy/ka)	gamma (Gy/ka)	cosmic ray (Gy/ka)	depth (m)	water (%)	total (Gy/ka)
775	Q <sup>1</sup>	$1.43 \pm 0.09$	$0.96 \pm 0.03$	$0.21 \pm 0.01$	1.8	$20 \pm 5$	$2.62 \pm 0.10$
775	F <sup>2</sup>	$1.48 \pm 0.10$	$0.96 \pm 0.03$	$0.21 \pm 0.01$	1.8	$20 \pm 5$	$3.35 \pm 0.13$
776	Q <sup>1</sup>	$1.18 \pm 0.08$	$0.83 \pm 0.02$	$0.23 \pm 0.01$	1.1	$25 \pm 5$	$2.25 \pm 0.08$
777	Q <sup>1</sup>	$1.22 \pm 0.08$	$0.87 \pm 0.02$	$0.23 \pm 0.01$	0.92	$20 \pm 5$	$2.33 \pm 0.08$

<sup>1</sup> For quartz minerals, we relied on an internal alpha dose rate contributions of  $0.014 \pm 0.007$  Gy/ka.

<sup>2</sup> For K-feldspar minerals, we relied on an external alpha and internal beta dose rate contributions of  $0.13 \pm 0.08$  and  $0.57 \pm 0.03$  Gy/ka, respectively.

The beta dose rate absorption efficiencies were adjusted according to the specific grain size and mineral used for equivalent dose measurement (Nathan, 2011). External beta and gamma contributions were attenuated for water content (Zimmerman, 1971). The energy-to-dose rate conversion coefficient relied on the update by Guérin et al. (2011). Cosmic ray contributions were calculated from Prescott and Hutton (1988; 1994).

#### 4. Uncertainty budget

The breakdown of the uncertainties, between the total random and systematic sources, are presented in table 8. The random uncertainties reflect the standard error on the best estimate (i.e. from the minimum age model) for the equivalent dose (in seconds of laboratory-induced irradiation). The systematic uncertainties reflect here the combined (in quadrature) components of the environmental dose rate and calibration of the beta source on the luminescence system.

Most of the age uncertainties, here, are derived from the random sources. Given the fairly old ages of both samples, their natural luminescence signal (square symbol; Figure 2) lies in the < curving > part of the luminescence growth curve. Small variation in the measured natural luminescence signal will produce large variation in the interpolated equivalent dose (dashed line; Figure 2). In addition, systematic uncertainties reflect our imperfect understanding of the burial conditions of the samples,

along with temporal changes. For example, the water content constantly fluctuates, unless in extreme and constant conditions (i.e. arid desert, permafrost). Burial depth is also another unknown quantity: it is assumed, here, that the samples were instantly buried to their current depth. For both parameters, water content and depth, a model could be devised, where both values would change over time, hence the dose rate thus final IRSL age. Such a model could be put in place, even with simple, guestimates. Simply lets of know of your interest.

Table 8. Random and systematic uncertainties (In years), at 1 sigma

ISGS code	Sample	Age (ka)	1 $\sigma$ (random)	1 $\sigma$ (systematic)
775	LT1	20.266 $\pm$ 1.248	$\pm$ 0.944	$\pm$ 0.817
776	LT3	17.448 $\pm$ 1.118	$\pm$ 0.886	$\pm$ 0.682
777	R	21.776 $\pm$ 1.360	$\pm$ 1.069	$\pm$ 0.841

## 5. Conclusion

In summary, there is a slightly excess in  $^{226}\text{Ra}$ , relative to its direct parent,  $^{238}\text{U}$  for sample ISGS 777 ( $1.16 \pm 0.06$ ). It is not a cause for concern. The dose rate was calculated using present-day values. The samples were well-behaved in their luminescence light-response. However, they suffer from having a low characteristic dose, ranging from 24 to 32 Gy, in average. This value is lower than the equivalent doses for these samples. Hence, it is possible that the final age is slightly underestimated. In addition, all samples were partially-bleached, at deposition. Our best age estimated is provided by the minimum age model.

Sebastien Huot

Visiting Research Scholar - Geochemistry

Illinois State Geological Survey

## References

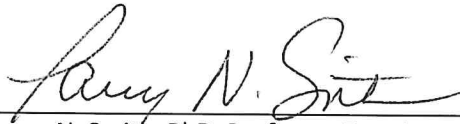
- Arnold, L.J., Roberts, R.G., 2009. Stochastic modelling of multi-grain equivalent dose ( $D_e$ ) distributions: Implications for OSL dating of sediment mixtures. *Quaternary Geochronology* 4, 204-230. <http://doi.org/10.1016/j.quageo.2008.12.001>
- Brooks, C., Hart, S.R., Wendt, I., 1972. Realistic use of two-error regression treatments as applied to rubidium-strontium data. *Reviews of Geophysics* 10, 551-577. <http://doi.org/10.1029/RG010i002p00551>
- Galbraith, R.F., Roberts, R.G., Laslett, G.M., Yoshida, H., Olley, J.M., 1999. Optical dating of single and multiple grains of quartz from Jinmium rock shelter, northern Australia: part I, experimental design and statistical models. *Archaeometry* 41, 339-364. <http://doi.org/10.1111/j.1475-4754.1999.tb00987.x>



- Gilmore, G.R., 2008. Practical gamma-ray spectrometry, 2nd ed. John Wiley & Sons, Ltd.  
<http://doi.org/10.1002/9780470861981>
- Huntley, D.J., Baril, M.R., 1997. The K content of the K-feldspars being measured in optical dating or in thermoluminescence dating. *Ancient TL* 15, 11-13.
- Huntley, D.J., Hancock, R.G.V., 2001. The Rb contents of the K-feldspar grains being measured in optical dating. *Ancient TL* 19, 43-46.
- Huot, S., Lamothe, M., 2003. Variability of infrared stimulated luminescence properties from fractured feldspar grains. *Radiation Measurements* 37, 499-503.  
[http://doi.org/10.1016/S1350-4487\(03\)00014-3](http://doi.org/10.1016/S1350-4487(03)00014-3)
- Kolb, T., Fuchs, M., 2018. Luminescence dating of pre-Eemian (pre-MIS 5e) fluvial terraces in Northern Bavaria (Germany) – Benefits and limitations of applying a pIRIR225-approach. *Geomorphology* 321, 16-32. <http://doi.org/10.1016/j.geomorph.2018.08.009>
- Ludwig, K.R., 2003. Mathematical-statistical treatment of data and errors for Th-230/U geochronology, 52. In: Bourdon, B., Henderson, G.M., Lundstrom, C.C., Turner, S.P. (Eds.), *Uranium-Series Geochemistry*. Mineralogical Society of America, pp. 631-656.
- Murray, A.S., Funder, S., 2003. Optically stimulated luminescence dating of a Danish Eemian coastal marine deposit: a test of accuracy. *Quaternary Science Reviews* 22, 1177-1183.
- Murray, A.S., Wintle, A.G., 2000. Luminescence dating of quartz using an improved single-aliquot regenerative-dose protocol. *Radiation Measurements* 32, 57-73.  
[http://doi.org/10.1016/S1350-4487\(99\)00253-X](http://doi.org/10.1016/S1350-4487(99)00253-X)
- Murray, A.S., Wintle, A.G., 2003. The single aliquot regenerative dose protocol: potential for improvements in reliability. *Radiation Measurements* 37, 377-381.  
[http://doi.org/10.1016/S1350-4487\(03\)00053-2](http://doi.org/10.1016/S1350-4487(03)00053-2)
- Olley, J.M., Caltcheon, G.G., Roberts, R.G., 1999. The origin of dose distributions in fluvial sediments, and the prospect of dating single grains from fluvial deposits using optically stimulated luminescence. *Radiation Measurements* 30, 207-217.
- Vandenbergh, D., De Corte, F., Buylaert, J.P., Kučera, J., Van den haute, P., 2008. On the internal radioactivity in quartz. *Radiation Measurements* 43, 771-775.

## SIGNATURE PAGE

This is to certify that the thesis prepared by Carlos Montejo entitled "Quaternary Geology of Portions of the McGregor Peak, Murr Peak, Marion, and Hubbart Reservoir, 7.5' Quadrangles, Flathead County, Montana" has been examined and approved for acceptance by the Department of Geological Engineering, Montana Technological University, on this 12th day of July, 2021.



---

Larry N. Smith, PhD, Professor Emeritus  
Department of Geological Engineering  
Chair, Examination Committee



---

Kaleb Scarberry, PhD, Associate Professor, Geologist  
Montana Bureau of Mines and Geology  
Member, Examination Committee



---

Paul W. Conrad, PhD, Professor  
Department of Mining Engineering  
Member, Examination Committee